



Norwegian University of  
Science and Technology

# Upgrading of Roskrepp hydropower plant to a pumped storage plant: Necessary reconstruction of the surge tank.

**Anne Leroquais**

Civil and Environmental Engineering

Submission date: January 2018

Supervisor: Leif Lia, IBM

Co-supervisor: Anton Schleiss, EPFL

Norwegian University of Science and Technology  
Department of Civil and Environmental Engineering



# M.Sc. THESIS IN HYDRAULIC ENGINEERING

Candidate: Ms. Anne Leroquais

Title: Upgrading of Roskrepp hydropower plant to a PSP: Reconstruction of the surge tank.

## 1. Background

In Norway and many countries in Europe, installation of unregulated power sources such as wind power, solar power and small hydro will grow in the years to come. This may result in more investments and construction of hydropower pumped storage plants (PSP). A PSP may be used for several purposes:

- Storing of energy
- Generation of peak power
- Balancing of energy production and electric grids

Already there is increased interest in PSP. The power company Sira-Kvina currently studying the possibility of upgrading the existing Roskrepp hydropower plant. Roskrepp power plant was commissioned in 1979, and has a single 50 MW Francis unit with nominal head 83 m and nominal discharge of approximately 70 m<sup>3</sup>/s.

One of the main problems with upgrading to PSPs is the uncertainty whether the tunnel system is capable of dealing with the increased loads (flow and pressure). The headrace tunnel in Roskrepp power plant is 3.5 kilometers and includes one surge tank and one brook intake. The tunnel is in general unlined and has an asphalt cover on the invert, which previously have proven vulnerable to rapid pressure fluctuations. New reversible units will result in increased and more frequent mass oscillations in the system. In this regard, the effect on the hydraulic transients in the tunnel system must be evaluated.

## 2. Main content for the thesis

The thesis shall cover, though not necessarily be limited to the main content listed below.

### 2.1 Literature and desk study

The candidate shall carry out a literature study of both dynamic flow design of power plants, and the design and operation of Roskrepp power plant.

### 2.2 Main tasks

The candidate must collect available background material such as reports, operational strategy, former studies, maps and drawings for Roskrepp power plant. Related to this material the following must be carried out:

- 1 Field trip to site and verification of drawings
- 2 In-situ measurement of hydraulic transients at Roskrepp power plant
- 3 Modeling of Roskrepp power plant in the numerical model LVTRANS
- 4 Calibration and validation
- 5 Calculation of mass oscillations after an upgrade to PSP

- 6 Propose a new design of the surge tank to allow the upgrade
- 7 Conclusions
- 8 Presentation

### **3 Supervision and data input**

Professor Leif Lia and Adjunct Associate Professor Kaspar Vereide will supervise and assist the candidate, and make relevant information available.

Discussion with and input from colleagues and other research or engineering staff at NTNU and EPFL, Lausanne, is recommended. Discussion with Sira-Kvina power company or other power companies is recommended. Significant inputs from other shall be referenced in a convenient manner.

Main contact person in Sira-Kvina kraftselskap will be: Kaspar Vereide

The research and engineering work carried out by the candidate in connection with this thesis shall remain within an educational context. The Roskrepp power plant is selected as a study objects. The candidate and the supervisors are therefore free to introduce assumptions and limitations which may be considered unrealistic or inappropriate in a contract research or a professional context.

### **4 Report format and reference statement**

The report should be written with a text editing software, and figures, tables, photos etc. should be of good quality. The report should contain an executive summary, a table of content, a list of figures and tables, a list of references and information about other relevant sources. The report should be submitted electronically in B5-format .pdf-file in DAIM, and three paper copies will automatically be handed in to the department.

The executive summary should not exceed 450 words, and should be suitable for electronic reporting.

The Master's thesis should be submitted within 19<sup>th</sup> of January 2018.

Trondheim 18<sup>th</sup> of September 2017

---

Leif Lia  
Professor  
Department of Hydraulic and Environmental Engineering  
NTNU



## Abstract

The scope of this thesis is to build a 1D numerical model of a hydraulic powerplant, transform it to simulate the upgrade of the powerplant into a pumped storage system, establish the issues that would emerge from it in the surge tanks and test several solutions to solve them.

The 1D numerical software LVTrans is used to calculate the hydraulic transient in the whole system and simulate the water table movements inside the surge tanks. It uses the Method Of Characteristics to solve the differential equations describing the transient flows.

The transformation of the Roskrepp powerplant, located in the south of Norway, into a pumped storage powerplant is used as a case study. The powerplant includes two separate surge tanks. The main one is a variable surge tank located between the upstream reservoir and the turbine. The second one is smaller and placed near the exit of the turbine, in the downstream part.

The model is build based on the drawings of the powerplant and a calibration is carried out by using data gathered during a field trip.

The upgrade of the model consider the implementation of a 50 MW pump in parallel with the turbine. The results show that the surge tank is sufficient to absorb the mass oscillations taking place in the upstream part of the system. The downstream surge tank is however unable to keep the water table within its boundaries and should be upgraded.

Three solutions are proposed to upgrade the downstream surge tank. The first is to expand the section of the existing surge tank. The second is to transform the surge tank into a variable surge tank by adding an upper and a lower chamber. The third is to implement a throttle at the bottom of the surge tank.

The solutions are tested by implementing them in the LVTrans model and the results show that they are successful in increasing the surge tank capacity to absorb the mass oscillations. An optimal design is proposed for each of them.

Finally, an economic analysis is performed to estimate the costs associated with their implementation.



## Résumé

L'objectif de cette étude est de construire un modèle numérique 1D d'un aménagement hydraulique, de le modifier afin de simuler la transformation de l'aménagement en aménagement de pompage turbinage, d'établir les problèmes qui en émergerait au niveau des cheminées d'équilibre et de tester des solutions pour les résoudre.

Le logiciel de modélisation numérique 1D LVTrans est utilisé pour calculer les conditions hydraulique dans tout le système et simuler les déplacements du plan d'eau dans les cheminées d'équilibre. Il utilise la méthode des caractéristiques pour résoudre les équations différentielles décrivant les flux hydrauliques.

La transformation de l'aménagement de Roskrepp, situé dans le sud de la Norvège, en aménagement de pompage turbinage est utilisé comme étude de cas. L'aménagement comprend deux cheminées d'équilibre indépendantes. La principale est une cheminée à chambre d'expansion située entre le réservoir amont et la turbine. La seconde est plus petite et placée près de la sortie de la turbine, dans la partie aval.

Le model est construit en se basant sur les plans de l'aménagement et un calibrage est réalisé en se basant sur des données récupérées lors d'une sortie sur le terrain.

La transformation du modèle prend en compte l'implémentation d'une pompe de 50 MW en parallèle avec la turbine. Les résultats montrent que la cheminée d'équilibre est suffisante pour absorber les oscillations de masse dans la partie amont. La cheminée d'équilibre aval n'est cependant pas capable d'absorber le trop plein d'eau et devrait être modifiée.

Trois solutions sont proposées pour modifier la cheminée d'équilibre aval. La première est d'élargir la section de la cheminée. La seconde est de transformer la cheminée en cheminée à chambre d'expansion en y ajoutant deux chambres. La troisième est d'implémenter un goulot d'étranglement à la base de la cheminée.

Les solutions sont testées en les implémentant dans le modèle et les résultats montrent qu'elles augmentent bien la capacité de la cheminée à absorber les oscillations de masse. Une optimisation du dimensionnement de chaque solution est réalisée.

Finalement, une analyse économique est réalisée pour estimer les coûts liés à leur implémentation.



## Acknowledgement

I'm sincerely grateful to my main supervisors, Prof. Anton Schleiss of EPFL in Switzerland and Prof. Leil Lia of NTNU in Norway for giving me the opportunity to realize my thesis in Norway and discover this beautiful country.

My deepest thanks to Kaspar Vereide and Ola Haugen Havrevoll for guiding me and answering all of my questions. This thesis would not have been the same without their inputs.

Finally, I'm really grateful for the warm welcoming that I received from everyone in Trondheim and for the kindness that was shown to me all along this semester.

Lausanne 19<sup>th</sup> of January 2018



Anne Leroquais



# Contents

Abstract .....	1
Résumé .....	3
Acknowledgement .....	5
List of Figures .....	11
List of Tables .....	13
List of Symbols .....	15
1 Introduction .....	17
1.1 LVTrans .....	17
1.2 Roskrepp Powerplant .....	17
1.3 Pumped storage plant and surge tanks .....	18
2 Theory .....	19
2.1 General hydraulic concepts .....	19
2.1.1 Governing equations .....	19
2.1.1.1 Continuity equation .....	19
2.1.1.2 Momentum equation .....	22
2.1.1.3 Simplification .....	23
2.1.2 Method of characteristics .....	24
2.1.3 Hydraulic losses .....	28
2.1.3.1 Friction losses .....	29
2.1.3.2 Singular losses .....	30
2.1.3.3 Hydraulic losses in LVTrans .....	31
2.2 Theory related to the surge tank .....	32
2.2.1 Design criteria of the surge tank .....	32
2.2.2 Water hammer .....	32
2.2.2.1 Concept .....	33
2.2.2.2 Calculation of the wave celerity .....	35
2.2.2.3 Instantaneous closing of the valve .....	36
2.2.2.4 Non-instantaneous closing of the valve .....	37
2.2.3 Mass oscillation .....	38
2.2.3.1 Concept .....	38

---

2.2.3.2	Amplitude .....	40
2.2.3.2.1	Momentum equation.....	40
2.2.3.2.2	Continuity equation .....	42
2.2.3.2.3	Maximal amplitude of the oscillations .....	42
2.2.3.2.4	Simplified method .....	44
2.2.4	Stability condition .....	44
2.2.5	Types of surge tank .....	46
2.2.5.1	Simple surge tank.....	46
2.2.5.2	Throttled surge tank .....	46
2.2.5.3	Variable surge tank .....	46
2.2.5.4	Closed surge tank.....	47
2.2.5.5	Differential surge tank .....	48
3	Method.....	50
3.1	Model of the Roskrepp powerplant.....	50
3.1.1	Model construction.....	50
3.1.1.1	Tunnels.....	51
3.1.1.2	Surge tanks.....	52
3.1.1.2.1	Upstream surge tank .....	52
3.1.1.2.2	Downstream surge tank .....	54
3.1.1.3	Creek shaft .....	54
3.1.1.4	Turbine .....	55
3.1.2	Calibration .....	55
3.1.2.1	Data available.....	56
3.1.2.1.1	Report from 1980.....	56
3.1.2.1.2	Field trip .....	57
3.1.2.1.3	Data conversion .....	58
3.1.2.2	Normal operation calibration .....	61
3.1.2.3	Shutdown calibration .....	64
3.1.2.3.1	Considerations on the turbine opening .....	65



---

3.1.2.3.2	Upstream the turbine .....	69
3.1.2.3.3	Downstream.....	74
3.2	Transformation into a pumped storage system.....	76
3.2.1	Model.....	77
3.2.2	Simulation .....	78
3.2.2.1	Load cases studied .....	78
3.2.2.2	Water levels in the surge tanks .....	80
3.2.3	Upgrade impact .....	81
3.3	Solutions proposal .....	82
3.3.1	Simulation scenarios.....	82
3.3.2	Alternatives .....	82
3.3.2.1	Enlargement of the surge tank .....	83
3.3.2.2	Transformation into a variable surge tank .....	83
3.3.2.3	Implementation of a throttle.....	84
3.3.2.3.1	Simulated values.....	85
3.3.2.3.2	Design of a symmetrical throttle .....	85
3.3.3	Economic analysis.....	86
3.3.3.1	Enlargement of the surge tank .....	87
3.3.3.2	Variable surge tank .....	87
3.3.3.3	Throttle.....	89
4	Results .....	91
4.1	Current surge tank.....	91
4.2	Solutions proposal.....	92
4.2.1	Alternative I – Surge tank enlargement.....	92
4.2.2	Alternative II – Variable surge tank .....	93
4.2.3	Alternative III – Throttled surge tank.....	95
4.2.3.1	Symmetric .....	95
4.2.3.2	Asymmetric.....	97
4.2.3.3	Throttle design .....	97
4.3	Economic analysis.....	98
5	Discussion .....	101
5.1	Calibration.....	101

5.2	Upgrade of the model.....	102
5.3	Solutions.....	104
5.3.1	Surge tank enlargement .....	104
5.3.2	Variable surge tank.....	104
5.3.3	Throttle .....	105
5.3.4	Economic analysis.....	105
6	Conclusion.....	107
	ANNEX.....	109

## List of Figures

Figure 2.1. Control volume (---) in a loaded pipe .....	19
Figure 2.2. Axial forces applied to a control volume in a loaded pipe.....	22
Figure 2.3. Characteristic lines AP et BP .....	25
Figure 2.4. Characteristic lines used in the solving of a loaded pipe problem.....	26
Figure 2.5. Solving of a pipe problem using the MOC .....	28
Figure 2.6. Moody diagram.....	30
Figure 2.7. Water hammer concept .....	34
Figure 2.8. Water hammer oscillation with a linear closing of the valve.....	37
Figure 2.9. Mass oscillations depending on the friction characteristic $\sigma$ for an a) Instantaneous opening b) Instantaneous closing of the valve .....	39
Figure 2.10. Forces inside the waterway of an hydro-power plant .....	40
Figure 2.11. Extreme values of Z for an instantaneous a) opening and b) closing of the valve.....	43
Figure 2.12. Extreme values of Z for a gradual a) opening and b) closing of the valve .....	44
Figure 2.13. Throttled surge tank .....	46
Figure 2.14. Alternative for the design of the upstream surge tank in Roskrepp power plant .....	47
Figure 2.15. Closed surge tank.....	48
Figure 2.16. Differential surge tank according to Johnson (1915).....	49
Figure 3.1. LVTrans model from the intake to the pipe connection I.....	50
Figure 3.2. LVTrans model from the pipe connection I to the outlet.....	51
Figure 3.3. Tunnel sections in the powerplant .....	51
Figure 3.4. Cross-section of the tunnels working as chambers in the upstream surge tank .....	53
Figure 3.5. Simplified schema of the upstream surge tank introduced in the model .....	53
Figure 3.6. Cross-section of the downstream surge tank.....	54
Figure 3.7. Drawing of the secondary intake in the Skjervevatn Lake .....	54
Figure 3.8. Power produced during the measurements .....	57
Figure 3.9. Butterfly valve and location of the upstream sensor (1) .....	58
Figure 3.10. Turbine and general locations of the upstream (1) and downstream (2) sensors .....	59
Figure 3.11. Pressure measured before the opening of the butterfly valve .....	59
Figure 3.12. Comparison of the measured and simulated hydraulic heads upstream the turbine .....	62
Figure 3.13. Comparison of the measured and simulated hydraulic head downstream the turbine .....	62
Figure 3.14. Hydraulic head based on the measurements upstream the turbine during the shutdown..	64
Figure 3.15. Hydraulic head based on the measurements downstream the turbine during the shutdown .....	65
Figure 3.16. Upstream and downstream pressure and turbine opening during the shutdown.....	66
Figure 3.17. Downstream hydraulic head and turbine opening during the turbine start up .....	67
Figure 3.18. Downstream hydraulic head, water level in reservoir and turbine opening during the shutdown .....	68
Figure 3.19. Adjusted downstream hydraulic head .....	69
Figure 3.20. Simulated hydraulic head from the calibrated model compared to the measured one.....	70
Figure 3.21. Simulated upstream hydraulic head with / without creek shaft .....	71
Figure 3.22. Simulated upstream hydraulic head for different creek shaft diameters .....	71
Figure 3.23. Simulated upstream hydraulic head for different friction coefficients in the creek shaft .	72
Figure 3.24. Simulated upstream hydraulic head for different friction coefficients in the surge tank ..	73
Figure 3.25. Simulated upstream hydraulic head for different surge tank diameters.....	73
Figure 3.26. Simulated hydraulic head from the calibrated model compared to the adjusted one.....	75
Figure 3.27. Simulated downstream hydraulic head for different friction coefficients in the surge tank .....	75
Figure 3.28. Simulated downstream hydraulic head for different surge tank diameters .....	76

---

Figure 3.29. LVTrans upgraded model from the intake to the pipe connection I .....	77
Figure 3.30. LVTrans upgraded model from the pipe connection I to the lower reservoir .....	77
Figure 3.31. Extreme simulated water level in the upstream surge tank .....	81
Figure 3.32. Extreme simulated water level in the downstream surge tank .....	81
Figure 3.33. Estimated cost in NOK per meter of blasted tunnel, for different cross-section areas .....	88
Figure 3.34. Estimated cost of a plug implemented in an addit tunnel .....	89
Figure 4.1. Extreme simulated water level in the downstream surge tank .....	91
Figure 4.2. Highest water level in the surge tank for different surge tank diameters .....	92
Figure 4.3. Lowest water level in the surge tank for different surge tank diameters .....	93
Figure 4.4. Highest water level in the variable surge tank for different chambers area .....	94
Figure 4.5. Lowest water level in the variable surge tank for different chambers area .....	94
Figure 4.6. Highest water level in the variable surge tank for different throttles .....	96
Figure 4.7. Lowest water level in the variable surge tank for different throttles .....	96
Figure 4.8. Lowest water level in the variable surge tank for an asymmetrical throttle .....	97

## List of Tables

Table 3.1. Area and equivalent diameter of the tunnel sections.....	52
Table 3.2. Cross-sections and boundaries of the different parts of the upstream surge tank .....	52
Table 3.3. Equivalent diameter of the creek shaft .....	55
Table 3.4. Parameters of the turbine.....	55
Table 3.5. Total heads estimated according to the report from 1980 .....	56
Table 3.6. Water level in the reservoirs during the measurements.....	57
Table 3.7. Sensors level.....	60
Table 3.8. Pipes diameters at the sensors levels .....	61
Table 3.9. Average measured power and hydraulic heads. ....	61
Table 3.10. Comparison between the simulated and the measured hydraulic heads upstream and downstream the turbine .....	63
Table 3.11. Average hydraulic head for different opening of the turbine .....	67
Table 3.12. Optimized set of parameters in the upstream section .....	69
Table 3.13. Downstream surge tank parameters in the calibrated model.....	74
Table 3.14. Surge tanks boundaries according to the drawings .....	76
Table 3.15. Pump parameters in the upgraded model .....	78
Table 3.16. Scenarios of turbine and pump operations .....	79
Table 3.17. Water level combinations and power produced in the worst-case scenarios.....	80
Table 3.18. Worst configurations for the upgraded model.....	80
Table 3.19. Extreme design values in the surge tanks and corresponding simulated ones .....	82
Table 3.20. Simulation scenarios used to test the solutions .....	82
Table 3.21. Simulated diameters .....	83
Table 3.22. Chambers configurations.....	84
Table 3.23. Surge tank boundaries after the implementation of a throttle .....	85
Table 3.24. Singular loss coefficients in the surge tank .....	85
Table 4.1. Maximum and minimum water level reached for each combination .....	94
Table 4.2. Maximum and minimum levels simulated with different symmetrical throttles.....	96
Table 4.3. Estimated cost of the enlargement of the surge tank.....	98
Table 4.4. Estimated cost of the transformation of the surge tank into a variable surge tank .....	99
Table 4.5. Estimated cost of the implementation of a throttle.....	100



## List of Symbols

Symbol	Unit	Description
$A$	$m^2$	Area
$C_v$	$m^5/s^2$	Loss coefficient in LVTrans
$D$	$m$	Diameter
$H$	$m$	Total head
$L$	$m$	Length
$Q$	$m^3/s$	Discharge
$a$	$m/s$	Wave propagation velocity
$f$	–	Friction factor
$h$	$m$	Hydraulic head
$p$	$Pa$	Pressure
$t$	$s$	Time
$v$	$m/s$	Velocity
$\zeta$	–	Singular loss coefficient
$\rho$	$kg/m^3$	Density
$\nu$	$m^2/s$	Kinematic viscosity
$\eta$	–	Efficiency
$\tau$	$N/m^2$	Shear stress





# 1 Introduction

The scope of this thesis is to build a 1D numerical model of a powerplant, transform it to simulate the upgrade of the powerplant into a pumped storage system, establish the issues that would emerge from it in the surge tanks and test several solutions to solve them. The 1D numerical software LVTrans will be used to calculate the hydraulic transient in the whole system and simulate the water table movements inside the surge tanks.

## 1.1 LVTrans

LVtrans (Lab View Transient Pipe Analysis) is a 1D-simulation software for loaded flow in pipe systems. It uses the Method of Characteristics, described in the theory chapter, to solve the partial differential equations that describe transient flows in a system. Those equations, called equation of motion and continuity equation, are also introduced in the theory chapter.

LVTrans is object based and uses LabVIEW (Laboratory Virtual Instrument Engineering Workbench) as graphical interface. Each element of a powerplant is represented as an object in which are introduced several input parameters. Pipes, surge tanks, constant level, turbine and pumps are introduced and characterised by the user who can then connect them together to form an entire system.

LVTrans is especially designed to simulate hydro-powerplant and allows the user to control the power produced by the turbine and to start or stop a pump at all time during the simulation. The results are exhibited for each object in the form of graphs and can be loaded as lists of values.

## 1.2 Roskrepp Powerplant

The model built in LVTrans is based on the Roskrepp powerplant located in the south of Norway. It is part of the network of hydraulic powerplants taking place along the Sira and Kvina rivers and owned by the company Sira Kvina Kraftselskap.

The Roskrepp powerplant is small in term of power produced, with an installed capacity of 50 MW, but is strategically placed as the first of several powerplants placed along the Kvina river. Its operation impacts everything that happens downstream and its adaptability is therefore important in the overall production flexibility of the company. For this reason, the

transformation of the Roskrepp powerplant in a pumped storage system is considered to enhance the control of the company over the produced power.

### **1.3 Pumped storage plant and surge tanks**

The addition of a pump into a hydraulic powerplant allows for a better flexibility in terms of power produced. It gives the possibility to pump water in the upstream reservoir when the electricity demand is low and to use the stored energy when needed. A pumped storage system can then be viewed as a large-scale battery.

The addition of a pump however creates new hydraulic conditions by moving the water on the upward direction and increases the water hammer that can be experienced in the powerplant. It then becomes possible to have situations in which the water flowing in the system is abruptly stopped and then changes direction in a short span of time. The surge tanks in the system should then be tested to check their behaviour in those kind of situations. The main risk would be that the water table goes out of the surge tank boundaries because of the increased mass oscillations.

## 2 Theory

The theory used in the LVTrans software is introduced in this chapter. First the governing equations, the method of characteristics and the computation of hydraulic losses are developed. Then the theory related to the surge tanks including the water hammer and the mass oscillations is introduced.

### 2.1 General hydraulic concepts

The general hydraulic concepts used in LVTrans are introduced in this part.

#### 2.1.1 Governing equations

Two fundamental equations are used to describe the water flow in a loaded unsteady state. The first one is based on the principle of mass conservation while the other one is derived from the second law of Newton. Those equations are used as core principles in the computation of the flows in LVTrans.

##### 2.1.1.1 Continuity equation

The principle of mass conservation states that the mass increase of water inside a control volume, as described in Figure 2.1, in a certain amount of time, is equal to the mass entering the control volume minus the one exiting it during this time.

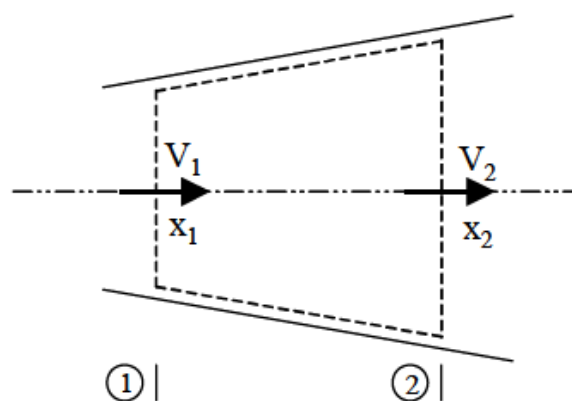


Figure 2.1. Control volume (---) in a loaded pipe<sup>1</sup>

<sup>1</sup> (Boillat & De Souza, 2004)

In the case of a loaded pipe, with  $x$  the longitudinal coordinate,  $t$  the time,  $A(x, t)$  the cross section of the pipe and  $\rho$  the water density, the mass variation over time of the water volume is expressed by  $\delta x \cdot \delta(\rho A)/\delta t$ . The difference in mass entering and exiting the control volume is formulated  $\delta(\rho AV)$  with  $V(x, t)$  the water velocity.

The principle of mass conservation, applied to a loaded pipe, can then be written as following:

$$\frac{\delta}{\delta t}(\rho A) + \frac{\delta}{\delta x}(\rho AV) = 0 \quad (2.1)$$

By expanding equation (3.2), equation (2.2) is deduced.

$$A \frac{\delta \rho}{\delta t} + \rho \frac{\delta A}{\delta t} + \rho A \frac{\delta V}{\delta x} + \rho V \frac{\delta A}{\delta x} + AV \frac{\delta \rho}{\delta x} = 0 \quad (2.2)$$

The total derivative of a quantity  $i$  can be expressed as shown in equation (2.3). By using this rule, equation (2.4) can be derived from equation (2.2)

$$\frac{di}{dt} = \frac{\delta i}{\delta t} + \frac{\delta i}{\delta x} \frac{dx}{dt} \quad (2.3)$$

$$\frac{1}{\rho} \frac{d\rho}{dt} + \frac{1}{A} \frac{dA}{dt} + \frac{\delta V}{\delta x} = 0 \quad (2.4)$$

The water elasticity modulus  $E_a$  can be written as:

$$E_a = \frac{dp}{d\rho/\rho} \quad (2.5)$$

An elastic linear relationship between the strain and the stress in the pipe walls is admitted. With  $\sigma_2$  the radial stress,  $\sigma_1$  the axial stress,  $\mu$  the Poisson's ratio and  $E_p$  the pipe elasticity modulus, the strain can then be defined as:

$$\varepsilon = \frac{\sigma_2 - \mu_1 \sigma_1}{E_p} \quad (2.6)$$

As a simplification, it is admitted that expansion joints are set all along the pipe. The axial stress  $\sigma_1$  is therefore null. The strain becomes:

$$\varepsilon = \frac{\sigma_2}{E_p} \quad (2.7)$$

If the wall's thickness  $e$  is low and constant, then the radial stress can be written, with  $D$  the pipe diameter:

$$\frac{d\sigma_2}{dt} = \frac{d}{dt} \left( \frac{pD}{2e} \right) = \frac{p}{2e} \frac{dD}{dt} + \frac{D}{2e} \frac{dp}{dt} = E_p \frac{d\varepsilon}{dt} \quad (2.8)$$

For a circular cross-section with a radius  $R$ , the section area is defined by  $A = \pi R^2$ , then  $dA/dt = 2\pi R(dR/dt)$  and  $d\varepsilon = dR/R = dD/D$ . With those values, equation (2.8) is written:

$$E_p \frac{d\varepsilon}{dt} = \frac{pD}{2e} \frac{d\varepsilon}{dt} + \frac{D}{2e} \frac{dp}{dt} \quad (2.9)$$

Hence:

$$\frac{d\varepsilon}{dt} = \frac{dp/dt}{\frac{2eE_p}{D} - p} \quad (2.10)$$

Considering that  $dA/A = 2d\varepsilon$ , the following equation ensues:

$$\frac{1}{A} \frac{dA}{dt} = \frac{dp/dt}{\frac{eE_p}{D} - \frac{p}{2}} \quad (2.11)$$

By introducing equations (2.5) and (2.11) into equation (2.4), the terms  $dp/dt$  and  $(1/A) \cdot (dA/dt)$  are eliminated and the following equation is found.

$$\frac{\delta V}{\delta x} + \left[ E_a^{-1} + \left( \frac{eE_p}{D} - \frac{p}{2} \right)^{-1} \right] \frac{dp}{dt} = 0 \quad (2.12)$$

In practice, the pressure  $p$  is usually much lower than the value  $eE_p/D$ . Thus, in most case equation (2.12) can be reduced to the following form:

$$\frac{\delta V}{\delta x} + \frac{1}{E_a} \left[ 1 + \frac{DE_a}{eE_p} \right] \frac{dp}{dt} = 0 \quad (2.13)$$

Finally, the propagation velocity of a fluid with low compressibility is considered, according to equation (2.14).

$$a^2 = \left( \frac{\rho}{E_a} + \frac{\rho D}{E_p e} \right)^{-1} \quad (2.14)$$

The continuity equation can then be written in its standard form:

$$\text{Continuity equation} \quad \frac{\delta p}{\delta t} + V \frac{\delta p}{\delta x} + \rho a^2 \frac{\delta V}{\delta x} = 0 \quad (2.15)$$

### 2.1.1.2 Momentum equation

The second law of Newton states that the acceleration of a system multiplied by its mass is equal to the sum of the forces applied to it. In the case of a control volume as seen in Figure 2.2 and by admitting a fluid with low compressibility and pipe's walls with low deformability, the application of the second law of Newton yields:

$$m \frac{dV}{dt} \frac{1}{dx} = \rho A \frac{dv}{dt} = \frac{\sum F_i}{dx} \quad (2.16)$$

The axial forces applied to the control volume include the pressures forces  $F_i = (pA)_i$  on the control sections, the resultant of the pressure applied to the walls  $F_p = (1/2)(p_1 + p_2)(A_1 - A_2)$ , the axial component of the gravity force  $F_g = \rho g A \sin(\theta) \Delta x$  with  $\theta$  the pipe slope and the friction force  $F_f = \tau_0 \pi D \Delta x$  where  $\tau_0$  is the shear stress between the fluid and the pipe walls. Those forces are illustrated in Figure 2.2.

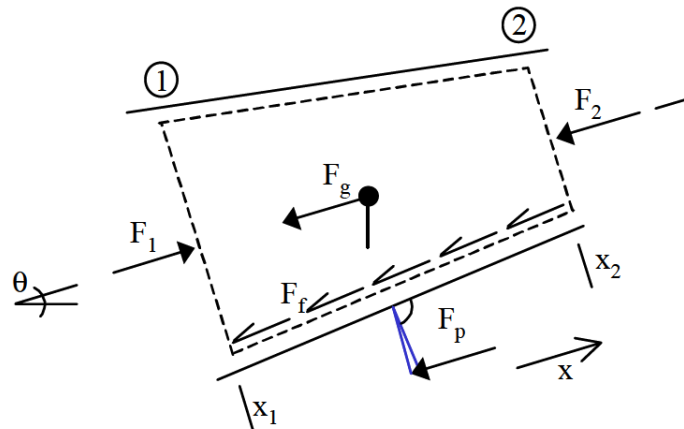


Figure 2.2. Axial forces applied to a control volume in a loaded pipe<sup>2</sup>

The forces sum applied to the control volume can then be written as following.

$$\sum F = p_1 A_1 - p_2 A_2 - \frac{1}{2} (p_1 + p_2) (A_1 - A_2) - \rho g A \sin(\theta) \Delta x - \tau_0 \pi D \Delta x \quad (2.17)$$

By dividing the equation by  $\Delta x$  and simplifying the terms, equation (2.19) is obtained.

$$\frac{\sum F}{\Delta x} = \frac{(p_1 - p_2)(A_1 + A_2)}{2\Delta x} - \rho g A \sin\theta - \tau_0 \pi D \quad (2.18)$$

<sup>2</sup> (Boillat & De Souza, 2004)

This equation is inserted into equation (2.14) and considering that  $\Delta x$  tends toward  $\delta x$ , it simplifies into equation (2.19).

$$\rho A \frac{dv}{dt} + A \frac{\delta p}{\delta x} + \rho g A \sin\theta + \tau_0 \pi D = 0 \quad (2.19)$$

The shear stress can be generally stated as:

$$\tau_0 = \frac{1}{4} \rho g D S_f \quad (2.20)$$

Where  $S_f$  is a dimensionless value called friction slope. It represents the resistance force per weight unit. By replacing  $\tau_0$  in equation (2.19), considering  $A = \pi D^2/4$  and applying (2.3) to  $dV/dt$ , the following equation is found.

$$\rho A \frac{\delta V}{\delta t} + \rho A V \frac{\delta V}{\delta x} + A \frac{\delta p}{\delta x} + \rho g A \sin\theta + \rho g A S_f = 0 \quad (2.21)$$

Finally, the momentum equation is deduced by dividing the previous equation by  $\rho A$ .

$$\text{Momentum equation} \quad \frac{\delta V}{\delta t} + V \frac{\delta V}{\delta x} + \frac{1}{\rho} \frac{\delta p}{\delta x} + g(\sin\theta + S_f) = 0 \quad (2.22)$$

### 2.1.1.3 Simplification

An unsteady gradually varied flow can be described by the continuity equation (2.23) and the momentum equation (2.24).

$$\frac{\delta p}{\delta t} + V \frac{\delta p}{\delta x} + \rho a^2 \frac{\delta V}{\delta x} = 0 \quad (2.23)$$

$$\frac{\delta V}{\delta t} + V \frac{\delta V}{\delta x} + \frac{1}{\rho} \frac{\delta p}{\delta x} + g(\sin\theta + S_f) = 0 \quad (2.24)$$

Those equations form the foundation of the computation of unsteady flows inside loaded pipes. The terms  $V(\delta p/\delta x)$ ,  $V(\delta V/\delta x)$  and  $\sin\theta$  can usually be deemed as negligible and be removed from the equations. The governing equations can then be written in the following simplified forms.

$$\frac{\delta p}{\delta t} + \rho a^2 \frac{\delta V}{\delta x} = 0 \quad (2.25)$$

$$\frac{\delta V}{\delta t} + \frac{1}{\rho} \frac{\delta p}{\delta x} + gS_f = 0 \quad (2.26)$$

The pressure  $p$  can be considered in terms of height by stating the hydraulic head  $h = p/\rho g + z$  with  $z$  the distance between the pipe's axe and a reference height. Then for a horizontal pipe, it can be stated that  $\delta p/\delta t = (\rho g) \cdot \delta h/\delta t$  and  $\delta p/\delta x = (\rho g) \cdot \delta h/\delta x$ . The water velocity inside the pipe  $V$  can be transformed in a discharge  $Q$  by multiplying it by the cross-section area  $A$ . It ensues that  $\delta V/\delta x = (1/A)(\delta Q/\delta x)$  and  $\delta V/\delta t = (1/A)(\delta Q/\delta t)$ . Finally, the friction slope  $S_f$  is expressed in equation (2.27) by using the Darcy-Weisbach formula  $\tau_0 = \frac{1}{8} \rho f V |V|$

$$S_f = \frac{fQ|Q|}{2gDA^2} \quad (2.27)$$

All those simplifications lead to the simplified equation of continuity (2.28) and momentum equation (2.29).

$$\rho g \frac{\delta h}{\delta t} + \frac{\rho a^2}{A} \frac{\delta Q}{\delta x} = 0 \quad (2.28)$$

$$\frac{1}{A} \frac{\delta Q}{\delta t} + g \frac{\delta h}{\delta x} + \frac{fQ|Q|}{2DA^2} = 0 \quad (2.29)$$

### 2.1.2 Method of characteristics

The governing equations, even in their simplified forms, pose a system of equations with partial derivations, making it complex to solve. It is then necessary to use numerical method of resolution such as the method of characteristics (MOC), the finite difference method or the finite element method, amongst others. The MOC is the most popular method and the one used in LVTrans. It offers the user a correct simulation of steep waves while being easy to program and fast to compute.

The MOC applied to the case of a loaded pipe is based on the simplified governing equations in the following form, where  $R = f/(2DA)$ .

$$L_1 = \frac{\delta Q}{\delta t} + gA \frac{\delta h}{\delta x} + RQ|Q| = 0 \quad (2.30)$$

$$L_2 = gA \frac{\delta h}{\delta t} + a^2 \frac{\delta Q}{\delta x} = 0 \quad (2.31)$$

A linear combination of the equations (2.30) and (2.31), as shown in (2.32), leads to equation (2.33).



$$\tilde{L} = L_1 + \lambda L_2 \quad (2.32)$$

$$\left(\frac{\delta Q}{\delta t} + \lambda a^2 \frac{\delta Q}{\delta x}\right) + \lambda g A \left(\frac{\delta h}{\delta t} + \frac{1}{\lambda} \frac{\delta h}{\delta x}\right) + RQ|Q| = 0 \quad (2.33)$$

The discharge  $Q$  and the hydraulic head  $h$  depend on the variables  $x$  and  $t$ , which means that, according to rule (2.3):

$$\frac{dQ}{dt} = \frac{\delta Q}{\delta t} + \frac{\delta Q}{\delta x} \frac{dx}{dt} \quad (2.34)$$

$$\frac{dh}{dt} = \frac{\delta h}{\delta t} + \frac{\delta h}{\delta x} \frac{dx}{dt} \quad (2.35)$$

By stating that  $\lambda a^2 = 1/\lambda = dx/dt$ , which means that:

$$\lambda = \pm \frac{1}{a} \quad (2.36)$$

Then, if  $dx/dt = +a$  equation (2.33) can be written:

$$\frac{dQ}{dt} + \frac{1}{a} g A \frac{dh}{dt} + RQ|Q| = 0 \quad (2.37)$$

And if  $dx/dt = -a$ :

$$\frac{dQ}{dt} - \frac{1}{a} g A \frac{dh}{dt} + RQ|Q| = 0 \quad (2.38)$$

By using the MOC, the initial system of equations (2.30) and (2.31) involving partial derivatives is converted in a system of equation (2.37) and (2.38) with only ordinary derivatives. However, those equations are only valid if their corresponding condition  $dx/dt = \pm a$  is valid. The lines in the plane ( $x - t$ ) in which those conditions are fulfilled are called characteristic lines. An illustration of those lines is presented in Figure 2.1.

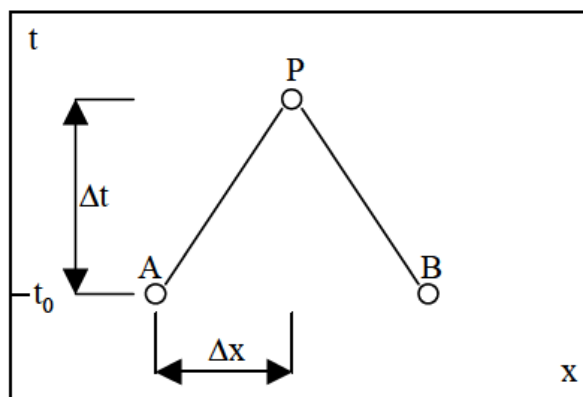


Figure 2.3. Characteristic lines AP et BP

The point  $P$  is placed on the plane  $(x - t)$  so that  $\Delta x_{AP} = a\Delta t_{AP}$ , with  $\Delta x_{AP}$  and  $\Delta t_{AP}$  the difference between the coordinates of the starting point  $A$  and  $P$ . Then, the line going from  $A$  to  $P$  is a characteristic line, since it satisfies the criteria  $dx/dt = a$ . The equation (2.37) is valid on this line. In the same way, if the point  $B$  is placed so that  $\Delta x_{PB} = -a\Delta t_{PB}$ , then the line going from  $P$  to  $B$  is a characteristic line satisfying the criteria  $dx/dt = -a$ . The equation (2.38) is valid on this line.

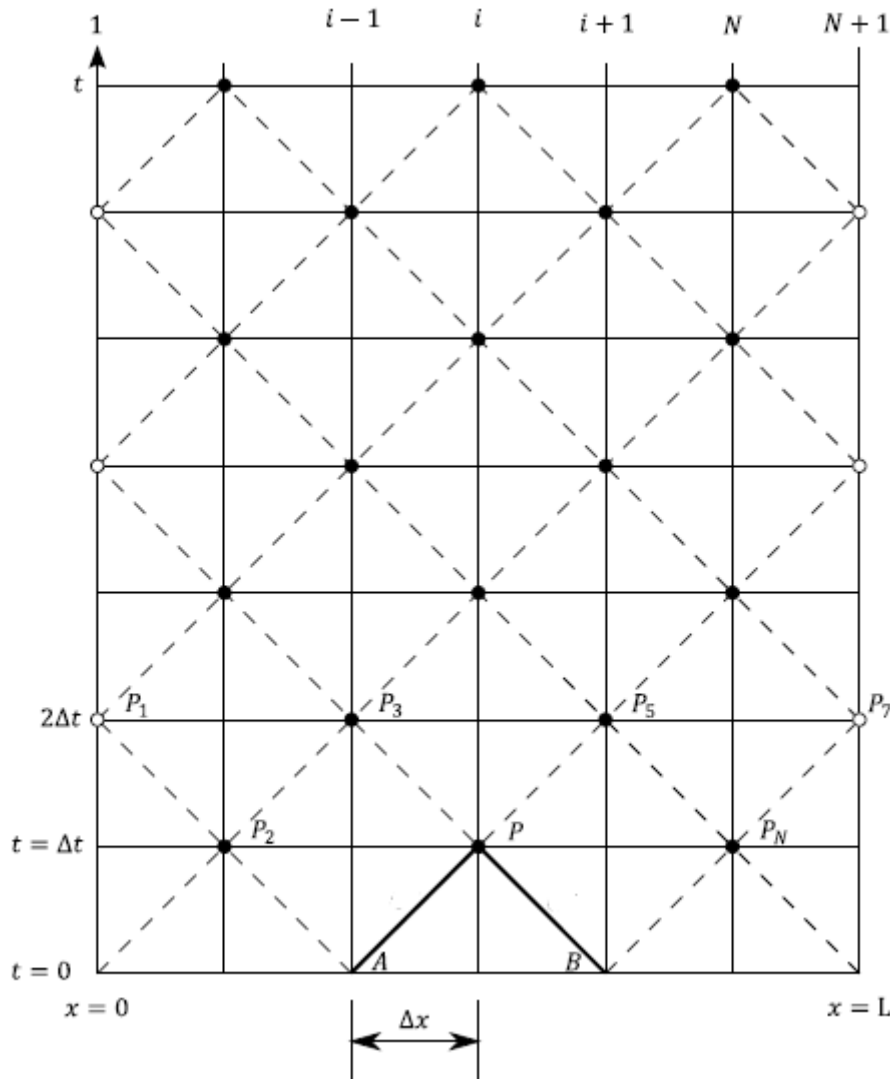


Figure 2.4. Characteristic lines used in the solving of a loaded pipe problem

The concept can be applied to a loaded pipe by dividing it into  $N$  parts with length  $\Delta x$ . The time step is then chosen as  $\Delta t = \Delta x/a$ . Figure 2.4 illustrates the division of the plane  $(x - t)$  according to the characteristic lines in the case of a pipe with length  $L$ . The lines  $AP$  and  $PB$  represent the lines where respectively equation (2.37) and equation (2.38) are valid. Then, if the values of  $h$  and  $Q$  are known at points  $A$  and  $B$ , it is possible to find the solution at point  $P$  by

integrating equation (2.37) along the line  $AP$  and equation (2.38) along the line  $PB$ . The integration along the line  $AP$  can be written:

$$\int_A^P dH + \frac{a}{gA} \int_A^P dQ + \frac{R}{gA} \int_A^P Q|Q|dx = 0 \quad (2.39)$$

The latter term in the previous equation can't be solved as it is, as the discharge at point  $P$  is unknown. An approximation by the trapezoidal rule is done to solve the integral. When solving this integral and the integral of equation (2.38) from  $P$  to  $B$ , the following equations are found.

$$\text{AP: } h_P - h_A + \frac{a}{gA} (Q_P - Q_A) + \frac{R}{gA} \Delta x Q_P |Q_A| = 0 \quad (2.40)$$

$$\text{PB: } h_P - h_B - \frac{a}{gA} (Q_P - Q_B) - \frac{R}{gA} \Delta x Q_P |Q_B| = 0 \quad (2.41)$$

This system of two equations with two unknown variables can be simplified as:

$$\text{AP: } h_P = h_A - B(Q_P - Q_A) - R^* Q_P |Q_A| \quad (2.42)$$

$$\text{PB: } h_P = h_B + B(Q_P - Q_B) + R^* Q_P |Q_B| \quad (2.43)$$

With  $B$  and  $R^*$ :

$$B = \frac{a}{gA} \quad (2.44)$$

$$R^* = R \frac{\Delta x}{gA} \quad (2.45)$$

The indexes  $A$ ,  $P$  and  $B$  are generalized into  $i - 1$ ,  $i$  and  $i + 1$ . Equations (2.42) and (2.43) can then be written in the simplified form:

$$\text{AP: } h_i = C_P - B_P Q_i \quad (2.46)$$

$$\text{BP: } h_i = C_M - B_M Q_i \quad (2.47)$$

With coefficients  $C_P$  and  $C_M$  as following:

$$C_{P/M} = h_{i\mp 1} \pm B Q_{i\mp 1} \quad (2.48)$$

And coefficients  $B_P$  and  $B_M$ :

$$B_P = B + R|Q_{i\mp 1}| \quad (2.49)$$

Finally, the solution of the system of two equations with two unknowns is displayed in equations (2.50) and (2.51).

$$h_i = \frac{C_P B_M + C_M B_P}{B_P + B_M} \quad (2.50)$$

$$Q_i = \frac{C_P - C_M}{B_P + B_M} \quad (2.51)$$

The hydraulic heads and the discharges along the pipe can then be deduced by using the values found at the previous time step and the boundary conditions, as illustrated in (▲)

Upstream boundary condition (▼) Downstream boundary condition  
 (■) Initial conditions (○) Computation point

Figure 2.5.

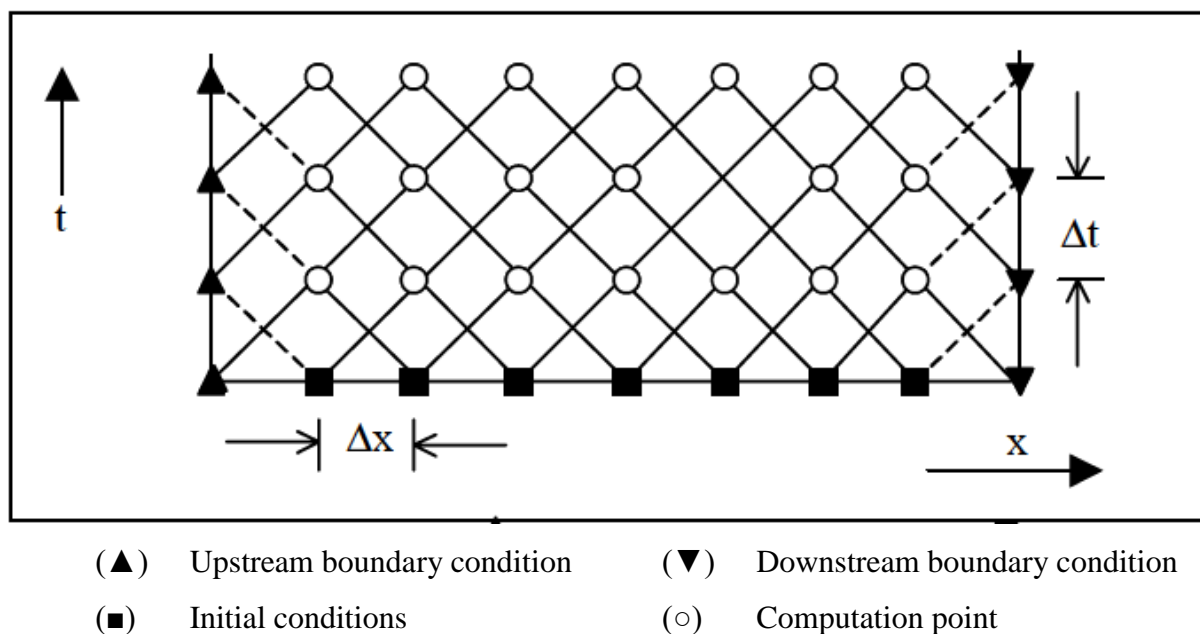


Figure 2.5. Solving of a pipe problem using the MOC

### 2.1.3 Hydraulic losses

When flowing, the water inevitably loses energy by rubbing against rough material or by forming turbulent zones resulting in energy dissipation. To simplify their computation in a hydraulic system, the head losses are divided into two types: the friction losses spread all along a pipe's length and the singular losses related to a sudden modification of the pipe.

### 2.1.3.1 Friction losses

The friction of the water against the pipe's walls creates head losses spread all along the pipe's length. To estimate them, one can use the Darcy-Weisbach equation (2.52) which introduces a head loss coefficient  $f$  dependent on the walls roughness and the flow regime.

$$\Delta H = f \frac{L}{D} \frac{v^2}{2g} \quad (2.52)$$

In the case of a laminar flow, the head loss coefficient  $f$  is independent of the walls roughness and can be computed by using the Reynolds number  $Re = vD/\nu$ , with  $\nu$  the kinematic viscosity of the fluid. For a circular pipe, the head loss coefficient is estimated as:

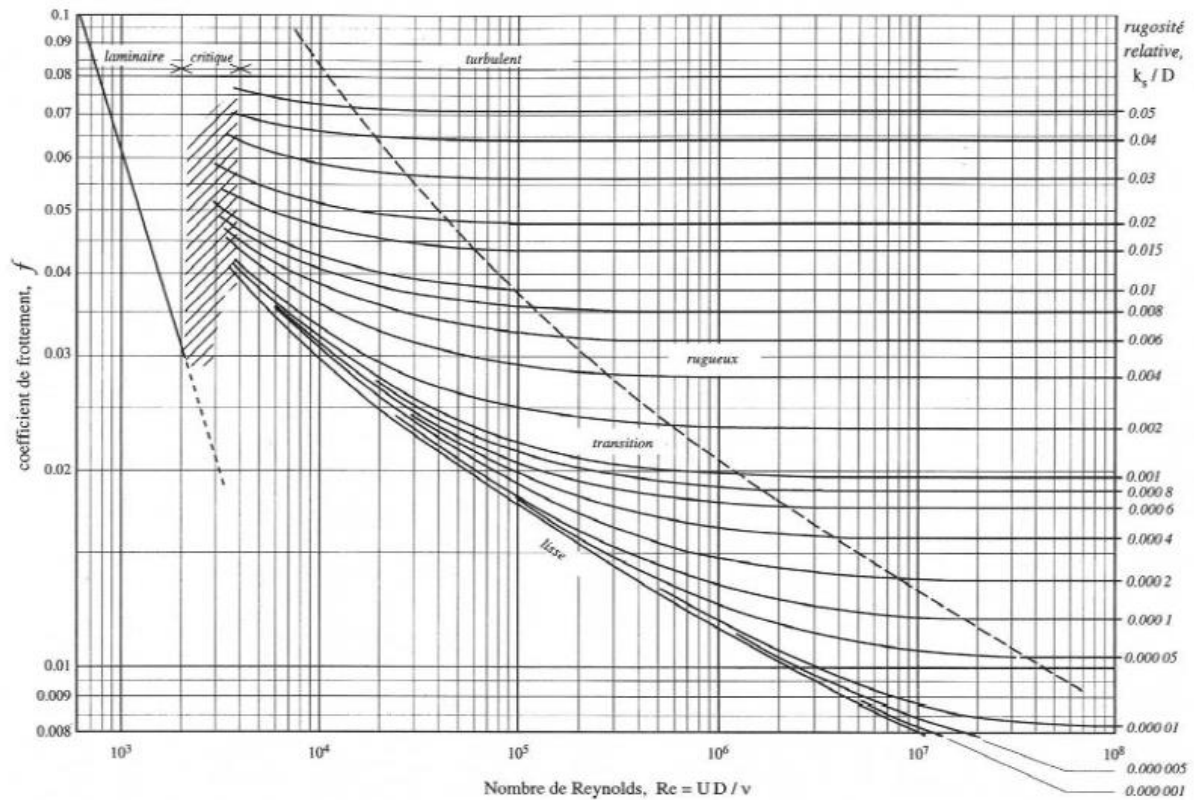
$$f = \frac{64}{Re} \quad (2.53)$$

In the case of a turbulent flow, it's common to use the Colebrook formula (2.54) in the case of circular pipes.

$$\frac{1}{\sqrt{f}} = -0.91 \ln \left( 0.27 \frac{k_s}{2R} + \frac{2.51}{\sqrt{f} Re} \right) \quad (2.54)$$

where:  $k_s$  [m]      Roughness of the pipe's walls  
 $R$  [m]      Pipe radius

Another way to estimate the head loss coefficient for both laminar and turbulent flows is by using the Moody diagram shown in Figure 2.6. The diagram is based on experimental data and reproduces equation (2.53) in its laminar part.

Figure 2.6. Moody diagram<sup>3</sup>

### 2.1.3.2 Singular losses

Singular losses represent the energy losses caused by a sudden modification in the pipe. It can be a change in the cross-section or direction of the pipe, or the entry of the flow in a reservoir, or its exit, amongst other possible causes.

The singular losses are usually estimated by using the general form:

$$\Delta H_s = \zeta \frac{v^2}{2g} \quad (2.55)$$

Where  $\zeta$  is the singular head loss coefficient. Its computation depends on the nature of the modification in the pipe causing the singular loss.

In the case of a sudden expansion of the cross-section, the water velocity used to estimate the singular loss is the upstream one  $v_1$ . The computation of the singular loss coefficient is different if the flow regime is laminar (2.57) or turbulent (2.58). The entry of water in a reservoir is computed by taking  $A_2 \rightarrow \infty$ .

<sup>3</sup> (Ancy, 2014)

$$\Delta H_s = \zeta \frac{v_1^2}{2g} \quad (2.56)$$

Laminar

$$\zeta = 2 - \frac{8 A_1}{3 A_2} + \frac{2 A_1^2}{3 A_2^2} \quad (2.57)$$

Turbulent

$$\zeta = \left(1 - \frac{A_1}{A_2}\right)^2 \quad (2.58)$$

In the case of a sudden constriction of the cross-section, the water velocity used to estimate the singular loss is the downstream one  $v_2$ . The computation of the singular loss coefficient for a turbulent flow is presented in equation (2.60). The coefficient takes the value  $\zeta = 0.5$  for water exiting a reservoir.

$$\Delta H_s = \zeta \frac{v_2^2}{2g} \quad (2.59)$$

$$\zeta = \left(1 - \frac{1}{0.59 + 0.41 \left(\frac{A_2}{A_1}\right)^3}\right)^2 \quad (2.60)$$

In the case of a sudden direction change, the head loss coefficient is computed with the Weissbach formula (2.61). The change of direction  $\theta$  is expressed in degree and  $R_c$  represents the radius of curvature.

$$\zeta = \frac{\theta}{90} \left(0.13 + 1.85 \left(\frac{R}{R_c}\right)^{\frac{7}{2}}\right) \quad (2.61)$$

If the change in direction is sudden, without radius of curvature, then the head loss coefficient can be estimated with the formula (2.62).

$$\zeta = \sin^2 \frac{\theta}{2} + 2 \sin^4 \frac{\theta}{2} \quad (2.62)$$

### 2.1.3.3 Hydraulic losses in LVTrans

In LVTrans, each object computes its head losses for each time step. Both types of losses are implemented in the software but some objects sometimes only consider one. For example, the “Pipe” objects only compute the friction losses and not the singular ones. For each object calculating the friction losses, the head loss coefficient  $f$  found in equation (2.52) must be

implemented in its parameters. The objects computing singular losses use another coefficient  $C_v$  which can be related to the coefficient  $\zeta$  in equation (2.55) by the following relation:

$$C_v [m^5/s^2] = \frac{Q^2}{2\Delta H_s} = \frac{A^2 g}{\zeta} \quad (2.63)$$

Two coefficients  $C_v$  must be implemented in the objects, one for each flow direction. This way, it is possible to simulate asymmetrical losses.

## 2.2 Theory related to the surge tank

In the case of high head power plants, it is common practice to use surge tanks to control the pressure transients induced by the regulation of the turbine discharge. By creating a water table closer to the turbine, the surge tank serves as an intermediate reservoir. The amount of water having to be accelerated or decelerated when opening or closing the turbines is then reduced, which improves the response time of the system. The surge tank also diminishes the maximum pressure reached in the waterway by reflecting the water hammer, a wave of pressure induced by a fast alteration of the discharge. However, the implementation of a surge tank creates mass oscillations between itself and the reservoir.

### 2.2.1 Design criteria of the surge tank

According to (Nabi, Habib-ur-Rehman, Kashif, & Tariq, 2011), the design of a surge tank relies on three criteria. Firstly, the location of the surge tank must be chosen so that the pressure variations caused by the water hammer are kept within reasonable limits. Secondly, the oscillations resulting from the discharge regulation at the turbine must be naturally dampened and must not be sustained or amplified. In other words, the surge tank must be stable. Lastly, the design of the surge tank must be chosen so that the water table is kept within its boundaries in any circumstances. The maximum upsurge should be contained unless a spillway is provided and the lowest down surge shouldn't allow air to enter the tunnel.

These criteria must be fulfilled while finding the best economical solution.

### 2.2.2 Water hammer

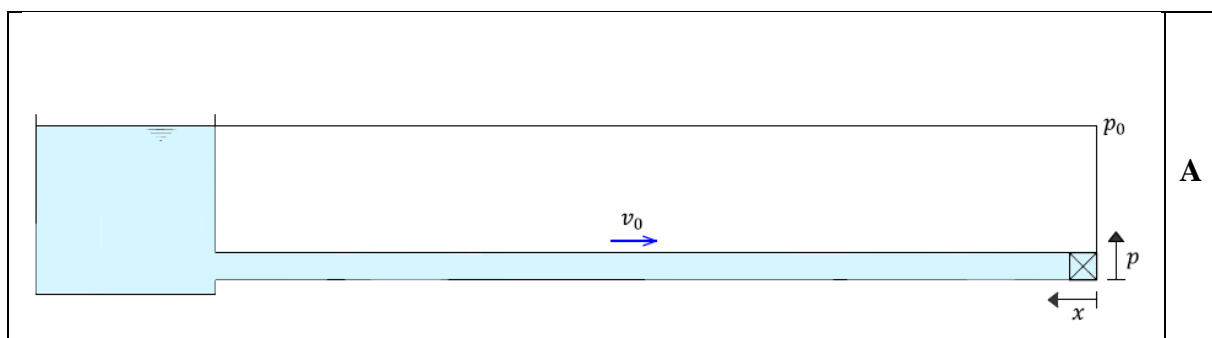
A fast alteration of the discharge in a loaded system creates the propagation of a wave of pressure inside the pipe. This phenomenon is called water hammer. In the case of a powerplant, the water hammer propagates from the turbine to the closest water table, generally the surge tank.



### 2.2.2.1 Concept

To illustrate the concept of the water hammer, a simple case is presented in Figure 2.7. A reservoir is linked directly to a valve by a single pipe and the hydraulic losses are deemed negligible. The water is initially flowing through the valve with a velocity  $v_0$ , with a pressure  $p_0$ , as seen in Figure 2.7.A. The instantaneous closing of the valve, illustrated in Figure 2.7.B, causes the water velocity to drop to zero directly upstream the valve. A wave of increased pressure then propagates with the wave speed velocity  $a$  toward the reservoir. The total pressure is then increased to  $p_0 + \Delta p$ . The water upstream the front of this wave is still flowing with a velocity  $v_0$  while the water downstream the front of the wave is still. The front of the wave reaches the reservoir after a time  $t = L/a$  with  $L$  being the length of the pipe. At this point, illustrated in Figure 2.7.C, all the water is still and the pressure inside the whole pipe is equal to  $p_0 + \Delta p$ . The pressure wave is then reflected by the reservoir and goes back to the valve with an opposite sign, as shown in Figure 2.7.D. The pressure inside the pipe goes back to  $p_0$  and the water flows toward the reservoir with a velocity  $v_0$ . When the front of the wave reaches the valve at time  $t = 2L/a$ , as illustrated in Figure 2.7.E, the water velocity inside the pipe is of  $-v_0$  and the pressure  $p_0$ . This induces a wave of reduced pressure  $p_0 - \Delta p$ , seen in Figure 2.7.F, propagating toward the reservoir and the velocity going back to zero downstream the front of this wave. The wave is then reflected when reaching the reservoir at time  $t = 3L/a$  and the water velocity gradually goes back to  $v_0$  with a pressure  $p_0$ . At time  $t = 4L/a$ , the entire system is similar to the initial situation, described in Figure 2.7.A, and the cycle is complete and ready to repeat itself.

In a theoretical system in which the head losses would be inexistent, this cycle could repeat itself infinitely. However, in reality the amplitude of the pressure oscillation  $\Delta p$  is damped by the head losses until it becomes negligible.



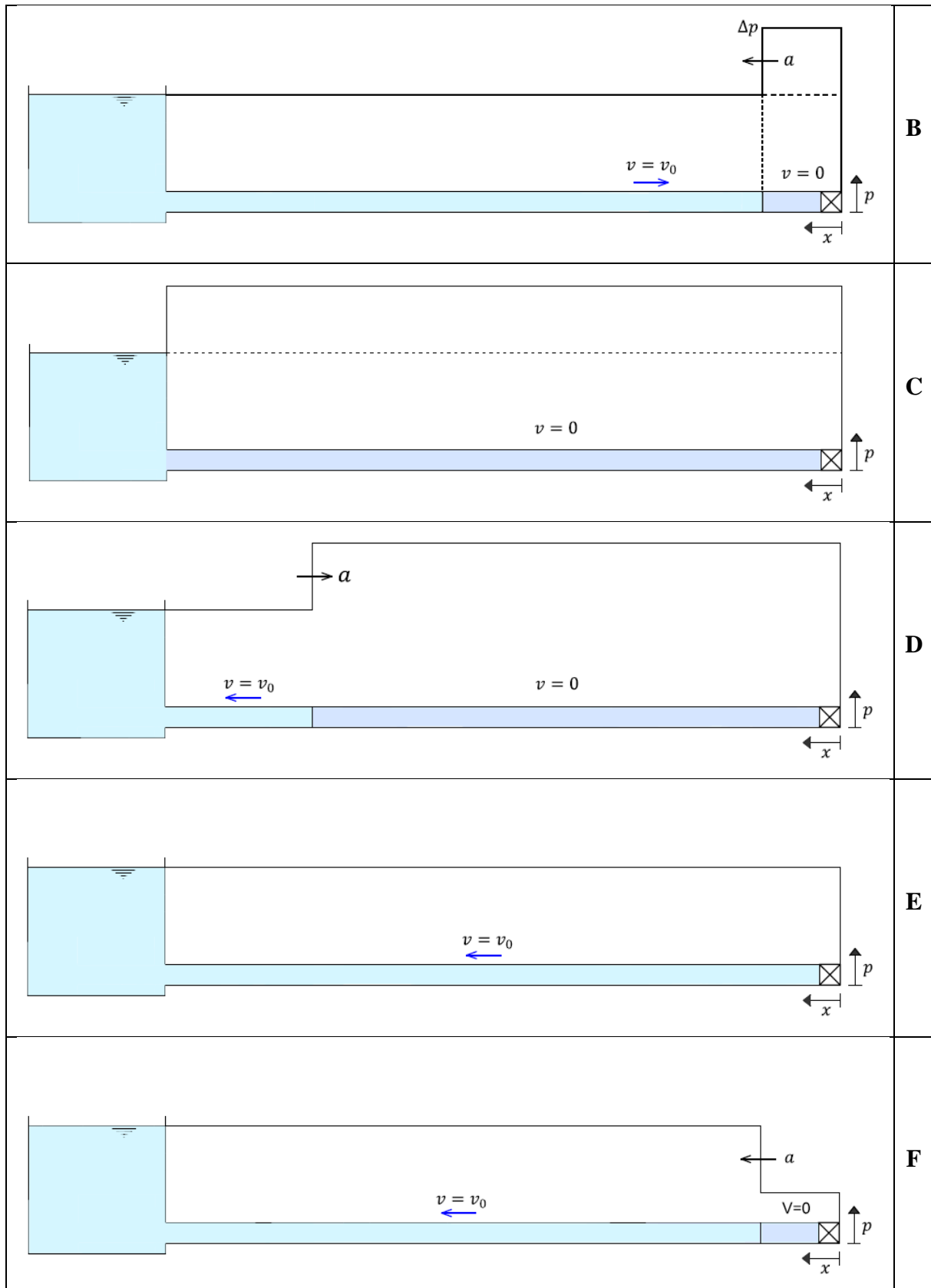


Figure 2.7. Water hammer concept

### 2.2.2.2 Calculation of the wave celerity

The wave celerity of the water hammer can be computed from the continuity equation, in which is included the pipe's dilatation and the water compressibility. In the case of a pipe put under pressure as a result of the closing of a valve, the continuity equation can be written as following (2.64). The pipe's walls are deemed thin and their dilatation is estimated according to equation (2.65). Finally, it is admitted that the wave celerity is significantly higher than the water's speed inside the pipe. Without this hypothesis, the water hammer celerity should be viewed as equal to  $a - v$ .

$$\text{Continuity equation} \quad \Delta v \cdot A \cdot \Delta t = \frac{\Delta p}{\rho_w \cdot a} \cdot \frac{\pi \cdot D^2}{4} \cdot \Delta t = \Delta Y_P + \Delta Y_W \quad (2.64)$$

$$\text{Pipe dilatation} \quad \Delta Y_P = \frac{\Delta p}{E_P} \cdot \frac{1}{e} \cdot \frac{D^3}{4} \cdot \pi \cdot a \cdot \Delta t \quad (2.65)$$

$$\text{Water compressibility} \quad \Delta Y_W = \frac{\Delta p}{E_W} \cdot a \cdot \Delta t \cdot \frac{D^2}{4} \cdot \pi \quad (2.66)$$

where:	$v$ [m/s]	Mean velocity of the water inside the pipe
	$A$ [m <sup>2</sup> ]	Section area
	$D$ [m]	Pipe diameter
	$E_P$ [N/m <sup>2</sup> ]	Pipe elasticity modulus ( $2.1 \cdot 10^{11}$ N/m <sup>2</sup> for steel)
	$E_W$ [N/m <sup>2</sup> ]	Water elasticity modulus ( $2 \cdot 10^9$ N/m <sup>2</sup> )
	$e$ [m]	Pipe's walls thickness
	$\Delta p$ [Pa]	Pressure added by the water hammer
	$a$ [m/s <sup>2</sup> ]	Wave celerity

By combining equations (2.64), (2.65) and (2.66), the wave celerity (2.67) is deduced:

$$a = \sqrt{\frac{1}{\rho_e} \cdot \left( \frac{1}{\frac{D}{e \cdot E_T} + \frac{1}{E_E}} \right)} \quad (2.67)$$

### 2.2.2.3 Instantaneous closing of the valve

Italian engineer Lorenzo Allievi was one of the first scientific working on the mathematical description of the water hammer phenomenon. He developed two differential equations characterizing the pressure wave, based on the conservation of momentum (2.68) and on the continuity equation (2.69). Head losses are deemed negligible which allows the momentum equation to be used.

$$\frac{\delta v}{\delta t} + g \cdot \frac{\delta h}{\delta x} = 0 \quad (2.68)$$

$$\frac{\delta v}{\delta x} + \frac{g}{a^2} \cdot \frac{\delta h}{\delta t} = 0 \quad (2.69)$$

where:  $h = \frac{p}{\rho \cdot g}$  [m] Hydraulic head

Allievis equations (2.70) and (2.71) propose general solutions for the set of equations (2.68) and (2.69).

$$h = h_0 + F\left(t - \frac{x}{a}\right) + f\left(t + \frac{x}{a}\right) \quad (2.70)$$

$$v = v_0 + \frac{g}{a} \cdot \left[ F\left(t - \frac{x}{a}\right) - f\left(t + \frac{x}{a}\right) \right] \quad (2.71)$$

where: F and f Mathematical functions defined by the initial and boundary conditions. They describe two waves going through the pipe in opposite directions, with the same velocity a. Their expression depends on the opening or closing conditions of the valve.

$h_0$  [m] Initial head (in steady state)

$U_0$  [m/s] Initial velocity (in steady state)

In the specific case of the instantaneous closing of the valve, Joukowski-Allievi equation (2.72) gives a maximal head:

$$h_{max} = h_0 + \frac{a \cdot U_0}{g} \quad (2.72)$$

where:  $h_{max}$  [m] Maximal hydraulic head reached at the valve

The water velocity in the section oscillates between  $v_0$  and  $-v_0$ .

### 2.2.2.4 Non-instantaneous closing of the valve

In the case of a non-instantaneous closing of the valve, the front of the wave becomes tilted and not vertical as in an instantaneous closing. The pressure increases gradually in the pipe until the maximal value is reached.

To simplify the comprehension of the phenomena observed in a non-instantaneous closing of the valve, the case of a linear closing is studied. It can be seen as an instantaneous closing carried out in small steps. The pressure increases linearly in the pipe and reaches its maximal value at the valve level at time  $t = 2L/a$ . If the valve is completely closed at this time, that is if  $2L/a < t_v$  with  $t_v$  the closing time, then the maximal pressure can be estimated in the same way as in an instantaneous closing case. However, if the pipe length is too short, as illustrated in Figure 2.8, then the total pressure at the valve level is reduced by the negative pressure reflected by the reservoir.

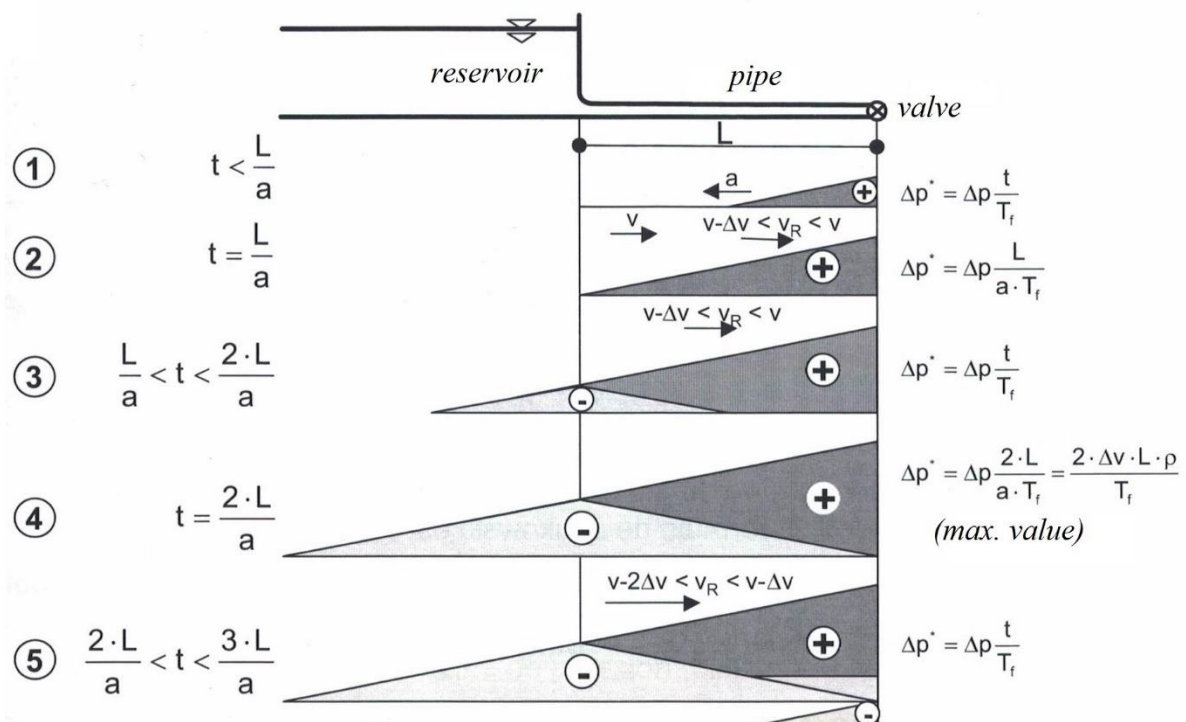


Figure 2.8. Water hammer oscillation with a linear closing of the valve

By taking into account this phenomenon, Michaud estimates a maximal pressure at the valve level for a linear closing as defined in the following equation (2.73).

$$p_{max} = p_0 + \frac{2 \cdot \Delta U \cdot L}{g \cdot t_v} \quad (2.73)$$

### 2.2.3 Mass oscillation

The implementation of a surge tank between the reservoir and the turbine, while useful in some aspects, creates mass oscillations between the reservoir and the surge tank resulting in the oscillation of the water table inside the latter. The amplitude of those oscillations should be carefully studied to avoid the water table to cross the boundaries of the surge tank.

#### 2.2.3.1 Concept

When opening or closing the turbines, the surge tank respectively provides or absorbs the needed water which make the water table drop or rise. This phenomenon creates a difference in potential energy between the surge tank and the reservoir, inducing a movement of the water table in the opposite direction. A water oscillation between the reservoir and the surge tank is then created. It is dissipated through hydraulic losses due to friction or singular losses.

Two oscillating pressure waves can then be observed in the penstock between the turbine and the surge tank. The first one, with a rather short period, comes directly from the water hammer which is reflected between the surge tank's water table and the turbine. The second one, with a longer period reaching several minutes, is induced by the oscillation of the water table inside the surge tank, making the pressure oscillate. The water hammer is almost imperceptible in the waterway connecting the reservoir to the surge tank because of the protection offered by the latter. Only the oscillation of the water table is perceived in this area.

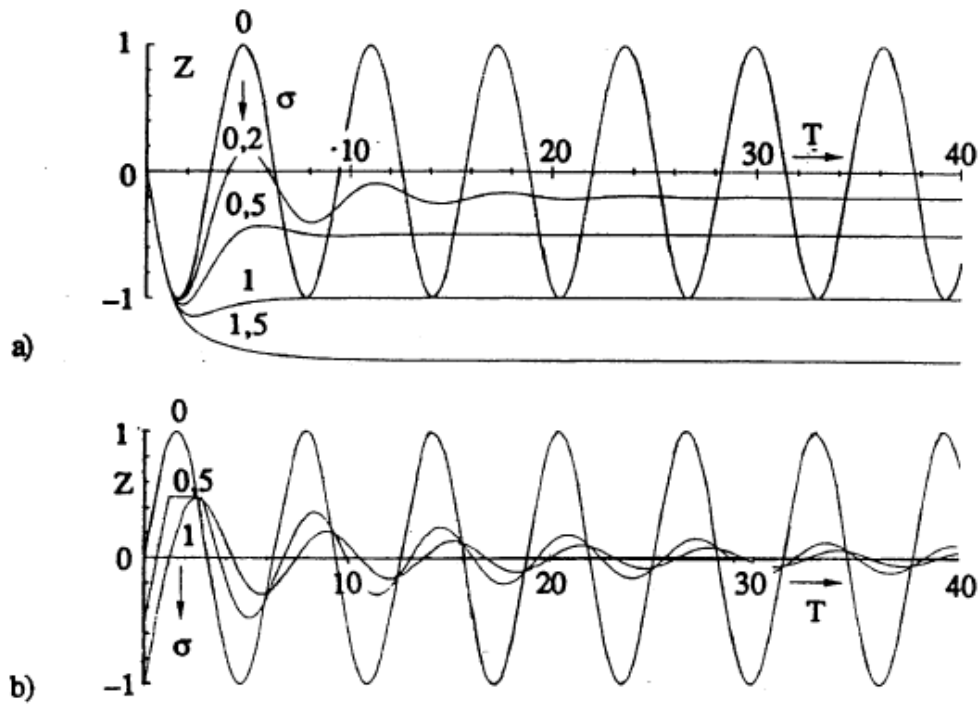


Figure 2.9. Mass oscillations depending on the friction characteristic  $\sigma$  for an a) Instantaneous opening b) Instantaneous closing of the valve

The amplitude and the dampening of the mass oscillations depend on how important the discharge alteration resulting in the water hammer is, but also on the type of surge tank implemented and its characteristics. The head losses between the reservoir and the surge tank are also essential in the estimation of the oscillations dampening. Figure 2.9 illustrates the oscillations evolution depending on the parameter  $\sigma$  representing the friction effect according to equation (2.76). The oscillations evolution is represented by using the dimensionless water level coordinates inside the surge tank  $Z$  (2.74) as vertical axis and the dimensionless time  $T$  (2.75) as horizontal axis.

$$Z = \frac{1}{v_{ww,0}} \cdot \left( \frac{g}{L} \cdot \frac{A_{st}}{A_{ww}} \right)^{\frac{1}{2}} \quad (2.74)$$

$$T = \left( \frac{g}{L_{ww}} \cdot \frac{A_{ww}}{A_c} \right)^{\frac{1}{2}} \quad (2.75)$$

$$\sigma = \frac{v_0}{v^*} \cdot \left( \frac{g \cdot L \cdot A_{st}}{A_{ww} \cdot v^{*2}} \right)^{\frac{1}{2}} \quad (2.76)$$

$$v^* = \bar{K} \cdot R_h^{\frac{2}{3}} \quad (2.77)$$

where: $v_{ww,0}$ [m/s]	Initial water velocity in the waterway
$L_{ww}$ [m]	Waterway length
$A_{st}$ [m <sup>2</sup> ]	Surge tank cross-section area
$A_{ww}$ [m <sup>2</sup> ]	Waterway cross-section area
$\bar{K}$ [m <sup>1/3</sup> /s]	Equivalent rugosity between the reservoir and the surge tank (includes friction and singular losses)

### 2.2.3.2 Amplitude

The calculation of the amplitude of the water table oscillations inside the surge tank is based on two fundamental equations, the momentum equation and the continuity equation.

#### 2.2.3.2.1 Momentum equation

The momentum equation is based on the analysis of the forces equilibrium in the waterway, between the reservoir and the surge tank, as represented in Figure 2.10.

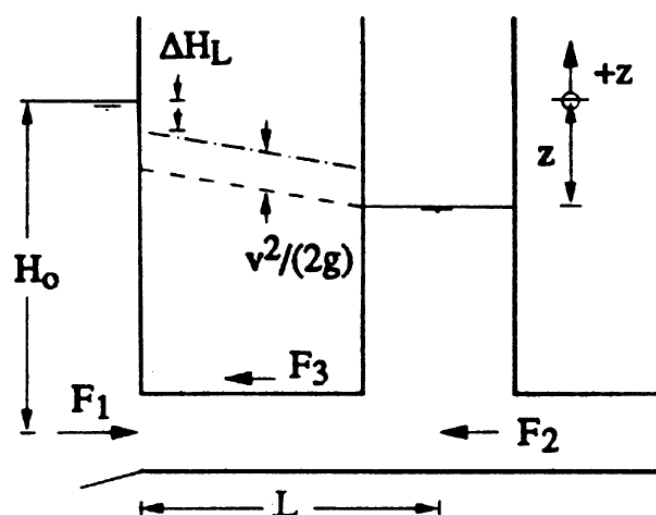


Figure 2.10. Forces inside the waterway of an hydro-power plant

Three forces are at play in the system. The first one represented in equation (2.78) is due to the water load in the reservoir. The second one, corresponding to equation (2.79), is due to the water load in the surge tank. The last one represents the friction force in the pipe and corresponds to equation (2.80).

$$F_1 = \rho \cdot g \cdot A_{ww} \cdot \left( H_0 - \Delta H_S - \frac{v_{ww}^2}{2 \cdot g} \right) \quad (2.78)$$

$$F_2 = \rho \cdot g \cdot A_{ww} \cdot (H_0 + z) \quad (2.79)$$



$$F_3 = \rho \cdot g \cdot A_{ww} \cdot \Delta H_F \quad (2.80)$$

where: $H_0$ [m]	Water height in the reservoir
$\Delta H_S$ [m]	Singular head loss at the pipe entrance
$v_{ww}$ [m/s]	Water velocity in the waterway
$z$ [m]	Height difference between the water level in the surge tank and the water level in the reservoir. $z$ is negative when the water level in the surge tank is below the water level in the reservoir.
$\Delta H_F$ [m]	Friction head loss in the pipe

Newton's second law states that the sum of the outside forces applied to a system is equal to the mass multiplied by the acceleration. If the waterway is taken as the system, then the sum of the outside forces (2.81) is found by subtracting  $F_2$  and  $F_3$  from  $F_1$ . The other member of the Newton's equation can be expressed as shown in equation (2.82).

$$\sum F_i = -\rho \cdot g \cdot A_{ww} \cdot \left( z + \Delta H_S + \Delta H_F + \frac{v_{ww}^2}{2 \cdot g} \right) \quad (2.81)$$

$$m \cdot a_{ww} = \rho \cdot A_{ww} \cdot L_{ww} \cdot \frac{dv_{ww}}{dt} \quad (2.82)$$

where:  $a_{ww}$  [m/s<sup>2</sup>] Water acceleration in the waterway

By combining the equations (2.81) and (2.82), the Newton's equation applied to the waterway (2.83) is deduced. The friction losses are estimated according to the Manning Strickler formula while the singular losses are expressed using equation (2.84). The equation (2.85) is then deduced, considering an equivalent rugosity  $\bar{K}$  according to equation (2.86).

$$\frac{dv_{ww}}{dt} + \frac{g}{L_{ww}} \cdot \left( z + \frac{v_{ww}^2}{2 \cdot g} + \Delta H \right) = 0 \quad (2.83)$$

$$\Delta H_S = \sum \zeta_i \cdot \frac{v_{vv}^2}{2g} \quad (2.84)$$

$$\frac{v_{ww}^2}{2 \cdot g} + \Delta H = \frac{v_{ww}^2}{2g} + \sum \zeta_i \cdot \frac{v_{ww}^2}{2g} + \frac{v_{ww}^2 \cdot L_{ww}}{K^2 \cdot R_h^{\frac{4}{3}}} = \frac{v_{ww}^2 \cdot L_{ww}}{\bar{K}^2 \cdot R_h^{\frac{4}{3}}} \quad (2.85)$$

$$\frac{1}{\bar{K}^2} = \frac{1}{K^2} + \frac{R_h^{\frac{4}{3}}}{2g \cdot L_{ww}} \cdot \left( 1 + \sum \zeta_i \right) \quad (2.86)$$

$$S_f = \frac{v_{ww} \cdot |U_{ww}|}{\bar{K}^2 \cdot R_h^{\frac{4}{3}}} \quad (2.87)$$

where: $\Delta H$ [m]	$= \Delta H_F + \Delta H_S$	Total head loss in the waterway
$\zeta_i$ [-]		Head loss coefficient
$K$ [ $m^{\frac{1}{3}}/s$ ]		Strickler rugosity coefficient
$R_h$ [m]		Hydraulic radius in the waterway

Finally, by combining the equations (2.83), (2.85) and (2.87), the latter being the friction slope, the momentum equation (2.88) is deduced. The analysis of the oscillations inside the surge tank is based partly on this equation.

$$\text{Momentum equation} \quad \frac{L_{ww}}{g} \cdot \frac{dv_{ww}}{dt} + z + S_f \cdot L_{ww} = 0 \quad (2.88)$$

### 2.2.3.2.2 Continuity equation

The continuity principle states that the discharge exiting the waterway must be equal to the sum of the discharges entering the surge tank and the penstock leading to the turbine. The water velocity in the surge tank is equated to the variation of  $z$ , the height difference between the water level in the surge tank and the water level in the reservoir, over time. The continuity equation can then be expressed as shown in equation (2.89).

$$\text{Continuity equation} \quad v_{ww} \cdot A_{ww} = \frac{dz}{dt} \cdot A_{st} + Q_{ps} \quad (2.89)$$

where:  $Q_{ps}$  [ $m^3/s$ ] Water discharge in the penstock

### 2.2.3.2.3 Maximal amplitude of the oscillations

The momentum equation (2.88) and continuity equation (2.89) are combined in equation (2.90).

$$\frac{L}{g \cdot a} \cdot \frac{d}{dt} \left( A_c \cdot \frac{dz}{dt} + Q_{cf} \right) + z + L + S_f = 0 \quad (2.90)$$

This second order differential equation can be solved for specific cases of opening and closing of the valve by defining initial conditions for  $z$  and  $dz/dt$ . The friction effect  $\sigma$  (2.76), the dimensionless water level coordinates inside the surge tank  $Z$  (2.74) and the dimensionless time  $T$  (2.75) are used to describe the behaviour of the water in different situations. Finally, the variables  $Z'$ ,  $Z''$  and  $\tau$  are defined as following.

$$Z' = \frac{dZ}{dT} \quad (2.91)$$

$$Z'' = \frac{d^2Z}{dT^2} \quad (2.92)$$

$$\tau = \left( \frac{g \cdot A_{ww}}{L_{ww} \cdot A_{st}} \right)^{\frac{1}{2}} \cdot t_v \quad (2.93)$$

where:  $t_v$  [s] Closing or opening time of the valve

Using these variables, several opening and closing cases can then be described by the following equations.

$$\text{Instantaneous opening} \quad Z'' + \sigma(Z' + 1)|Z' + 1| + Z = 0 \quad (2.94)$$

$$\text{Instantaneous closing} \quad Z'' + \sigma \cdot Z'|Z'| + Z = 0 \quad (2.95)$$

$$\text{Gradual opening} \quad Z'' + \sigma \left( Z' + \frac{T}{\tau} \right) \left| Z' + \frac{1}{\tau} \right| + Z + \frac{1}{\tau} = 0 \quad (2.96)$$

$$\text{Gradual closing} \quad Z'' + \sigma \left( Z' + 1 - \frac{T}{\tau} \right) \left| Z' + 1 - \frac{1}{\tau} \right| + Z - \frac{1}{\tau} = 0 \quad (2.97)$$

The maximal amplitude of the oscillations can then be expressed depending on the friction effect and the closing or opening time of the valve. The maximal and minimal dimensionless height in the surge tank in several cases of opening and closing of the valve are displayed in Figure 2.11 and Figure 2.12.

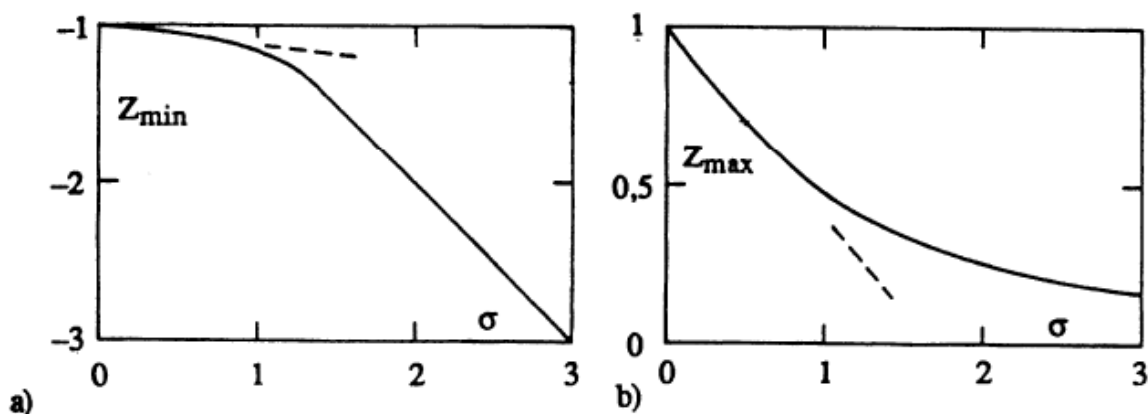


Figure 2.11. Extreme values of Z for an instantaneous a) opening and b) closing of the valve

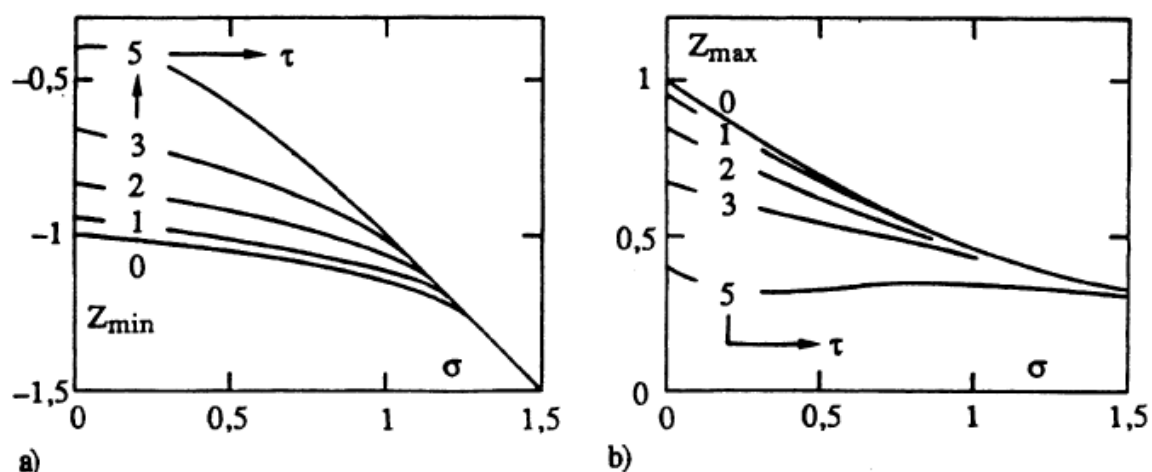


Figure 2.12. Extreme values of  $Z$  for a gradual a) opening and b) closing of the valve

### 2.2.3.2.4 Simplified method

A first estimation of the maximum and minimum levels reached by the water in the surge tank can be estimated by equating the potential energy in the water between the actual water level and the steady state water level to the kinetic energy of the water in the pipe from which is subtracted a certain amount of energy losses. The maximal and minimal levels reached by the water can then be approximated by the following equations.

$$\text{Instantaneous closing} \quad z_{max} = U_0 \cdot \sqrt{\frac{L \cdot A_{ga}}{g \cdot A_c}} - 0,6 \Delta H \quad (2.98)$$

$$\text{Instantaneous opening} \quad z_{min} = -U_0 \cdot \sqrt{\frac{L \cdot A_{ga}}{g \cdot A_c}} - 0,25 \Delta H \quad (2.99)$$

While being a rough estimation, these values can be used in a pre-design of the surge tank.

### 2.2.4 Stability condition

Besides being able to contain the oscillations of the water table within its boundaries, the surge tank also has to dampen them in order to make them disappear after a finite number of period. In a simple case where the oscillations are only affected by their interaction with the pipes and surge tank after their initiation, the frictions should ineluctably dampen them until they disappear. However, there are cases where the oscillations become unstable and where their amplitude increases with time instead of decreasing.

The most well-known case of unstable oscillations is related to the turbine's governing device. The discharge passing through the turbine is usually regulated so that it provides a constant

power. The power produced depends on the turbine flow, the hydraulic head at the turbine's level and on the turbine's yield, according to the equation (2.100).

$$P = \eta \cdot \rho \cdot g \cdot Q \cdot \Delta H \quad (2.100)$$

where: $\eta$ [-]	Turbine's yield
$Q$ [ $m^3/s$ ]	Turbine discharge
$\Delta H$ [ $m$ ]	Difference between the hydraulic heads just upstream and just downstream the turbine

When the water level goes down inside the surge tank, the hydraulic head upstream the turbine decreases. The discharge must then be increased to counterbalance this drop and keep a constant amount of power produced. The surge tank has to provide additional water due to this and the water level drops even more. Reversely, when the water level goes up in the surge tank, the discharge is decreased which amplifies the water rising. If the magnitude of this phenomenon is too high, then the oscillations amplitude rises over time instead of decreasing.

Several authors studied this phenomenon to propose design criteria to avoid it. The most famous one was developed by Thoma and dictates a minimal cross-section in the surge tank, according to equation (2.101).

$$\text{Thoma's formula} \quad A > A_L = \frac{A_{st} \cdot v^{*2}}{2 \cdot g \cdot (H - \Delta H)} \quad (2.101)$$

where: $A_L$ [ $m^2$ ]	Minimal cross-section in the surge tank
$v^*$ [ $m/s$ ]	Friction velocity, according to equation (2.77)
$H$ [ $m$ ]	Height difference between the upper reservoir and the turbine
$\Delta H$ [ $m$ ]	Head losses between the upper reservoir and the surge tank

If the penstock's length is significant compared to the waterway's, then the penstock's influence must be taken into account by adding a correction factor to the Thoma's formula. It's the Evangelisti's formula (2.102).

$$A_{st} > A_L \cdot \frac{1 + \frac{L_{tot} \cdot A_{ww}}{L \cdot A_{tot}}}{1 - 3 \cdot \frac{\Delta H_{tot}}{H - \Delta H}} \quad (2.102)$$

where: $L_{tot}$ [ $m$ ]	Total length of the waterway and the penstock
--------------------------	---

$A_{tot} [m^2]$  Total cross-section of the waterway and the penstock

$\Delta H_{tot} [m]$  Total head loss in the waterway and the penstock

### 2.2.5 Types of surge tank

Several types of surge tanks can be implemented in a hydropower plant. Each of them has its benefits and limitations and the choice of the optimal type will be different for each case.

#### 2.2.5.1 Simple surge tank

A simple surge tank consists of a vertical shaft linked in its bottom to the water way coming from the upstream reservoir and the penstock going to the turbine. The water table's oscillations are dampened only by the friction of the water against the water way's and the shaft's walls. It's the easiest type of surge tanks to build and design but it requires a large volume as the dampening of the oscillations isn't the most effective.

#### 2.2.5.2 Throttled surge tank

It is possible to create an additional singular head loss in the surge tank by adding a throttle in it, as shown in Figure 2.13. By doing so, the oscillations are dampened more effectively which allows for a smaller surge tank. The implementation of a throttle can however reduce the surge tank's capacity to protect the waterway from the water hammer.

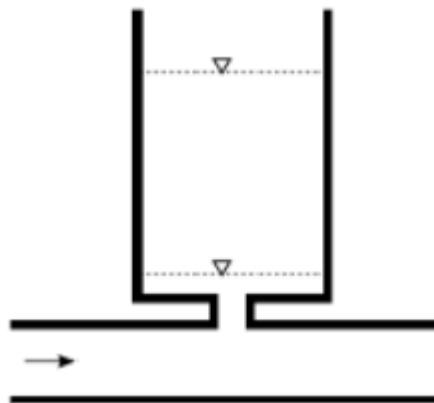


Figure 2.13. Throttled surge tank<sup>4</sup>

#### 2.2.5.3 Variable surge tank

A variable surge tank is made up of a main shaft coupled with one or more expansion chamber. An example of such surge tank is presented in Figure 2.14, with two chambers, one at the top

<sup>4</sup> (Adam, De Cesare, & Schleiss)

and one at the bottom of the shaft. The chambers reduce the oscillations amplitude by expanding the cross-section at strategic places.

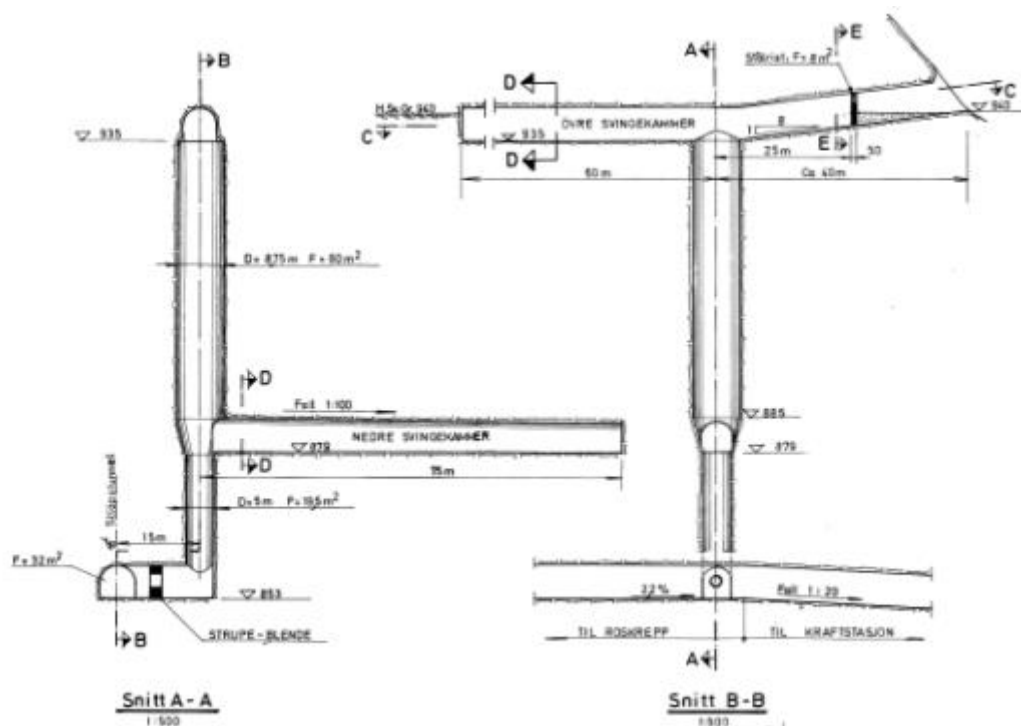
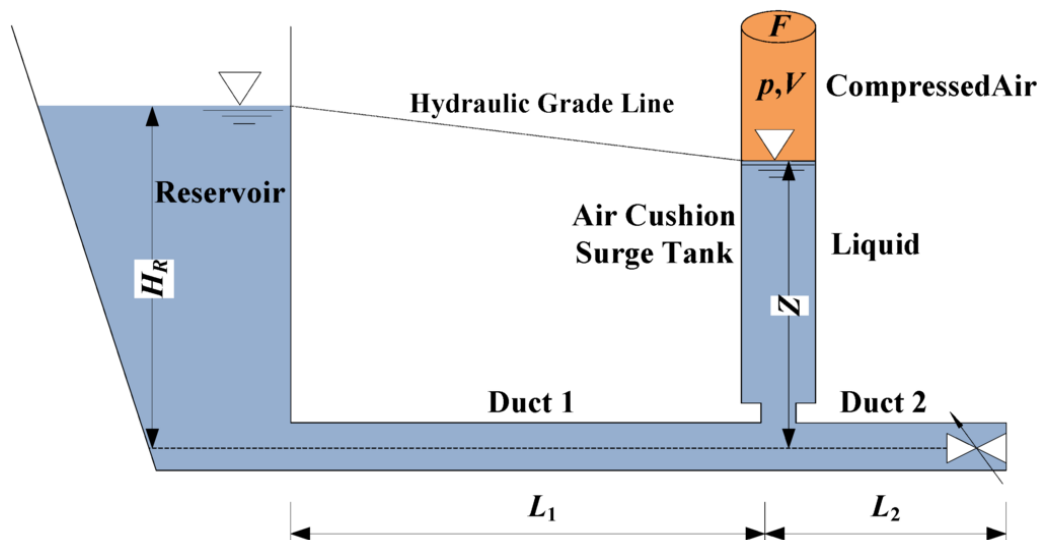


Figure 2.14. Alternative for the design of the upstream surge tank in Roskrepp power plant

#### 2.2.5.4 Closed surge tank

A closed surge tank is made of an excavated cave filled with compressed air, as illustrated in Figure 2.15. The amount of pressure applied to the water table is then related to its movement inside the surge tank. The water displacements are slowed down when the water level is rising and exceeds the static level of water and when the water level is going down and passing under the static level. This type of surge tank allows for a lower excavation's volume which reduces the costs. However, its implementation requires a good rock quality to avoid the air leaking out of the chamber and the installation of an air compressor. It is possible to reinforce the cave walls by covering it with steel but this technique is too expensive in most of the cases. Consequently, the closed surge tanks are mainly found in Norway, where the rock quality is generally good.

Figure 2.15. Closed surge tank<sup>5</sup>

### 2.2.5.5 Differential surge tank

Differential surge tank includes a main shaft coupled with additional chambers linked in a way that a differential flow is created. A classical layout is presented in Figure 2.16. In this case, the main shaft is connected in its top and bottom to one chamber surrounding it. The top of the shaft creates a spillway pouring inside the chamber while a throttle connects them in the bottom. This way, the water rises faster in the main shaft and spills out in the chamber, which creates an energy dissipation. When going down, the main shaft empties itself faster while the water in the chamber goes through the throttle, which creates another energy dissipation.

A differential surge tanks has a powerful dampening capacity, which allows for lower excavation volumes and reduces the costs. However, it requires a specific expertise to be designed and built as it can be considered as one of the most complex type of surge tank.

<sup>5</sup> (Wang, Yang, & Nilsson, 2015)



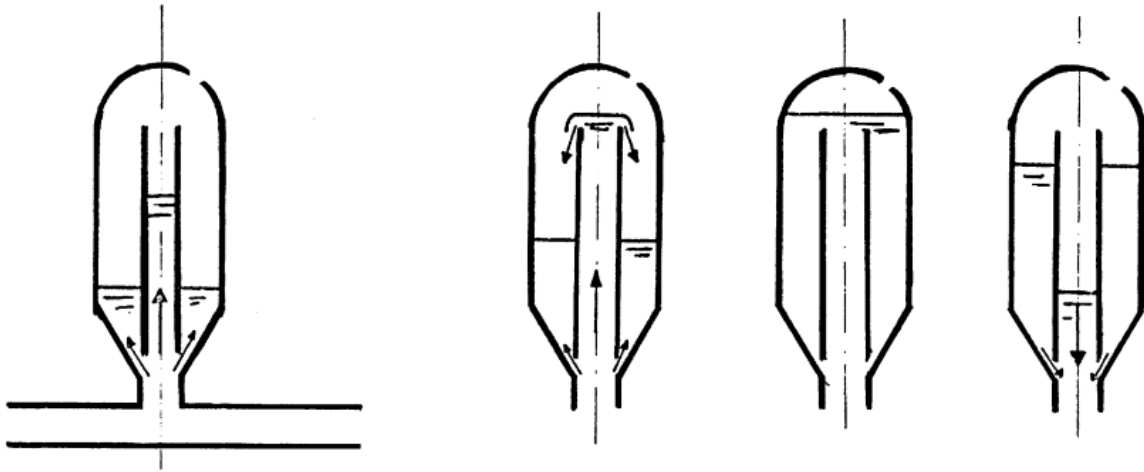


Figure 2.16. Differential surge tank according to Johnson (1915)

## 3 Method

This chapter presents the construction and calibration of the LVTrans model of the Roskrepp powerplant. The transformation of the model to reflect the upgrade of the powerplant into a pumped storage system and its use to simulate the water level in the surge tanks is then presented. Finally, solutions to increase the capacity of the downstream surge tank are studied.

### 3.1 Model of the Roskrepp powerplant

This chapter describe the different steps carried out to build the LVTrans model of the Roskrepp power plant. The purpose of the model is to depict as accurately as possible the oscillations inside both surge tanks during normal operations and emergency shutdowns.

#### 3.1.1 Model construction

The model layout, displayed in Figure 3.1 and Figure 3.2, is based on the drawings of the powerplant provided by the Sira-Kvina power company. Most of them have been made for the construction of the plant and are therefore inaccurate. There are no “as build” drawings, and no 3D scans, which would have been necessary to accurately capture the unlined tunnel surface. The tunnels have been drilled and blasted and are unlined, which usually leads to a larger section than in the drawings. To counter this lack of precision, the main parameters influencing the water level in the surge tanks are studied in the calibration phase detailed in chapter 3.1.2.

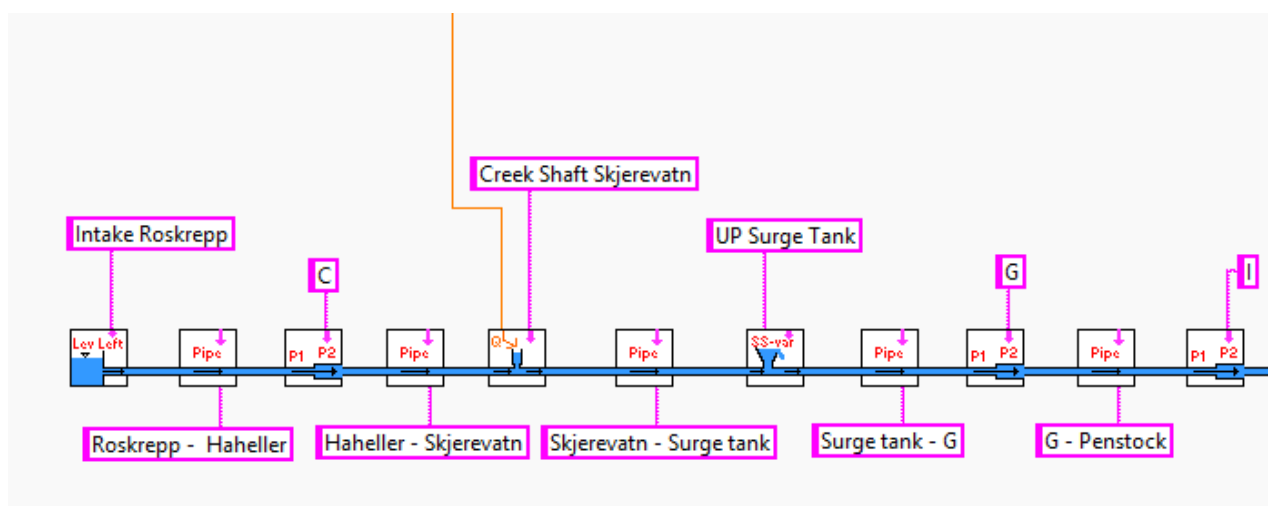


Figure 3.1. LVTrans model from the intake to the pipe connection I

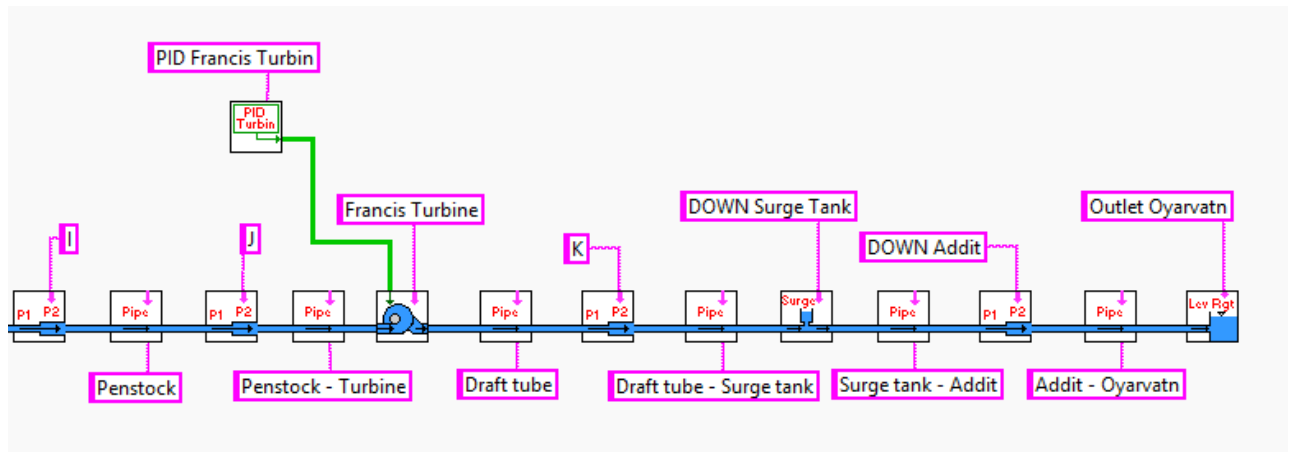


Figure 3.2. LVTrans model from the pipe connection I to the outlet

### 3.1.1.1 Tunnels

According to the drawings, two tunnel sections can be found in the powerplant. At the time of its initial construction, all the tunnels had a section similar to the section (C – C) presented in Figure 3.3, with a layer of asphalt covering the invert. However, the pressure oscillations in the water destroyed the asphalt and a renovation had to be carried out in 2007. The tunnels between the reservoir and the Haheller addit and between the surge tank and the turbine have been cleaned up so that they do not have asphalt anymore. Their new section is displayed in Figure 3.3 (D - D). The asphalt between the Haheller addit and the surge tank has been renovated and the other parts of the powerplant were not damaged. They consequently still have a section similar to section (C – C) of Figure 3.3. The areas and equivalent diameters drawn from the drawings are displayed in Table 3.1.

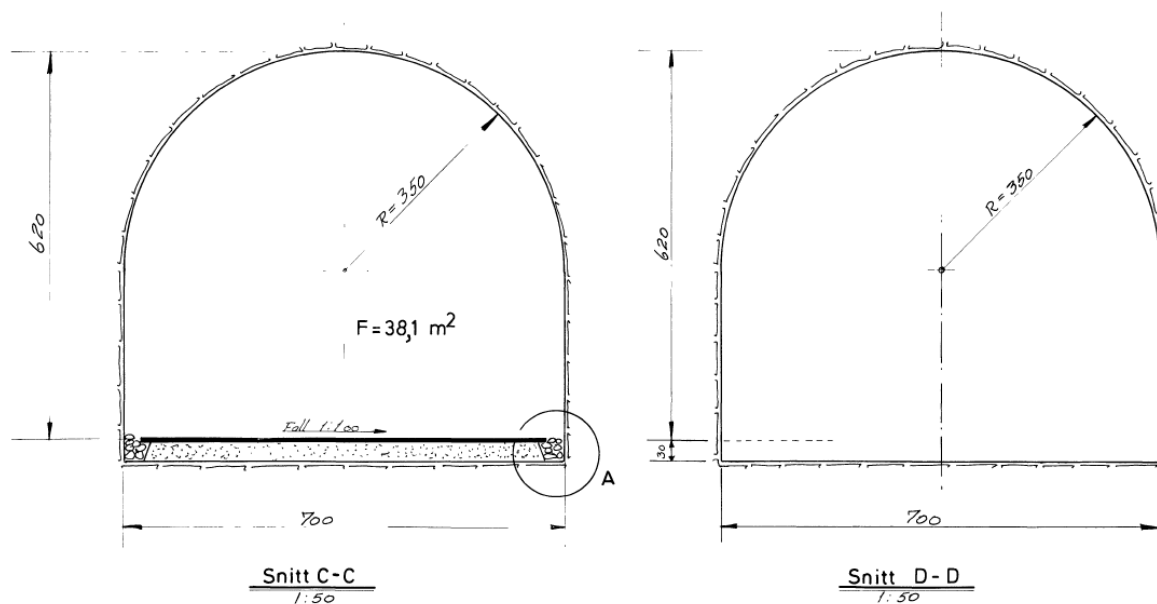


Figure 3.3. Tunnel sections in the powerplant

Section	A [m <sup>2</sup> ]	D [m]
C - C	38.1	6.97
D - D	40.2	7.16

Table 3.1. Area and equivalent diameter of the tunnel sections

### 3.1.1.2 Surge tanks

Two surge tanks have been constructed in the powerplant, one upstream and one downstream of the turbine, to regulate the pressure spikes caused by the discharge regulation. The upstream one is a variable surge tank while the downstream one is a simple shaft, with a lower capacity. Their drawings are available in annex F and G.

#### 3.1.1.2.1 Upstream surge tank

A variable area surge tank is set up around 350 meters upstream the turbine. Its lower chamber is a tunnel leaving the main one at 865 meters elevation and is going up until its top reaches 885 meters, where an intersection takes place. On one way, the tunnel goes on at the same level for 75 meters while on the other, a 5 meters vertical transition leads to a shaft going up to 935 meters, where it meets the upper chamber. This one is a tunnel of around 110 meters long, staying at a constant level. The cross-section areas of the tunnels and the shaft composing the surge tank are displayed in Table 3.2.

	Cross section area [m <sup>2</sup> ]	Lower boundary [m]	Upper boundary [m]
<b>Lower chamber</b>	34	865	885
<b>Transition</b>	28 → 60	885	890
<b>Shaft</b>	60	890	936
<b>Upper chamber</b>	34	936	940

Table 3.2. Cross-sections and boundaries of the different parts of the upstream surge tank

The main tunnel has a height of 6.2 meters, meaning that the lowest water level that can be reached without air entering the main tunnel is at 872.2 meters. As a simplification, a 873 meters elevation is considered in the following parts. The highest water level that can be reached is 942 meters if a 6 by 6 section is considered in the upper chamber.

This surge tank is reproduced in LVTrans. The horizontal areas of the different parts, associated with their height above the bottom of the surge tank must be introduced as parameters.

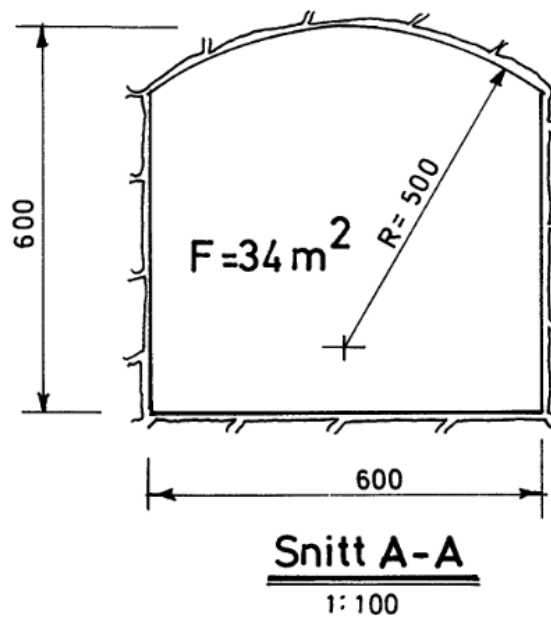


Figure 3.4. Cross-section of the tunnels working as chambers in the upstream surge tank

As a simplification, the tunnel cross-section is viewed as a square with a 6 meters side. In reality, it is shaped as shown in Figure 3.4. The first part of the lower chamber is a tilted tunnel with a 1:8 slope while the second part of the lower chamber and the upper chamber are considered to have no slope. The simplified schema of the surge tank depicted in the model is displayed in Figure 3.5.

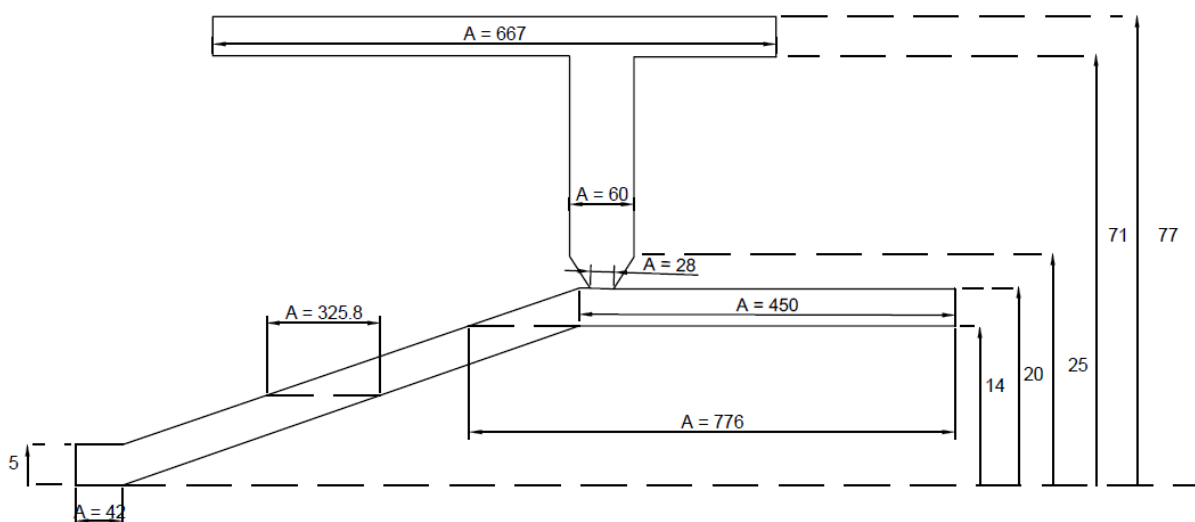


Figure 3.5. Simplified schema of the upstream surge tank introduced in the model

### 3.1.1.2.2 Downstream surge tank

The downstream surge tank is a simple shaft going from an elevation of 813.5 at its bottom to 840 meters at its top, where it reaches a service cavern. The tailrace tunnel exiting the shaft as a 6.2 meters height, which means that the actual lower boundary of the surge tank is at 819.7 meters. As a simplification, an 820 meters elevation is considered in the following parts.

The cross-section of the tunnel is depicted in Figure 3.6. In LVTrans, an equivalent diameter of 8.3 meters, with a  $90 \text{ m}^2$  section are considered as a first approximation. The diameter will later be calibrated to have a better model of the surge tank.

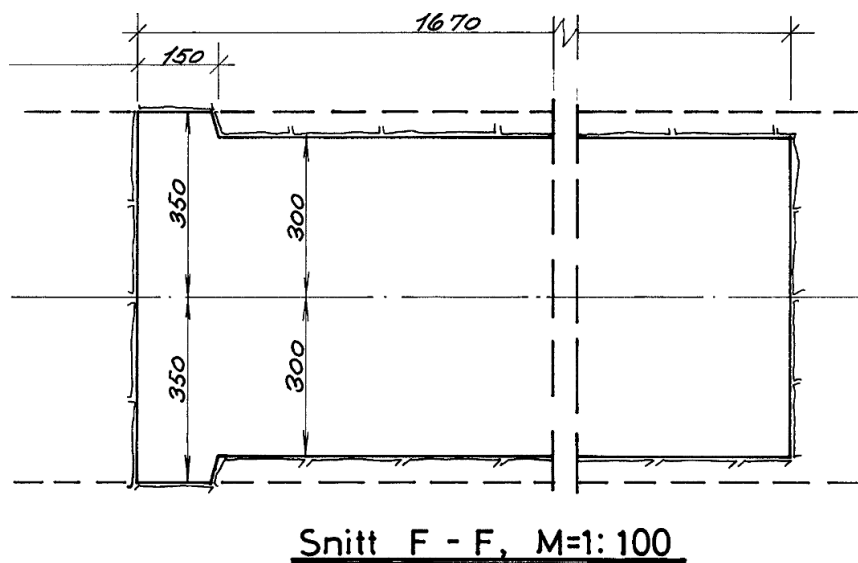


Figure 3.6. Cross-section of the downstream surge tank

### 3.1.1.3 Creek shaft

The Roskrepp powerplant includes a secondary intake in the Skjerevatn Lake. The water coming from this reservoir flows with a free surface inside the tunnel, displayed in Figure 3.7, until it reaches the water table. The intake tunnel works as a second upstream surge tank and is modelled as a creek shaft.

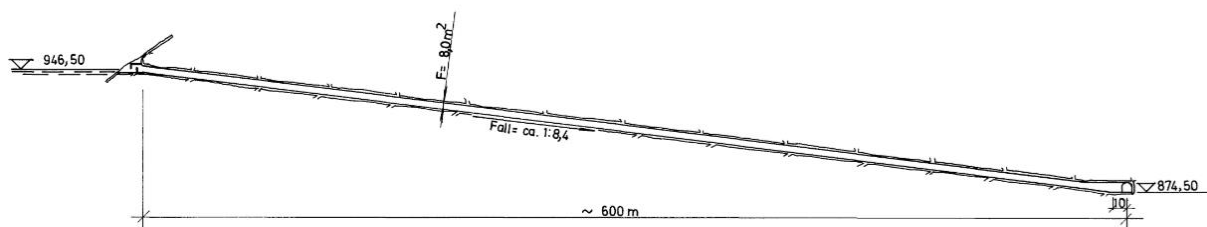


Figure 3.7. Drawing of the secondary intake in the Skjerevatn Lake

The tunnel goes from the reservoir at a 946 meters elevation to the main tunnel at 874.5 meters. To simplify the estimation of the water table area in the tunnel, its cross-section is considered as a square. The estimated equivalent horizontal diameter is shown in Table 3.3.

<b>Slope</b>	1 : 8.4
<b>Cross-section [m<sup>2</sup>]</b>	8
<b>Water table surface [m<sup>2</sup>]</b>	67
<b>Equivalent horizontal diameter [m]</b>	9.3

Table 3.3. Equivalent diameter of the creek shaft

The amount of water coming from this intake is very small compared to the one coming from the Roskrepp reservoir. The water discharge in the creek shaft is then deemed negligible and is set to 0.

### 3.1.1.4 Turbine

The turbine parameters introduced in the model are based on an Excel sheet provided with LVTrans. The frequency in the net, efficiency coefficient  $\eta$ , nominal head, nominal discharge and the number of pole pairs are given as an input and the sheet provides the parameters that should be introduced in LVTrans. All of those values are summed up in Table 3.4.

<b>INPUT</b>		<b>Parameters introduced in LVTrans</b>	
<b>Frequency [Hz]</b>	50	<b>H0 [m]</b>	83
<b><math>\eta</math></b>	0.947	<b>Q0 [m<sup>3</sup>/s]</b>	67
<b>H0 [m]</b>	83	<b>n [o/min]</b>	250.00
<b>Q0 [m<sup>3</sup>/s]</b>	67	<b>r1 [m]</b>	1.126
<b>Pole pairs</b>	12	<b>r2 [m]</b>	1.187
		<b>alpha1 [°]</b>	27.3
		<b>beta1 [°]</b>	78.0
		<b>beta2 [°]</b>	25.9
		<b>Poles</b>	24
		<b>P0 [MW]</b>	51.71
		<b>T0 [kgm]</b>	1975358

Table 3.4. Parameters of the turbine

### 3.1.2 Calibration

The calibration phase is a very important step in the construction of a model. It provides a direct comparison between the simulated results and measurements collected directly from the

system. By changing some parameters in the model and comparing the results with the measurements, the most significant parameters in the model can be identified. Their values can then be adjusted so that the simulation fits the reality as best as possible.

In the case of the Roskrepp model, the calibration is mostly based on the data provided by the measurements taken during the field trip. The steady-state situation is first studied, and then the transient situation with a shutdown is studied to complete the process.

### 3.1.2.1 Data available

Two sources of data are used to calibrate the model. The first one is a report<sup>6</sup> from the Norges Hydrodynamiske Laboratorier from 1980 and the second one, the most significant, is the measurements carried out during the field trip conducted in September 2017.

#### 3.1.2.1.1 Report from 1980

In 1980, the Sira-Kvina power company mandated the Norges Hydrodynamiske Laboratorier to conduct a series of pressure measurements<sup>6</sup> inside the Roskrepp powerplant to evaluate the head losses. The total pressure heads just upstream and downstream the turbine are estimated from the pressure measurements for two situations. In the first one, the power produced reaches 40 MW, for an estimated discharge of 46.5 m<sup>3</sup>/s while in the second one, the power reaches 50 MW for an estimated discharge of 58.3 m<sup>3</sup>/s. The water levels in the reservoirs are almost the same for both situations, with only a 30 centimetres difference in the downstream reservoir. The total head losses upstream the turbine are evaluated to 2.7 mWC in the first case and 4.1 mWC in the second. The downstream head losses are a lot smaller with only 8 cmWC in the first case and 0.2 mWC in the second. This correlates with the shorter tunnels between the turbine and the downstream reservoir. All those values are summarized in Table 3.5.

P [MW]	Q [m <sup>3</sup> /s]	Level Up. reservoir [m]	H <sub>up</sub> [mWC]	ΔH <sub>up</sub> [mWC]	Level Down. reservoir [m]	H <sub>down</sub> [mWC]	ΔH <sub>down</sub> [mWC]
40	46.5	928.2	925.5	2.7	828.22	828.3	0.08
50	58.3	928.2	924.1	4.1	828.3	828.5	0.2

Table 3.5. Total heads estimated according to the report from 1980

It is important to keep in mind that those measurements have been conducted in 1980 and that the situation inside the powerplant could have changed. However, they give a first idea of the amount of head losses that can be expected for a steady flow situation.

<sup>6</sup> Invalid source specified.



### 3.1.2.1.2 Field trip

In September 2017, a field trip was carried out in a collaboration between the NTNU and Sira-Kvina to perform a collection of measurements in the Roskrepp powerplant. The whole plant was at disposal the 19<sup>th</sup> of September to complete the measurements needed.

Two gauge pressure sensors were placed just upstream and downstream of the turbine and another sensor was monitoring the turbine opening. In addition, the power produced by the turbine, its rotational speed and the water levels in the upstream and downstream reservoirs were measured by the power plant installations. However, the water velocity and the turbine discharge were not known during the tests.

The tests started at around 9 in the morning, with the turbine completely closed for several hours. At 9:35, the turbine started up at full capacity until the power produced reached 50 MW. Then the power produced followed the curve displayed in Figure 3.8. Finally, an emergency shutdown was operated at 12:07.

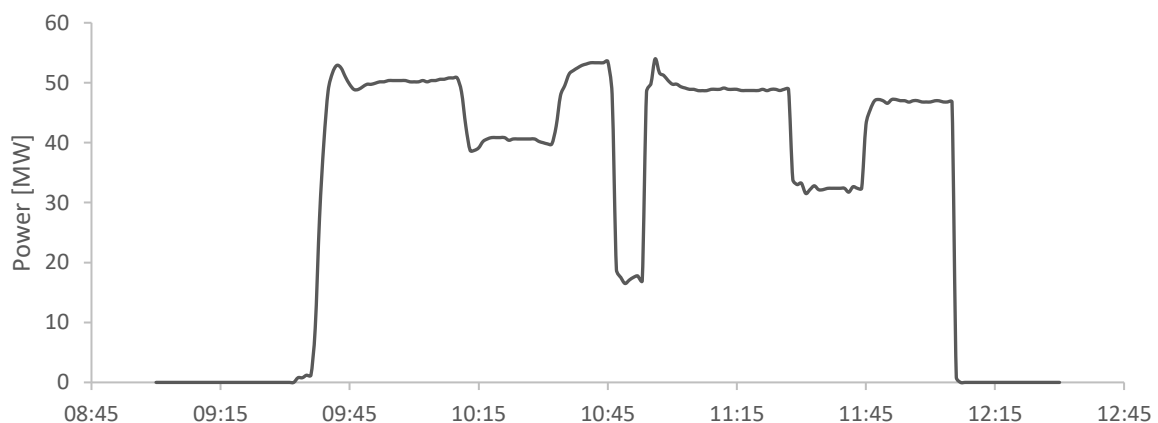


Figure 3.8. Power produced during the measurements

The water levels in the reservoirs during the measurements were almost constant with only a small drop of the level in the downstream reservoir. Their values are displayed in Table 3.6.

	<b>Upstream reservoir</b>	<b>Downstream reservoir</b>
<b>Water level at 9:00 [m]</b>	925.53	833.45
<b>Water level at 12:00 [m]</b>	925.53	833.39
<b>Value used in simulation [m]</b>	925.5	833.4

Table 3.6. Water level in the reservoirs during the measurements

### 3.1.2.1.3 Data conversion

When simulating an event, LVTrans gives results in the form of discharge, hydraulic head and total head. To be able to compare those with the measurements, some conversion must be completed. It is chosen to convert the pressure measurements into hydraulic heads, by using the following equation:

$$h_{measure} = \frac{p_{measure}}{\rho g} + z_{sens} \quad (3.1)$$

where:  $h_{measure}$  [mWC]      Hydraulic head associated with the pressure measured  
 $p_{measure}$  [Pa]              Pressure measured  
 $z_{sens}$  [m]                      Sensor elevation

The knowledge of the sensors locations is then crucial. The one situated upstream of the turbine is placed just at the exit of the butterfly valve. Its general location is represented in Figure 3.9 and Figure 3.10. The sensor located downstream of the turbine is placed just at its exit, as shown in Figure 3.10.

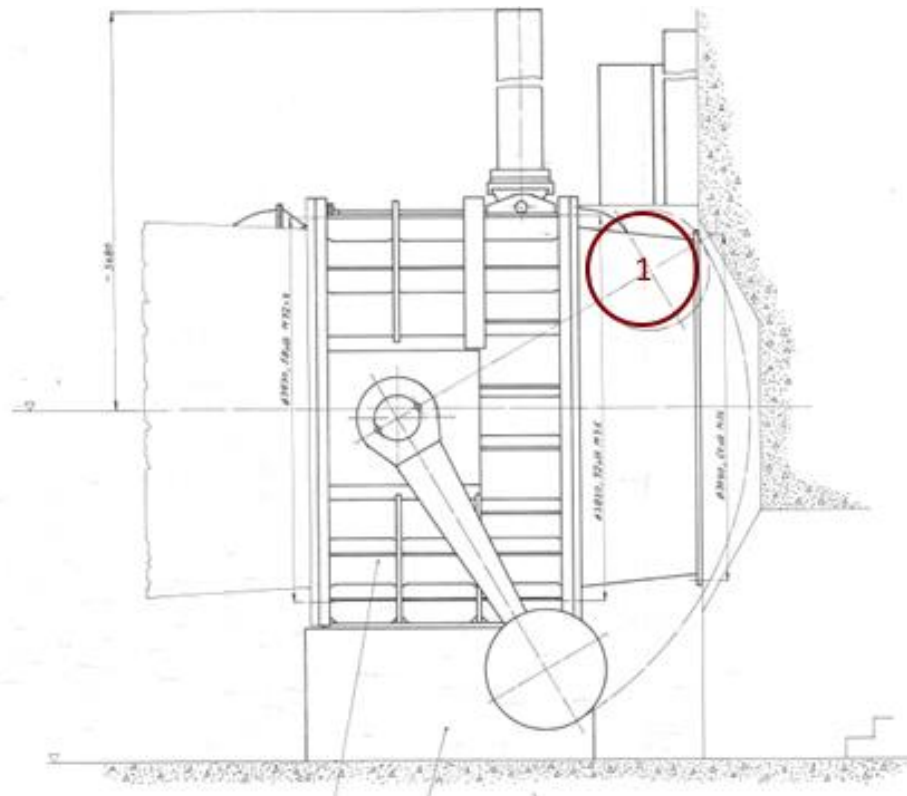


Figure 3.9. Butterfly valve and location of the upstream sensor (1)

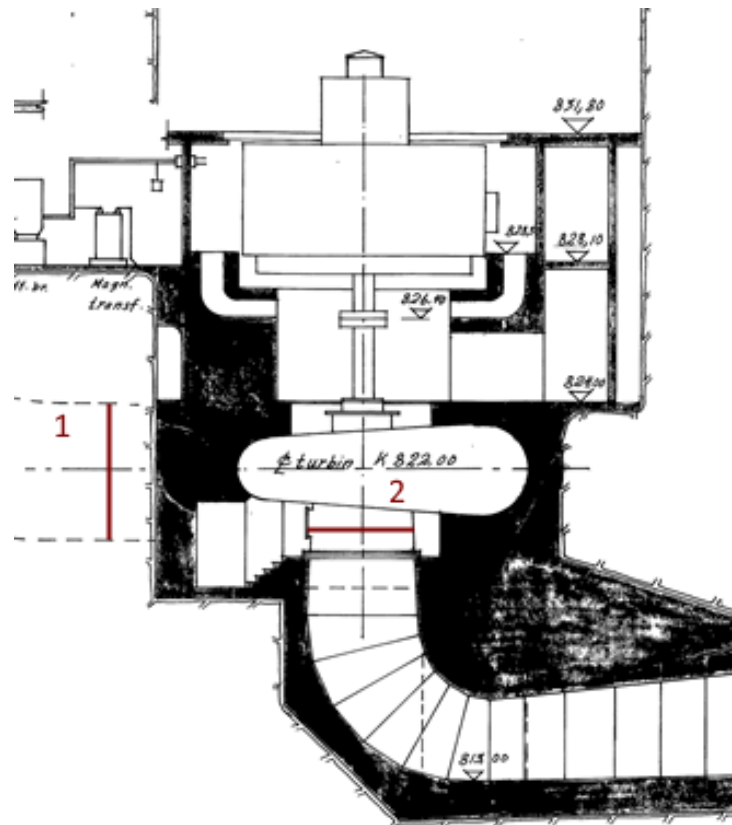


Figure 3.10. Turbine and general locations of the upstream (1) and downstream (2) sensors

### Sensors elevations

The sensors elevations are used to transform the measured pressures into hydraulic heads and compare it with the simulated hydraulic heads. To have a better precision their estimation is based on the pressure measurements rather than the drawings.

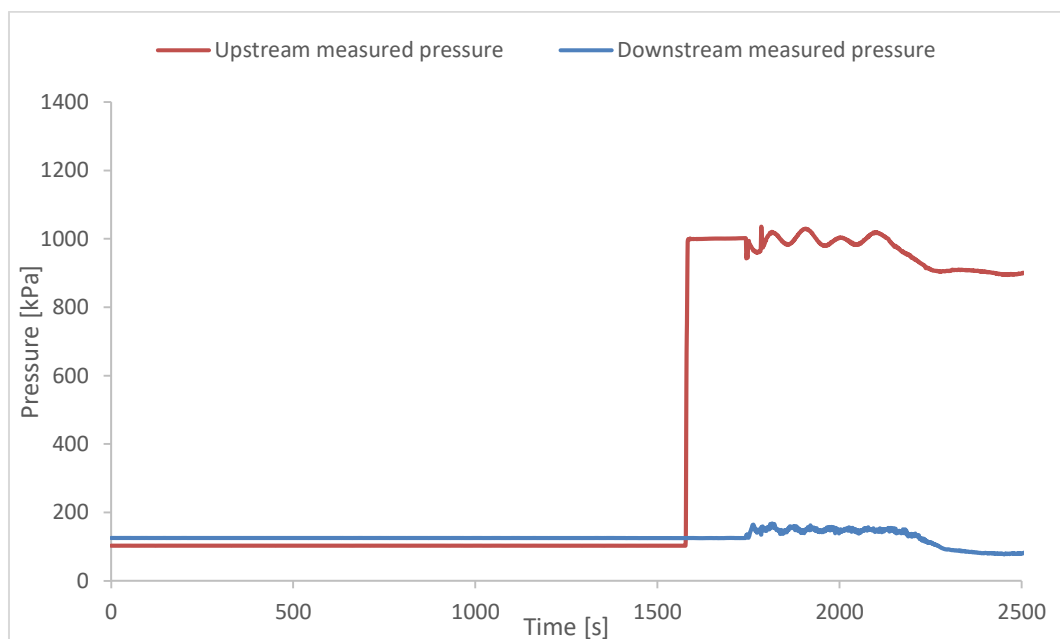


Figure 3.11. Pressure measured before the opening of the butterfly valve

The pressure measured before the opening of the butterfly valve, at the 1575<sup>th</sup> second in Figure 3.11, is used. The turbine is then completely closed and the water is still. With the butterfly valve closed, the pressure only comes from the height difference between the sensors and the water level in the downstream reservoir. The sensors elevations can be computed by the following equation:

$$z_{sensor} = z_{res} - \frac{p_0}{\rho g} \quad (3.2)$$

where:  $z_{res}$  [m] Water level in the downstream reservoir  
 $p_0$  [Pa] Pressure measured by the sensor before the opening of the butterfly valve

The computed sensor elevations are displayed in Table 3.7.

	Upstream	Downstream
Water level in the reservoir [m]	Not relevant	833.4
Initial measured pressure [kPa]	102.7	125.2
Sensor elevation [m]	823.0	820.7

Table 3.7. Sensors level

### Pipes diameters at sensor level

The pipe diameter is a crucial information to have a good simulation of the water velocity at the sensor level. To obtain the hydraulic head, LVTrans computes the total head and then remove the velocity head from it. If the velocity is wrong, then the hydraulic head will not be correct.

$$h_{sim} = H_{sim} - \frac{Q_{sim}^2}{2g \cdot A^2} \quad (3.3)$$

where:  $h_{sim}$  [mWC] Simulated hydraulic head  
 $H_{sim}$  [mWC] Simulated total head  
 $Q_{sim}$  [m<sup>3</sup>/s] Simulated discharge  
 $A$  [m<sup>2</sup>] Pipe diameter implemented in LVTrans

The pipes diameters, according to the drawings, are shown in Table 3.8.

	Upstream	Downstream
<b>D [m]</b>	3.4	9.08
<b>A [m<sup>2</sup>]</b>	2.94	6.79

Table 3.8. Pipes diameters at the sensors levels

### 3.1.2.2 Normal operation calibration

The model is calibrated to simulate as well as possible the steady state flow situations taking place during the normal operation of the powerplant. To facilitate the calibration, average values of the produced power and associated pressure are computed from the field trip data. They are displayed, along with the hydraulic heads drawn from the pressures, in Table 3.9.

From	To	Upstream			Downstream	
		P [MW]	Pressure [kPa]	Hydraulic head [mWC]	Pressure [kPa]	Hydraulic head [mWC]
09:53:00	10:05:00	50.3	913.0	924.2	86.2	829.5
10:19:00	10:29:00	40.7	946.6	919.5	106.4	831.5
10:42:00	10:46:00	53.4	901.4	914.9	78.7	828.7
10:50:00	10:51:00	17.1	993.3	924.2	141.4	835.1
11:11:00	11:23:00	48.8	920.4	916.8	88.3	829.7
11:36:00	11:40:00	32.4	964.9	921.3	125.3	833.5
11:54:00	12:03:00	46.9	928.2	917.6	90.7	829.9

Table 3.9. Average measured power and hydraulic heads.

The hydraulic heads simulated upstream and downstream the turbine in a steady state depend on the water levels in the reservoirs, the head losses between them and the turbine and on the discharge. The latter depends on the power produced by the turbine and its efficiency, on the water level in the reservoirs and on the head losses. The turbine efficiency is computed by LVTrans based on the parameters of the turbine and is admitted correct. The water levels and the power produced by the turbine being set to have the same conditions as during the measurements, only the head losses are calibrated.

The friction coefficients in the tunnels and the singular loss coefficient at the entrance or exit of the reservoirs are calibrated so that the hydraulic heads simulated upstream and downstream the turbine fit as well as possible the measurements. The conditions in which the measurements have been carried out are reproduced in the model with a power produced following the one displayed in Figure 3.8 and water level in the reservoirs as shown in Table 3.6. The simulated hydraulic heads upstream and downstream the turbine, compared with the measurements, are displayed in Figure 3.12 and Figure 3.13.

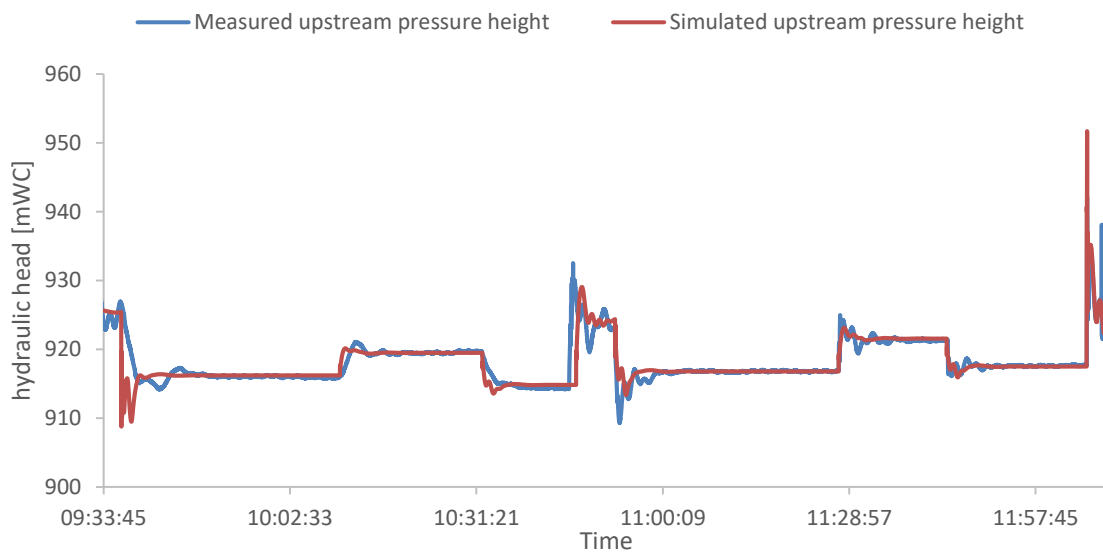


Figure 3.12. Comparison of the measured and simulated hydraulic heads upstream the turbine

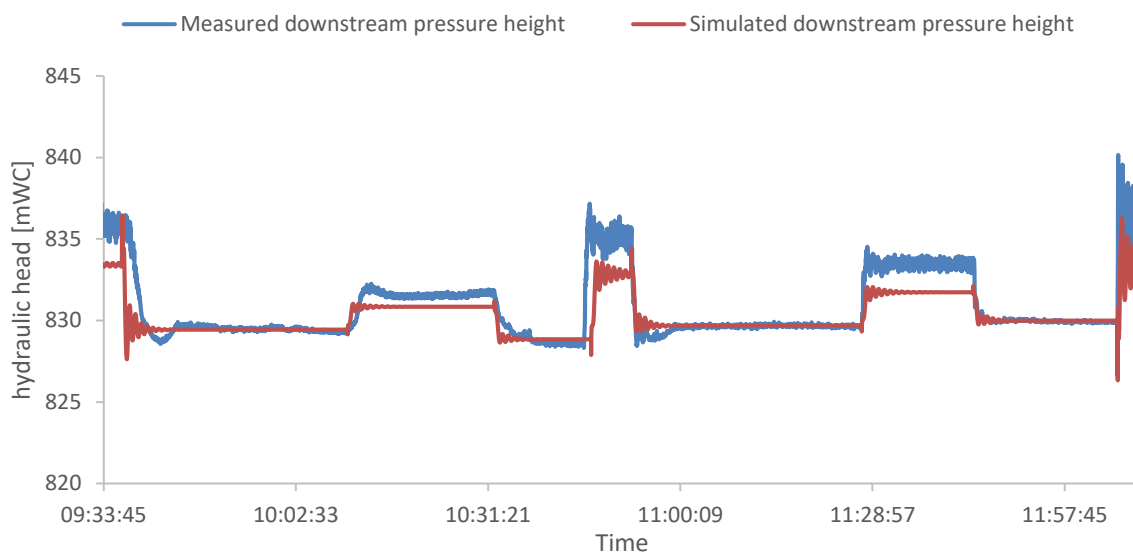


Figure 3.13. Comparison of the measured and simulated hydraulic head downstream the turbine

To better quantify the error between the simulated values and the measurements, the hydraulic heads simulated upstream and downstream the reservoir for the produced power given in Table 3.9 and their comparison with the measurements are summed up in Table 3.10.

P [MW]	Upstream hydraulic head [m]			Downstream hydraulic head [m]		
	Simulation	Measurements	Error	Simulation	Measurements	Error
17.1	924.1	924.2	-0.10	832.9	835.1	-2.25
32.4	921.5	921.3	0.18	831.8	833.5	-1.68
40.7	919.5	919.5	-0.02	830.9	831.5	-0.66
46.9	917.5	917.6	-0.08	830.0	829.9	0.07
48.8	916.8	916.8	0.02	829.6	829.7	-0.04
50.3	916.2	916.1	0.11	829.5	829.5	-0.02
53.4	914.8	914.9	-0.08	828.9	828.7	0.17

Table 3.10. Comparison between the simulated and the measured hydraulic heads upstream and downstream the turbine

According to these results, the upstream part is well represented in the model, with only a maximum error of 18 cm between the average measured hydraulic head and the simulated one. Moreover, the simulated curve seems to faithfully follow the measurements.

However, the simulated values in the downstream part diverge from the measurements when the power produced is lower than 50 MW. The measured hydraulic head reaches 835 mWC while the simulated one barely reach 833 mWC. The fact that the hydraulic head hit such a high value is difficult to explain, the water level in the reservoir being at 833.4 m. According to equation (3.4), an hydraulic head of 835 m at the turbine level would mean that the hydraulic losses between the turbine and the reservoir would be of at least 1.6 meters, without counting the velocity head. Such a high head loss seems unlikely, considering that in the 1980 report, the head losses in the downstream part reached only 20 cm for a discharge exceeding 50 m<sup>3</sup>/s.

$$h_{down,sens} = z_{res} + \Delta H_{loss} - \frac{v_{sens}^2}{2g} \quad (3.4)$$

where:

- $h_{sens,down}$  [mWC] Hydraulic head at the downstream sensor level
- $z_{res,down}$  [m] Water level in the downstream reservoir
- $\Delta H_{loss,down}$  [m] Head losses between the downstream reservoir and the turbine.
- $v_{sens,down}$  [m<sup>2</sup>/s] Water velocity at the downstream sensor level

An hypothesis could be that the pressure isn't homogeneously distributed in the pipe section at the sensor level. This could happen because of a local turbulence appearing when the turbine doesn't run at full load. Such a local turbulence can occur if there is an active rotating vortex rope (R. Goyal, M. J. Cervantes and B. Gandhi, "Vortex rope formation in a high head model Francis turbine," Journal of Fluid Engineering, 2016.) in the draft tube. The pressure near the pipe wall could then be higher than in its centre. This kind of phenomena can't be reproduced

by LVTrans. Such a local rise of pressure doesn't influence the water level in the surge tank and the hydraulic head being well represented when the turbine runs at a 50 MW power, the calibration is deemed acceptable.

### 3.1.2.3 Shutdown calibration

The shutdown calibration is based entirely on the pressure measurements realized during the field trip. Figure 3.14 and Figure 3.15 display the hydraulic head drawn from the pressure measurements upstream and downstream the turbine during the shutdown. The simulated results from LVTrans are compared to those two curves. To facilitate the visualisation, all the figures related to the shutdown are represented with an x-axis in seconds, starting at 12:01:20.

The situation of the shutdown monitored during the field trip is replicated in the LVTrans model to calibrate it. The power produced before the shutdown is set to 46.9 MW and the closing time to 6 s. For this part, the upstream flow doesn't influence what happens downstream and vice versa. The calibration can then proceed in two steps, first focusing on the upstream and then the downstream.

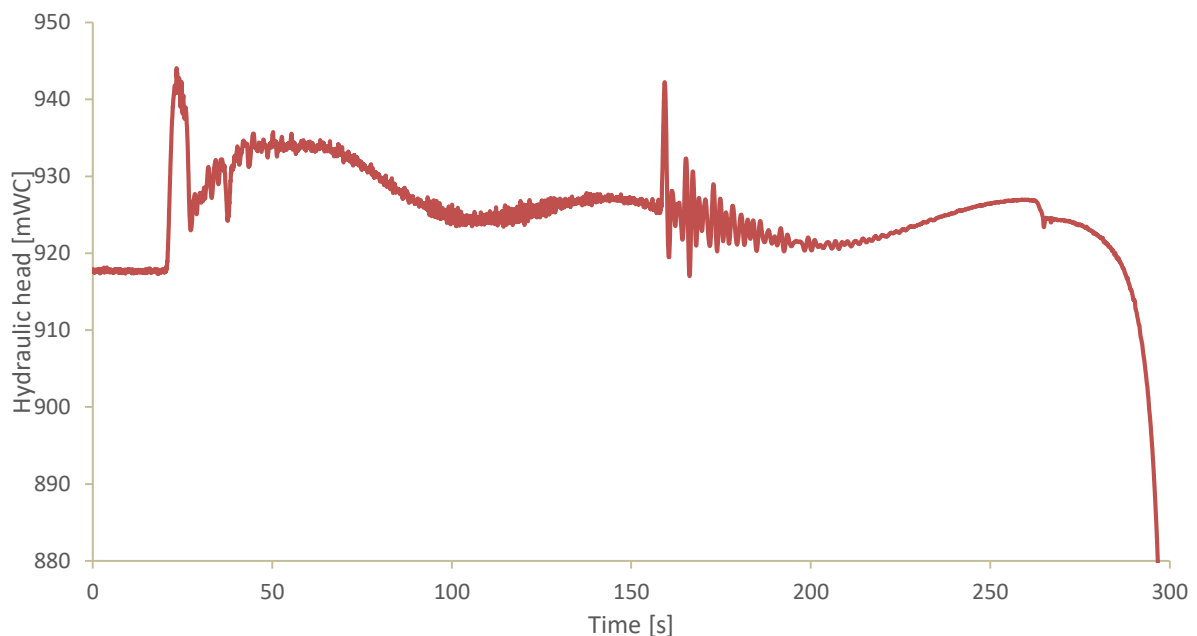


Figure 3.14. Hydraulic head based on the measurements upstream the turbine during the shutdown



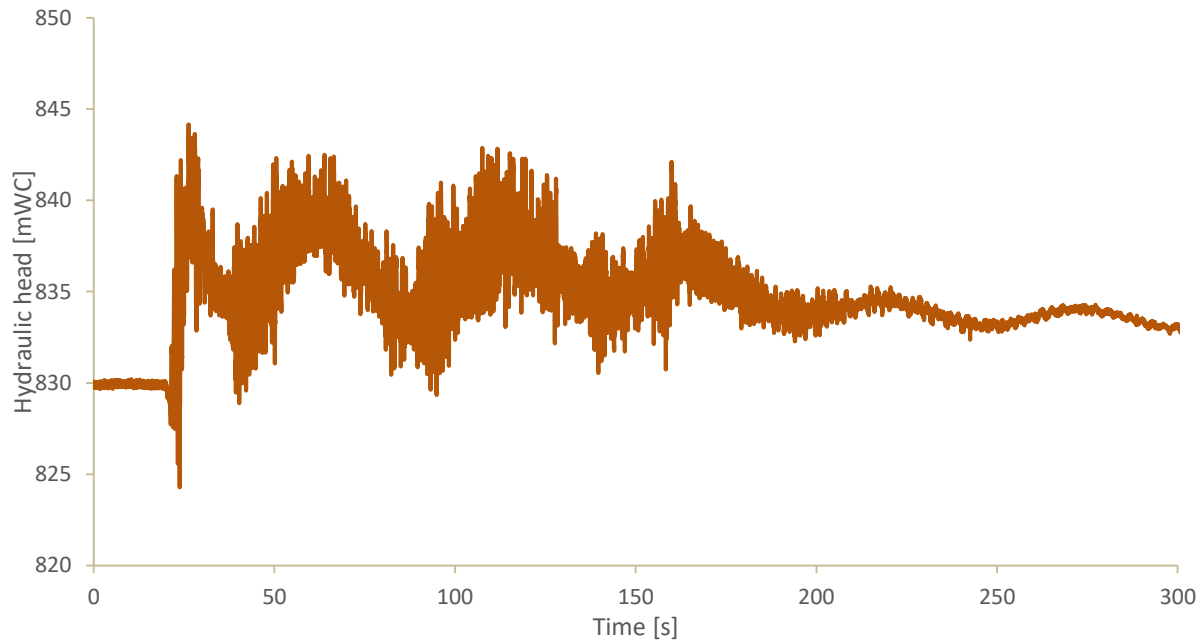


Figure 3.15. Hydraulic head based on the measurements downstream the turbine during the shutdown

### 3.1.2.3.1 Considerations on the turbine opening

During the shutdown, the turbine is first completely closed in 6 seconds, then stays shut for 10 seconds. After that, it re-opens a little bit and finally closes again around 130 seconds after the initial closing. The butterfly valve, placed upstream both sensors and the turbine, stays open during this entire operation and starts closing around 160 second after the initial closing. It is completely closed when the hydraulic head upstream the turbine drops as shown in Figure 3.16.

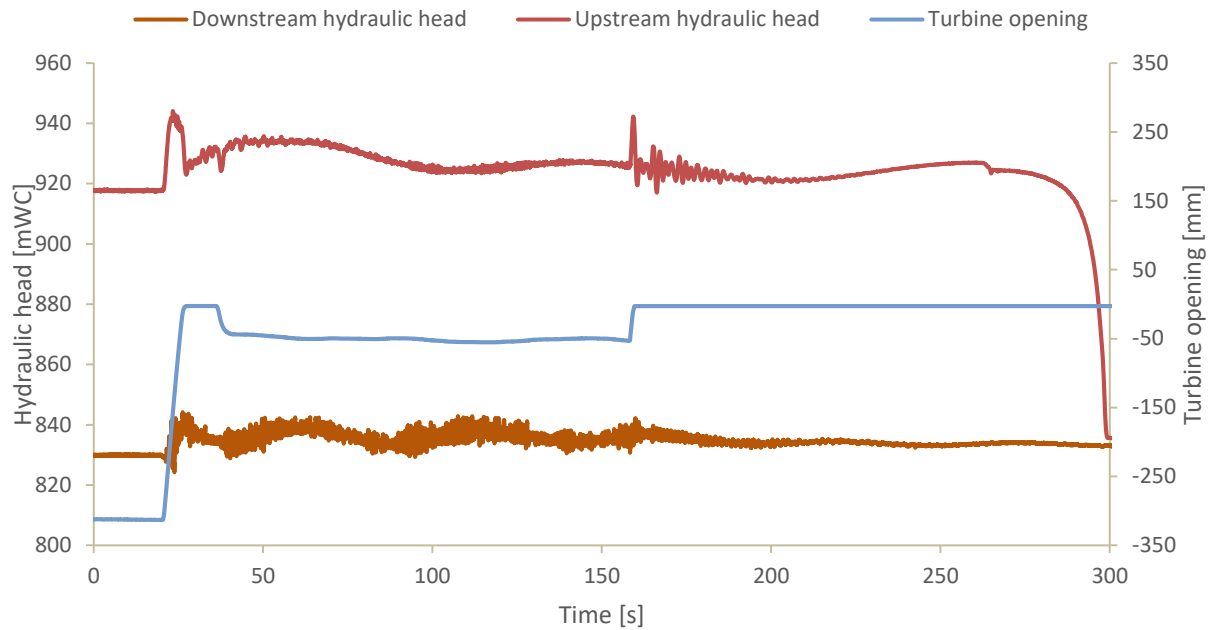


Figure 3.16. Upstream and downstream pressure and turbine opening during the shutdown

During the reopening of the turbine, a no-load operation takes place, which means that a little bit of water flows through the turbine without producing any power. This influences the pressure measurements, but cannot be simulated in the version of LVTrans used in this thesis.

To better understand the effects of this reopening, the measurements of the first opening of the turbine, that took place at around 9:30 in the morning, are studied. The turbine has then been closed for several hours and is open, first with a 100 mm opening and then with a 50 mm opening, matching the one observed during the shutdown, for around 6 minutes. The pressure measurements downstream the turbine during this opening, converted in hydraulic head, are displayed in Figure 3.17. To better visualize the pressure evolution, a moving average of the hydraulic head is represented.

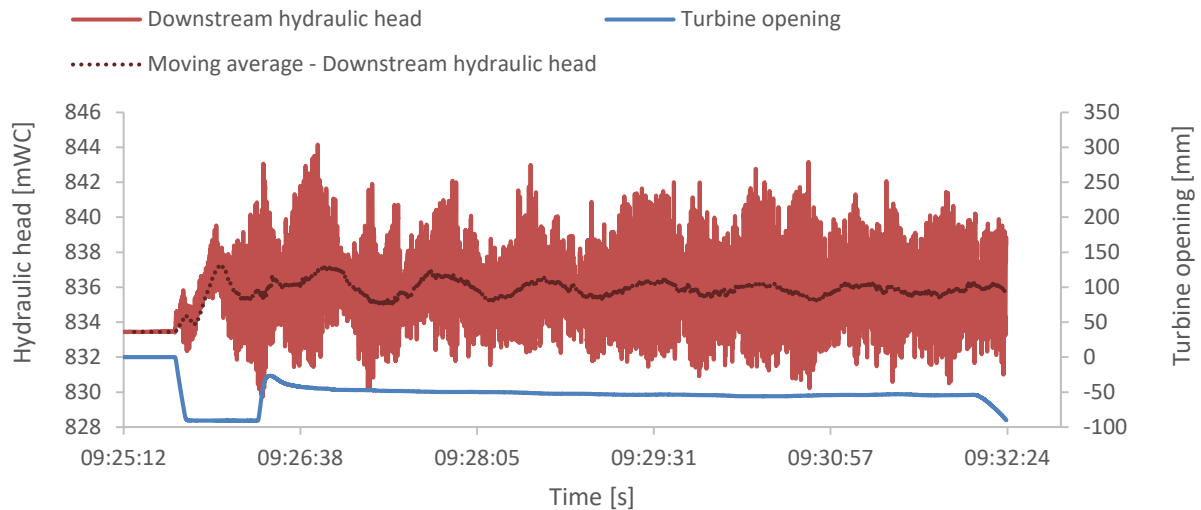


Figure 3.17. Downstream hydraulic head and turbine opening during the turbine start up

When the turbine is opened by only 50 mm, the hydraulic head downstream the turbine oscillates around an average of 835 mWC, that is 2.5 meters above the hydraulic head when the turbine is completely closed. The upstream hydraulic head oscillates around 925.1 mWC, 0.4 meters under the hydraulic head when the turbine is closed. Those values are summarized in Table 3.11.

	Opening [mm]	Downstream hydraulic head [mWC]	Upstream hydraulic head [mWC]
	- 53	835	925.1
	0	833.5	925.5
<b>Difference [m]</b>		<b>2.5</b>	<b>- 0.4</b>

Table 3.11. Average hydraulic head for different opening of the turbine

The difference in the upstream hydraulic head is small and could be explained by the velocity head and the head losses reducing it. Considering all the other uncertainties going with the model, it can be neglected.

However, the rise of the downstream hydraulic head is significant and can be observed in the shutdown measurements. As seen in Figure 3.18, the hydraulic head oscillations resulting from the shutdown are not centred on the water level in the downstream reservoir as it should theoretically be but a couple of meters above. When the turbine is completely closed for the second time, the hydraulic head starts going down until it reaches the water level in the reservoir. The fact that the hydraulic head is oscillating at much higher values than the water level in the reservoir during the shutdown can then be directly correlated with the turbine operating in a no-load function.

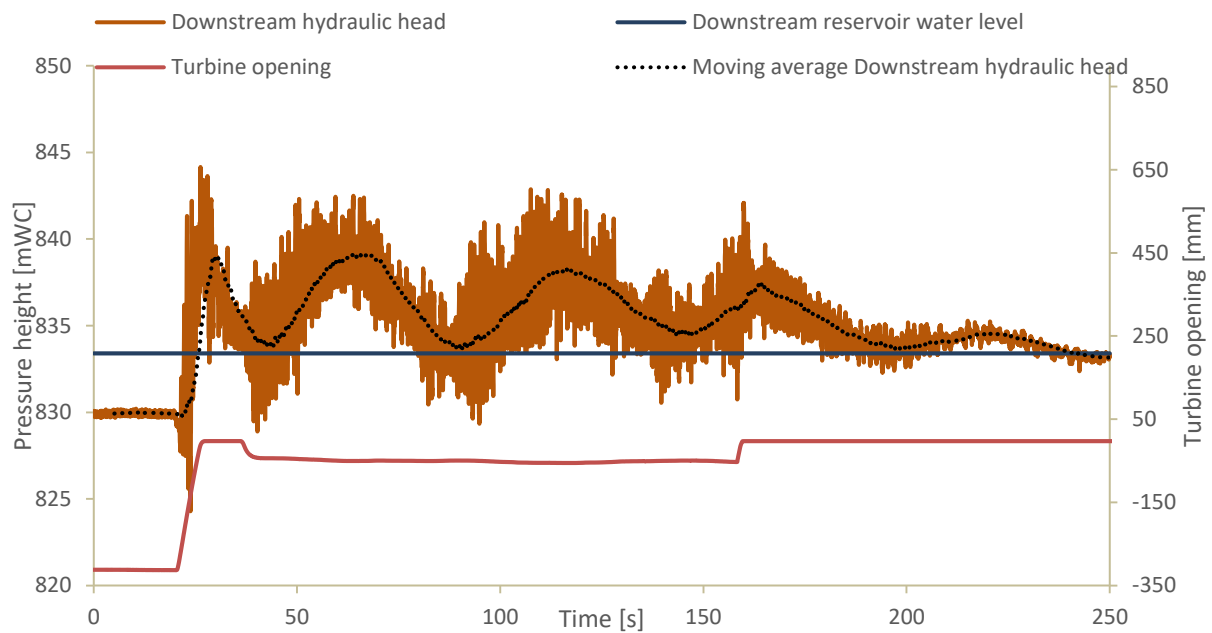


Figure 3.18. Downstream hydraulic head, water level in reservoir and turbine opening during the shutdown

Such an increase of hydraulic head down the turbine can not be explained by the hydraulic losses, even more considering that the rise of the velocity head should decrease the hydraulic head. Furthermore, if the head losses between the sensor and the surge tank, and the water velocity are considered small, it should be possible to assimilate the water table movements inside the surge tank with the moving average of the hydraulic head down the turbine. According to Figure 3.18, it should then almost reach 840 m. However, the visual observation of the water table movements inside the downstream surge tank during the shutdown contradicts this statement. It was indeed estimated that the highest level reached by the water was still several meters under the observation point located at a 840 m level.

Considering all the facts mentioned above, the hypothesis is made that the rise of pressure only appears locally and isn't perceptible in other parts of the powerplant. It could be related to a turbulence of the flow at the sensor level resulting in a local increase of pressure or something similar. The LVTrans software can not simulate this kind of phenomena. To be able to calibrate the model downstream the turbine, the hydraulic head coming from the measurements is adjusted by lowering it down by 2.5 meters, the value found in Table 3.11. This way, the oscillations are centred on the reservoir level and the calibration can be carried out.

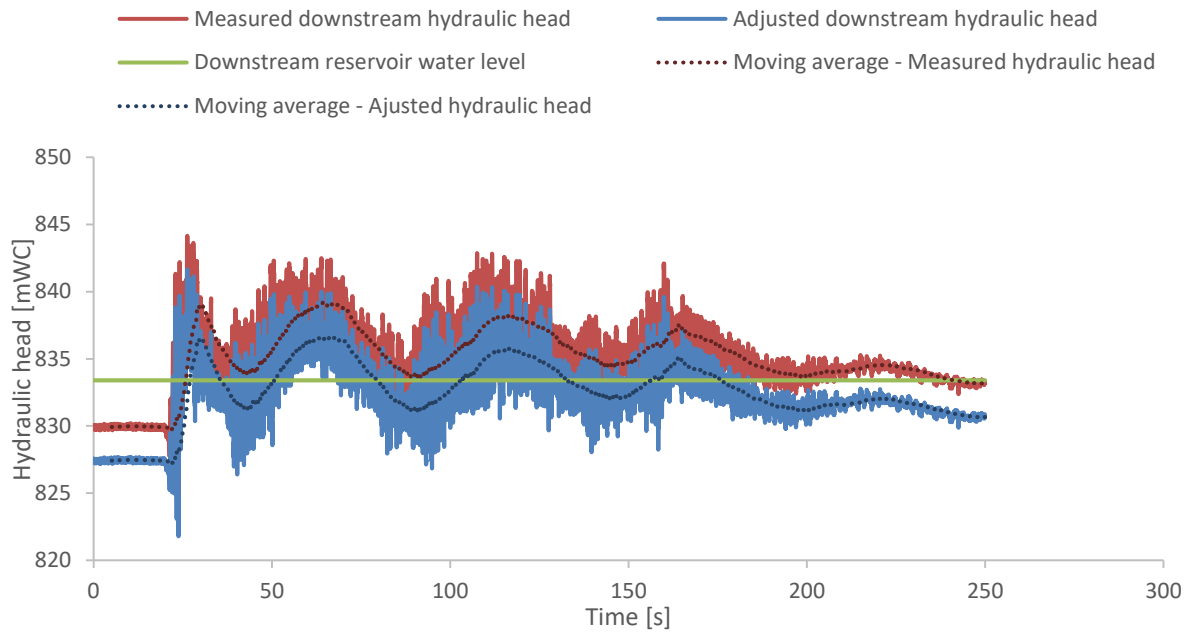


Figure 3.19. Adjusted downstream hydraulic head

### 3.1.2.3.2 Upstream the turbine

The pressure upstream the turbine is mainly influenced during the shutdown by the interaction between the surge tank and the creek shaft and their inner characteristics. Other parameters can impact it such as the tunnels diameters and lengths or the friction repartition between the reservoir, the creek shaft, the surge tank and the turbine. However, either their effects are small compared to the changes that can be caused by a modification of the creek shaft or surge tank parameters, or their values are considered known and should not be changed.

Among a large amount of tested combinations, the one which seems to provide the best results features the parameters shown in Table 3.12, with the diameter of the surge tank referring to its main shaft diameter. The hydraulic head simulated with this calibrated model, compared to the one coming from the measurements, is displayed in Figure 3.20.

	<b>D [m]</b>	<b>C<sub>vp</sub> [m<sup>5</sup>/s<sup>2</sup>]</b>	<b>C<sub>vm</sub> [m<sup>5</sup>/s<sup>2</sup>]</b>
<b>Creek shaft</b>	21	35	100000
<b>Surge tank</b>	60	100	100

Table 3.12. Optimized set of parameters in the upstream section

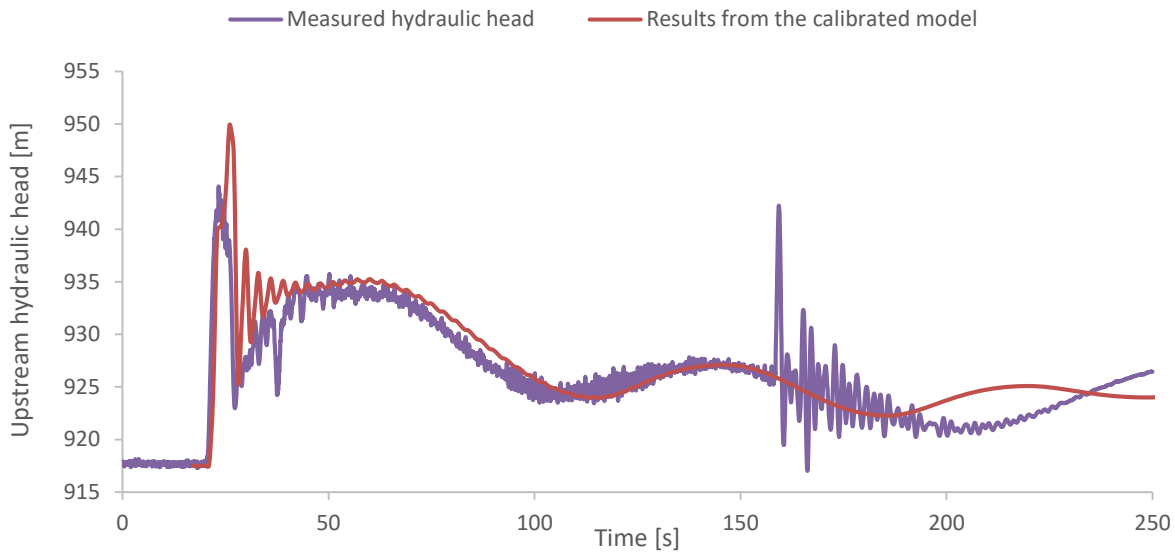


Figure 3.20. Simulated hydraulic head from the calibrated model compared to the measured one

The first spike reaching almost 945 mWC in the measured hydraulic head represents the water hammer caused by the turbine closing. As this thesis focuses on the water level in the surge tanks and not the water hammer, not much care is brought to the calibration of its value, which is why the simulated value reaches 5 mWC more than the measured one. The simulated values follow then well the measured ones in the larger oscillation that is issued by the mass oscillation. This oscillation follows the water table level in the surge tank, which is the main point of interest of this thesis. This tends to show that the water movements are well represented until the set of spikes at the 160<sup>th</sup> second, taking place when the turbine closes for the second time and the ball valve starts closing as seen in chapter 3.1.2.3.1. This phenomenon can not be simulated and it has been accepted that the simulated values aren't representing what is really happening after its occurrence.

To better visualize the impact of the parameters on the simulation results, the value of each of them are changed separately and the resulting hydraulic heads are plotted.

### Upstream creek shaft

Before studying the impacts of the variation of the creek shaft parameters, the effect of the implementation of the creek shaft in its whole is reviewed. As shown in Figure 3.21, the hydraulic head oscillation has both a way larger period and amplitude when no creek shaft is involved.

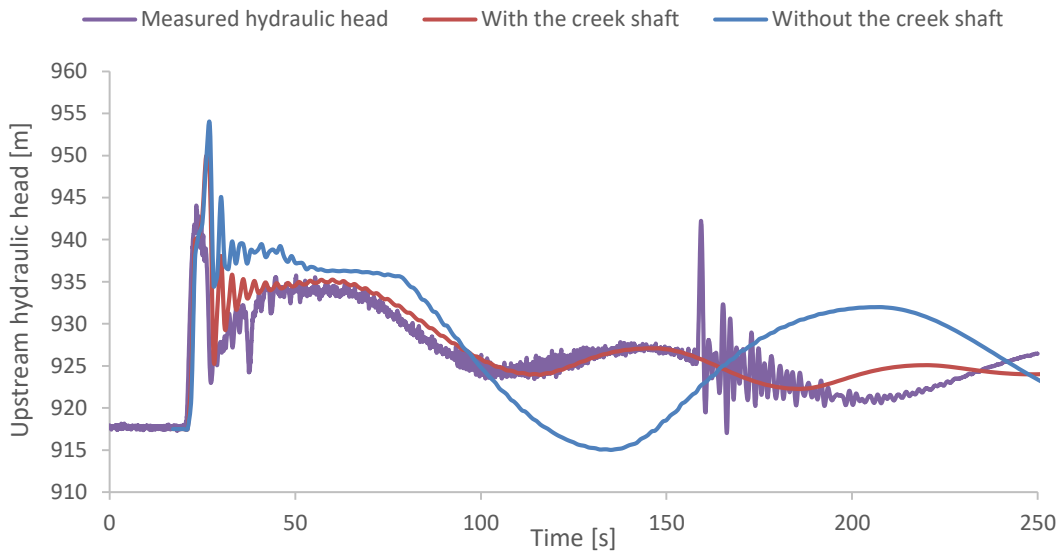


Figure 3.21. Simulated upstream hydraulic head with / without creek shaft

The equivalent diameter of the creek shaft according to the drawings measures about 8 meters, as seen in chapter 3.1.1.3. However, as shown in Figure 3.22, the water oscillation with this value is way too large and resembles the one simulated without any creek shaft. To obtain the right representation of the mass oscillations, a diameter of 21 meters must be implemented. This value seems really high but is necessary to correctly represent the oscillations.

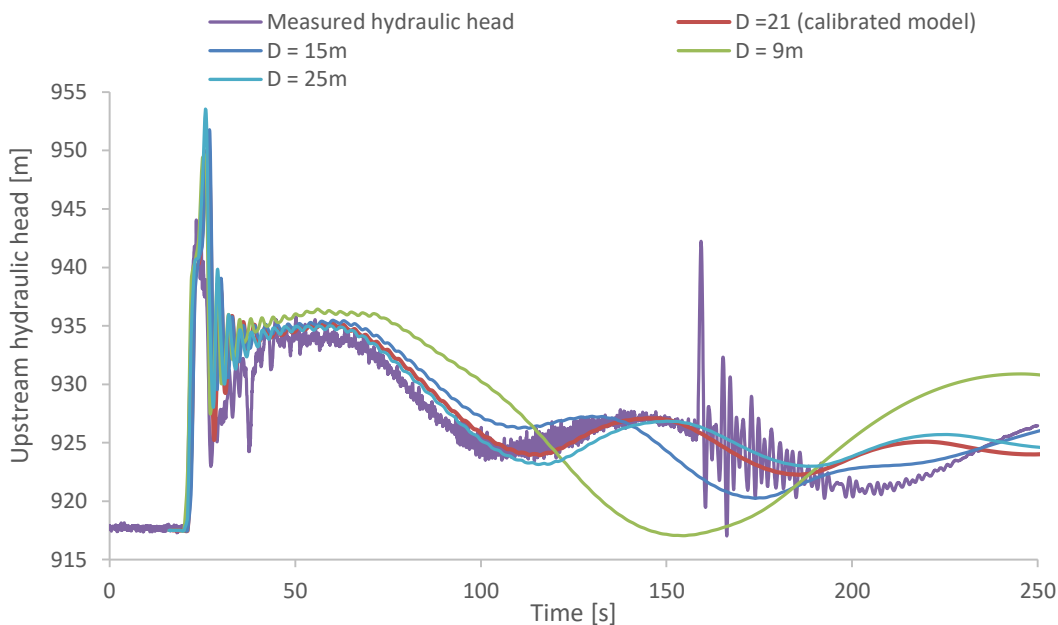


Figure 3.22. Simulated upstream hydraulic head for different creek shaft diameters

Finally, the friction coefficients in the creek shaft are studied. There are two of them: the first one,  $C_{vm}$ , characterizes the friction taking place during the rise of the water and the second one,  $C_{vp}$ , is used when the water is going down. As shown in Figure 3.23, when  $C_{vm}$  is too low, the hydraulic head rises too slowly after the end of the first drop down around the 100<sup>th</sup>

second. On the other hand, if  $C_{vp}$  is too high, the hydraulic head evolution doesn't follow the measurements at all. This results in a big difference in friction between the rising and the dropping of the water in the creek shaft that can't be explained by its design as there are no asymmetrical throttle of any kind. Furthermore, the friction coefficient  $C_{vp}$  is really low considering that a discharge of  $50 \text{ m}^3/\text{s}$  would result in a head loss of 36 mWC.

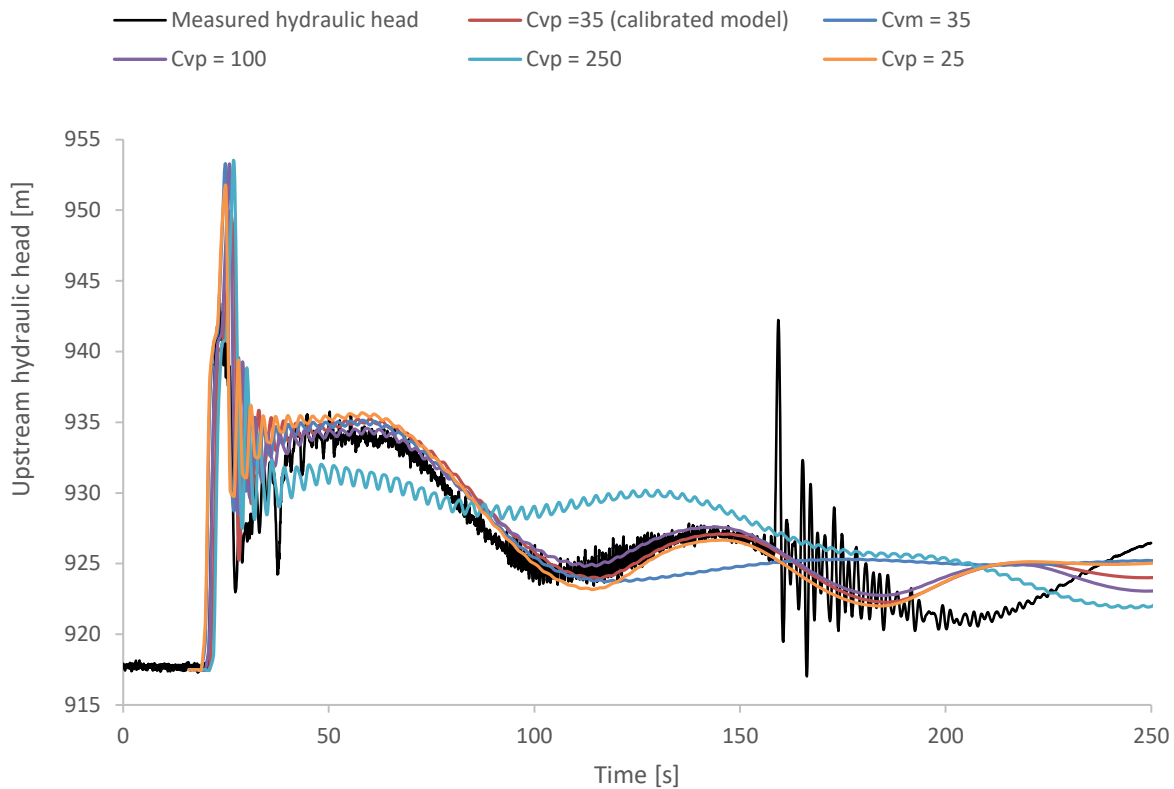


Figure 3.23. Simulated upstream hydraulic head for different friction coefficients in the creek shaft

### Upstream surge tank

The same process is realized with the upstream surge tank. First, several friction coefficients are tried out. As seen in Figure 3.24, if  $C_{vp}$  is too high, the water hammer isn't correctly dampened and the pressure oscillates too much. If it is too low, the dampening of the mass oscillations is too high. The value of  $C_{vm}$  doesn't influence much the results in this case, it is then chosen to take the same one as  $C_{vp}$ . In this case too, the friction coefficients seem too low to be realistic, as a  $50 \text{ m}^3/\text{s}$  discharge would result in a 12.5 mWC head loss.



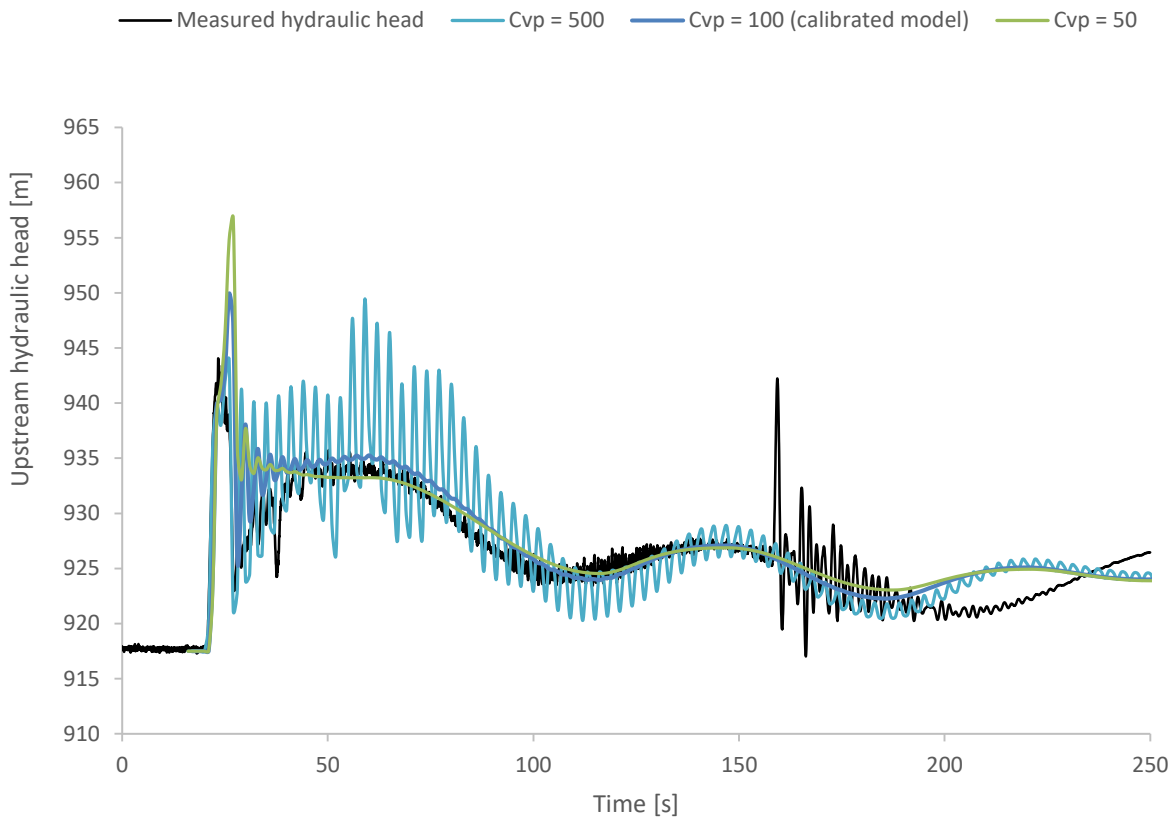


Figure 3.24. Simulated upstream hydraulic head for different friction coefficients in the surge tank

The diameter of the surge tank influences the mass oscillation period and amplitude. According to Figure 3.25, the period of the mass oscillation is depicted a little bit better with a 55 meters diameter of the main shaft in the surge tank. However, a 60 meter diameter gives a better amplitude and match the diameter found in the drawings, which is why it has been preferred in the calibrated model.

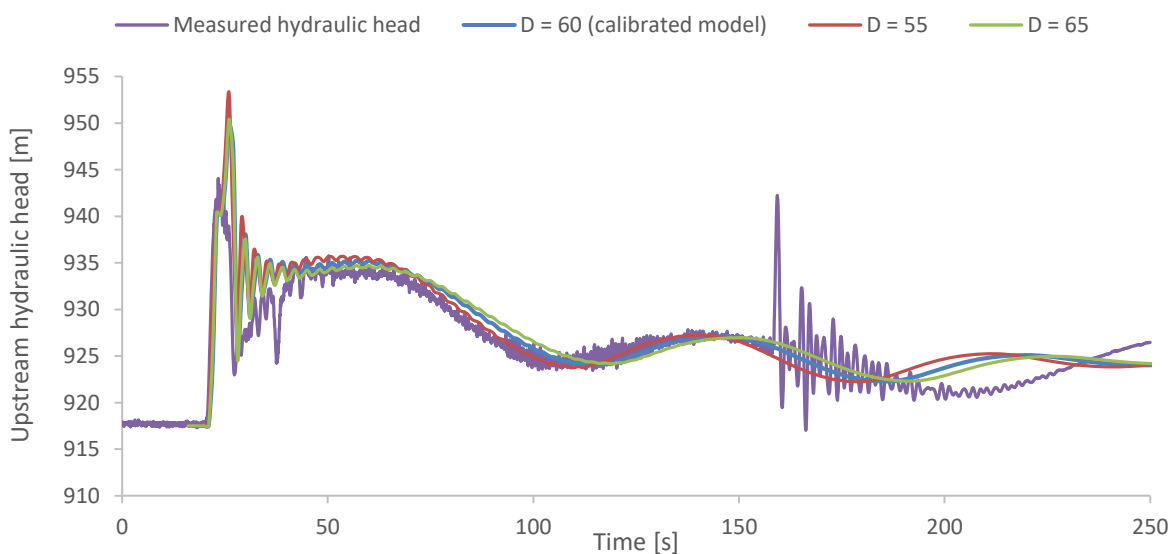


Figure 3.25. Simulated upstream hydraulic head for different surge tank diameters

### 3.1.2.3.3 Downstream

The downstream calibration of the shutdown is based on the adjusted hydraulic head presented in chapter 3.1.2.3.1, until the second closing of the turbine at the 160<sup>th</sup> second.

For this part of the model, the main parameters influencing the evolution of the pressure during the shutdown are related to the surge tank. As for the upstream calibration, many combinations of parameters have been tested and the one presenting the results with the best similarities is presented in Table 3.13.

<b>Cv [m<sup>5</sup>/s<sup>2</sup>]</b>	<b>D [m]</b>
700	10.3

Table 3.13. Downstream surge tank parameters in the calibrated model

The hydraulic head simulated with this calibrated model, compared to the one coming from the measurements, is displayed in Figure 3.26. The first drop and rise of the hydraulic head taking place between the 25<sup>th</sup> and the 50<sup>th</sup> seconds are not well represented by the model. The drop is related to the water hammer and water is still flowing while it occurs as the turbine is closing. It is therefore difficult to model it correctly without spending extensive time on it, which is not the purpose of this thesis. However, the measured rise of the hydraulic head above the reservoir water level around the 28<sup>th</sup> second is hard to explain. The water table in the surge tank should theoretically drop like it does in the simulation, which should make the hydraulic head at the turbine drop as well.

After the 50<sup>th</sup> second and the reopening of the turbine, the simulated hydraulic head follows the adjusted one pretty well until around the 160<sup>th</sup> second when the turbine closes definitively. The simulated results then gradually come closer to the measured values and reach them around the 220<sup>th</sup> second.

The amplitude and the period of the oscillations between the 50<sup>th</sup> and the 160<sup>th</sup> seconds are well represented, which support the hypothesis that the movements of the water table inside the surge tank are properly depicted in the model.

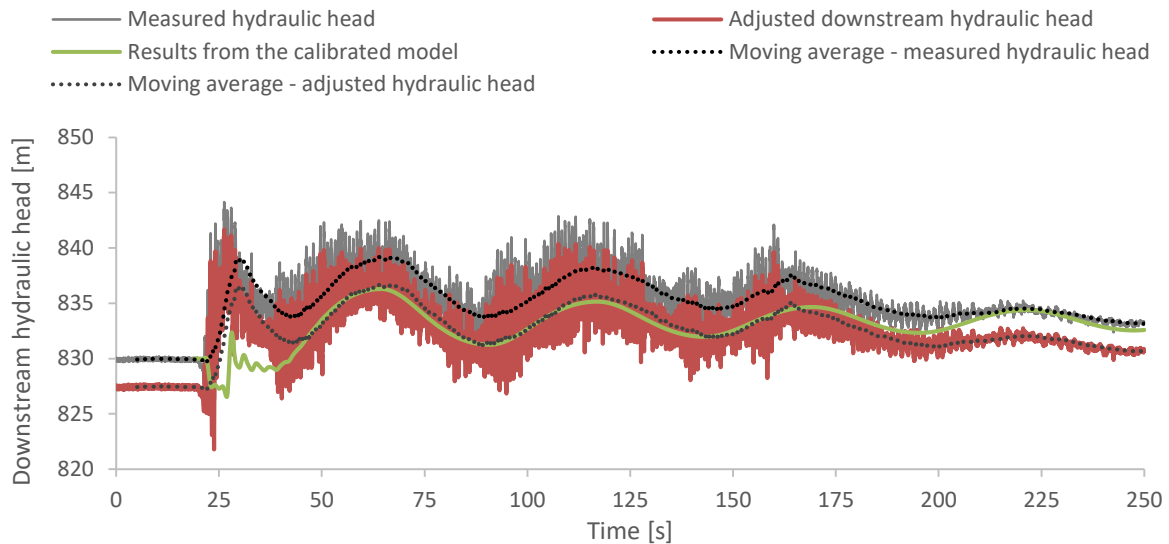


Figure 3.26. Simulated hydraulic head from the calibrated model compared to the adjusted one

As for the upstream calibration, the effects of the variation of the main parameters of the surge tank are studied in the following section.

### Downstream surge tank

The friction coefficients inside the surge tank are first considered. It is admitted that coefficients  $C_{vp}$  and  $C_{vm}$  have the same values. As seen in Figure 3.27, the amplitude of the simulated oscillations depends directly on the friction coefficient. A value of  $700 \text{ m}^5/\text{s}^2$  seems to make the best fit. This friction coefficient seems more realistic than the ones found in the upstream calibration. However, it is still low considering that a  $50 \text{ m}^3/\text{s}$  discharge would result in a  $3.6 \text{ mWC}$  head loss and no throttle of any kind is implemented in the surge tank.

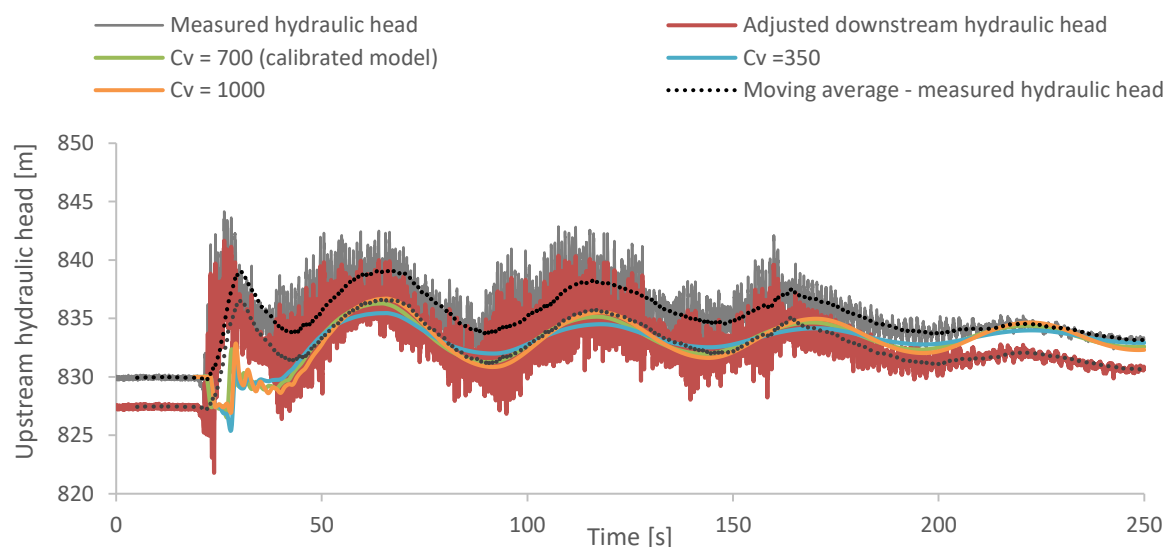


Figure 3.27. Simulated downstream hydraulic head for different friction coefficients in the surge tank

The surge tank diameter influences not only the amplitude of the simulated oscillations but also their period, as shown in Figure 3.28. The diameter that seems to make the best fit is equal to 10.3 meters, which is in the right range of values according to the drawings.

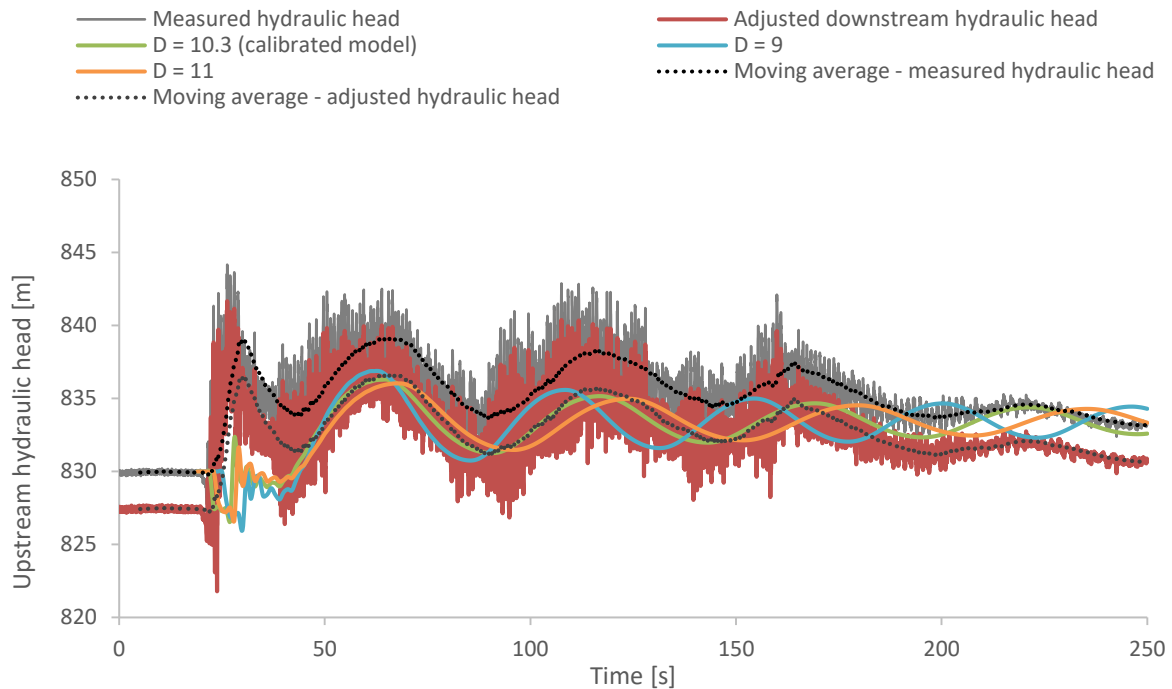


Figure 3.28. Simulated downstream hydraulic head for different surge tank diameters

### 3.2 Transformation into a pumped storage system

The calibrated model of the Roskrepp powerplant is now modified to simulate a pumped storage system and how this upgrade would affect the movements of the water level in the surge tanks. The purpose is to investigate whether the existing surge tanks need to be upgraded. This part describes the modifications operated on the model, along with the simulations carried out to determine the highest and lowest levels reached by the water in both surge tanks. The results are then compared to the surge tanks boundaries displayed in Table 3.14 to check if the surge tanks are able to absorb the mass oscillations in the new conditions generated by the pump addition.

	Upstream		Downstream	
	Max	Min	Max	Min
<b>Design from drawings [m]</b>	940	879	840	820

Table 3.14. Surge tanks boundaries according to the drawings

### 3.2.1 Model

The upgraded model simulates a situation where a pump is implemented in the powerplant in parallel with the turbine. Its layout is displayed in Figure 3.29 and Figure 3.30. To prevent cavitation, the pump is placed 10 meters below the turbine. It is recommended to avoid very small lengths in the model pipes as computational mistakes could distort the results. The position of the junctions between the pipes leading to the turbine and the ones leading to the pump are chosen accordingly.

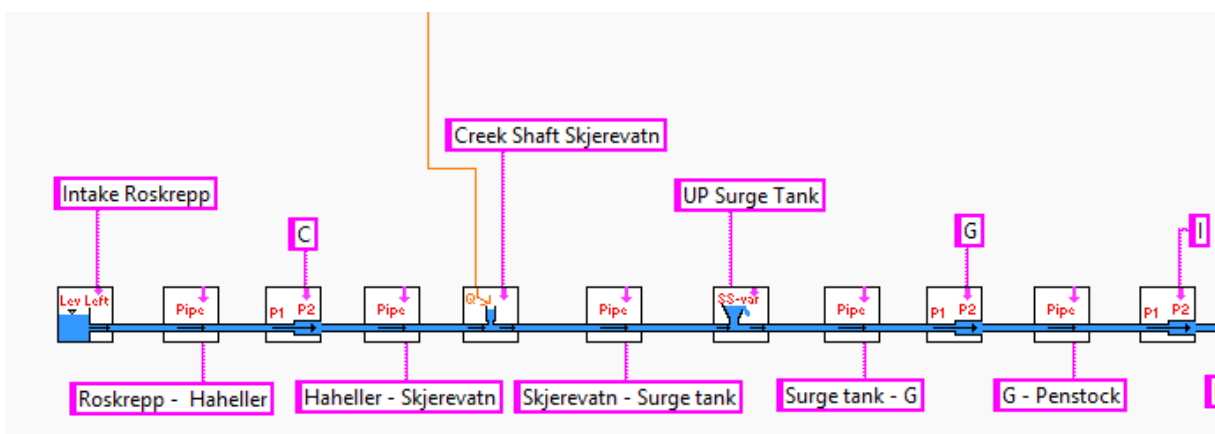


Figure 3.29. LVTrans upgraded model from the intake to the pipe connection I

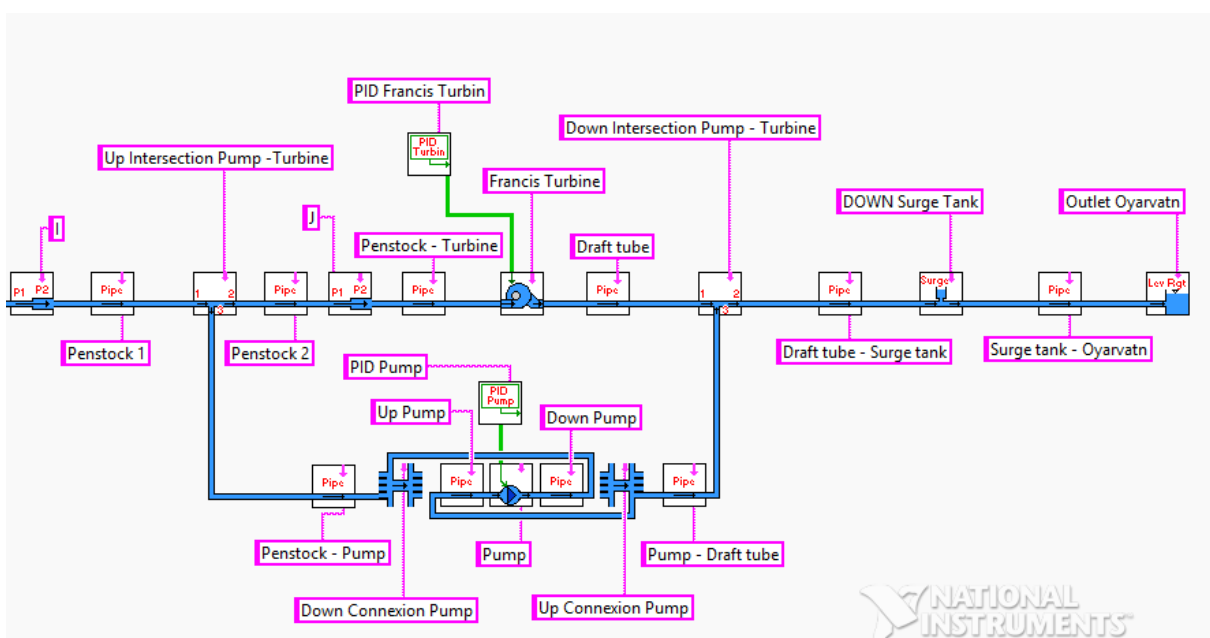


Figure 3.30. LVTrans upgraded model from the pipe connection I to the lower reservoir

The pump parameters used in the model are based on the excel sheet provided with the software in which the inputs summed up in Table 3.15 are introduced. The rated speed and the rated head

are similar to those of the turbine and the rated discharge is chosen so that the rated power is equal to 50 MW. The efficiency coefficient  $\eta$  is a conventional value used in a pump design.

Input		Parameters introduced in LVTrans	
Rated speed [rpm]	250	Nr [rpm]	250
$\eta$ [-]	0.9	Qr [m <sup>3</sup> /s]	55.2
Hr [m]	83	Hr [m]	83.00
Qr [m <sup>3</sup> /s]	55.21	Tr [Nm]	1909836
$\rho$ [kg/m <sup>3</sup> ]	1000	Pr [MW]	50
		I0 [kgm <sup>2</sup> ]	362137

Table 3.15. Pump parameters in the upgraded model

### 3.2.2 Simulation

The purpose of the simulations performed on the upgraded model is to evaluate the lowest and highest level that could be reached inside the surge tanks. The simulation scenarios are first established, then the simulation are carried out.

#### 3.2.2.1 Load cases studied

The worst-case scenarios are identified to simulate the highest and lowest water level that can be reached in the surge tanks. Two combinations of turbine and pump operations are established, the first one starting with the pump functioning at full power and the second with the turbine. The power produced by the latter when it is switched on is either 50 MW or the power produced with a maximum discharge of  $Q = 70 \text{ m}^3/\text{s}$ . The reservoirs levels are then chosen to create the worst-case scenarios. The 6 seconds closing time of the turbine used in the model calibration is regarded as the shortest possible and kept as it is for the following simulations.

#### Scenarios of turbine and pump operations

The first configuration starts with the pump running at full power and shutdown, with the turbine starting at the same time. The water level in the surge tank either rises (downstream) or drops (upstream) then changes direction. When the water level almost stops dropping (downstream) or rising (upstream), the turbines are shut down and the pump starts up. Finally, the pump is shut down after the water level rises again (downstream) or drops (upstream).

The same process is carried out in the second configuration but this time with the turbine running and being shut down in the beginning. Two cycles of turbine and pump being started then shut down are performed.

Both combinations are summed up in Table 3.16.

<b>Config. 1 – starts with pump at full power</b>	<b>Config. 2 – starts with turbines at full power</b>
(1) Pumping at full power	(1) Turbines at full power
(2) Shutdown pump	(2) Shutdown turbines
(3) Start-up turbines	(3) Start-up pump
(4) Shutdown turbines	(4) Shutdown pump
(5) Start-up pump	(5) Start-up turbines
(6) Shutdown pump	(6) Shutdown turbines
	(7) Start-up pump
	(8) Shutdown pump

Table 3.16. Scenarios of turbine and pump operations

## Water level in the reservoirs

According to the drawings, the highest water level that can be reached in the upper reservoir is 929 meters while its lowest is 890 meters. The water level in the lower reservoir stays between 825 meters and 837 meters. To provoke the largest mass oscillations in the downstream part, the water level in the upstream part must be set to have the highest possible discharge at the turbine before the shutdown. The more the head difference between the upstream and the downstream of the turbine is small and the more the discharge is high to produce a same power. The water level in the upstream reservoir must then be set to its lowest level, that is 890 meters, when the water level in the downstream surge tank is investigated. In the same way, the water level in the downstream reservoir must be set to its highest level, that is 837 meters, when the water level in the upstream surge tank is examined.

The power produced by the turbine during the worst-case simulations for different combination of water levels in the reservoirs is displayed in Table 3.17.

Upstream reservoir Water level [m]	Downstream reservoir Water level [m]	Power produced by the turbine [MW]
929	837	50
890	837	26.2
890	825	36.5

Table 3.17. Water level combinations and power produced in the worst-case scenarios

### Worst-case scenarios

The worst-case scenarios have been identified for the highest and lowest levels that can be reached inside both surge tanks and are displayed in Table 3.18. It should be noted that the configurations are specifically chosen for this model and that afterward, both will be tested for each water level combination in the reservoirs.

Scenarios	Upstream water level [m]	Downstream water level [m]	Config
<b>A</b> $z_{max}$ in upstream surge tank	929	837	2
<b>B</b> $z_{min}$ in upstream surge tank	890	837	1
<b>C</b> $z_{max}$ in downstream surge tank	890	837	1
<b>D</b> $z_{min}$ in downstream surge tank	890	825	2

Table 3.18. Worst configurations for the upgraded model

#### 3.2.2.2 Water levels in the surge tanks

The simulations are carried out on the upgraded model with the conditions described in Table 3.18. The water levels simulated in the upstream surge tank for scenarios A and B are displayed in Figure 3.31, along with the surge tank boundaries. Figure 3.32 shows the water levels in the downstream surge tanks for scenarios C and D, with the surge tank boundaries.

According to the simulations, the water level in the upstream surge tank would reach 880.7 meters at its lowest and 936.8 meters at its highest. In the downstream surge tank, the water level would move between 817.5 meters and 843.6 meters.



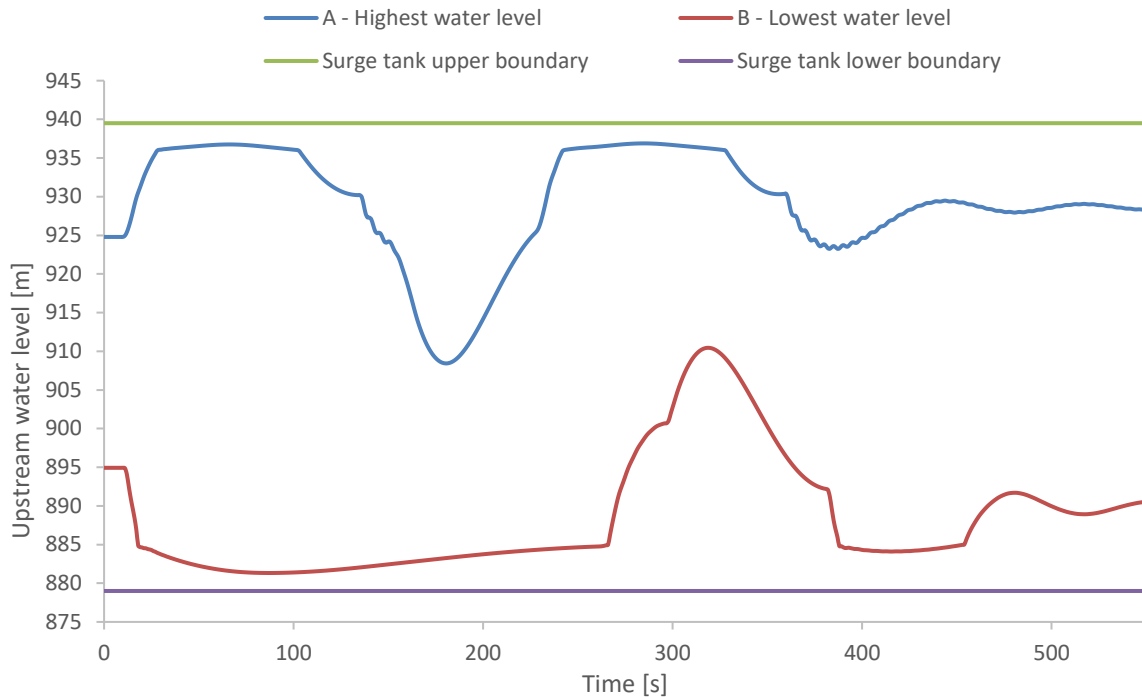


Figure 3.31. Extreme simulated water level in the upstream surge tank

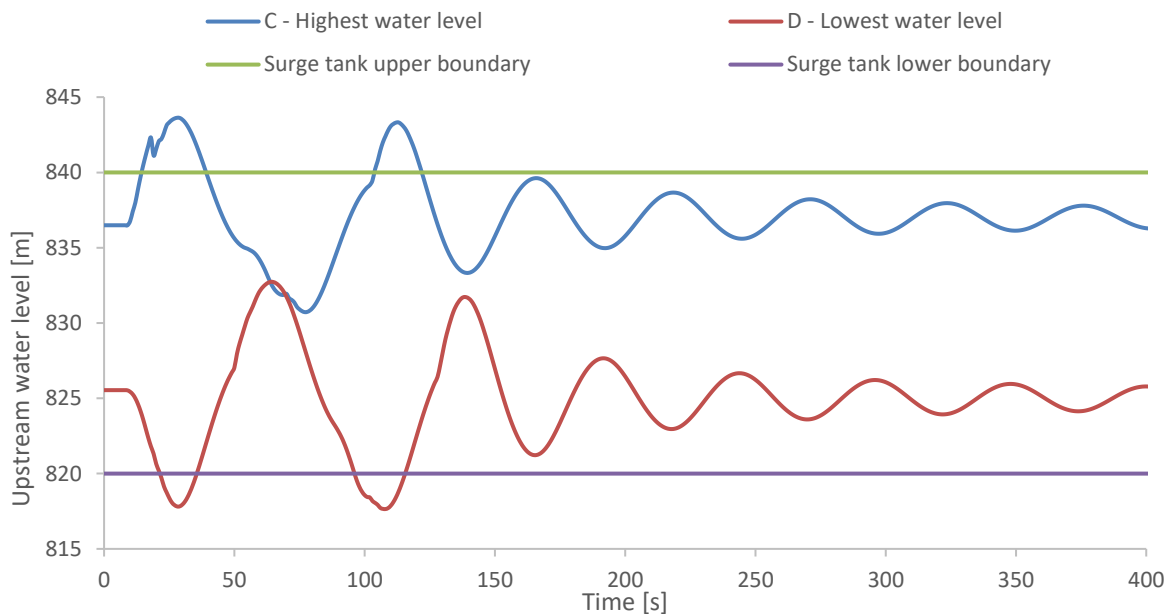


Figure 3.32. Extreme simulated water level in the downstream surge tank

### 3.2.3 Upgrade impact

The simulated maximum and minimum water levels in both surge tanks are summed up in Table 3.18 and compared with the surge tanks boundaries represented in the drawings. According to these simulations, the surge tank upstream the turbine is able to keep the water level between

its limits. It would therefore be possible to upgrade the powerplant without changing anything in the upstream surge tank.

However, the downstream surge tank's capacity is insufficient. The design maximum and minimum levels are largely exceeded in the simulations. Actions should then be taken to increase the downstream surge tank capacity.

	Upstream		Downstream	
	Max	Min	Max	Min
Simulated water level [m]	936.8	880.7	843.6	817.5
Surge tank boundary [m]	940	879	840	820

Table 3.19. Extreme design values in the surge tanks and corresponding simulated ones

### 3.3 Solutions proposal

According to the simulations, the upgrade of the Roskrepp powerplant into a pumped storage system would provoke a capacity insufficiency in the downstream surge tank. This part proposes three solutions that could be implemented to enhance the surge tank capacity so that the water table stays inside its boundaries. The solutions are implemented into the model presented in chapter 3.2.1 and tested to define their optimal designs. An economic analysis of each of them is then carried out.

#### 3.3.1 Simulation scenarios

The new models are tested in similar conditions as the ones described in chapter 3.2.2.1. However, this time both configurations of the pump and turbine are tested for each water levels combinations. Depending on the conditions, the configuration resulting in the largest mass oscillation amplitude is indeed different. The scenarios are summed up in Table 3.20.

Scenarios	Upstream water level [m]	Downstream water level [m]	Config.
<b>A</b> $z_{max}$	890	837	1
<b>B</b> $z_{min}$	890	825	1
<b>C</b> $z_{max}$	890	837	2
<b>D</b> $z_{min}$	890	825	2

Table 3.20. Simulation scenarios used to test the solutions

#### 3.3.2 Alternatives

This thesis is limited to the study of three different solutions to enhance the downstream surge tank capacity. The first one is an enlargement of the surge tank, the second is a transformation

into a variable surge tank and the third is an implementation of a throttle. This chapter describes those solutions and the simulations carried out to identify the optimal design of each of them.

### 3.3.2.1 Enlargement of the surge tank

A solution is to increase the equivalent diameter of the surge tank. The water then rises and falls at a slower pace and the amplitude of the oscillations decreases. In this case, the optimal design is the one able to keep the oscillations within the surge tank boundaries with the smaller excavation volume. To identify the optimal diameter several of them are tested. A selection of them is displayed in Table 3.21. The current surge tank cross-section is based on the values found in the calibration phase.

Test no.	D [m]	A [m <sup>2</sup> ]	Proposed dimensions [m x m]
<b>Current design</b>	10.3	83	5.6 x 15
<b>1</b>	22	380	12.7 x 30
<b>2</b>	24	452	15 x 30
<b>3</b>	26	531	15 x 35.4

Table 3.21. Simulated diameters

### 3.3.2.2 Transformation into a variable surge tank

A second solution is to transform the surge tank into a variable surge tank. This way, expansions are placed in strategic locations to slow down the water table movement and keep the oscillations within the surge tank boundaries. The excavated volume is then smaller than in the first solution.

The lower chamber is placed so that its top is at an 825 meters elevation. This way, when the water level in the downstream reservoir is at its lowest point, at 825 meters, the water table in the surge tank in steady state is still inside its main shaft. The bottom of the chamber joins the tail race tunnel at 820 meters. This facilitates the construction and this way, the surge tank is expanded near its boundary, which is a critical location.

The critical zone in the upper part of the surge tank is placed between the highest water level in the reservoir, at 837 meters, and the surge tank top, at 840 meters. To make the construction easier, the upper chamber is set to have a minimum height of 5 meters and is then placed between an 835 meters elevation and the top of the surge tank, at 840 meters.

Different combinations of chambers sections, displayed in Table 3.22, are tested in LVTrans. The optimal design keeps the water level within the surge tank boundaries for a minimal excavation volume.

Test no.	Upper chamber A [m <sup>2</sup> ]	Lower chamber A [m <sup>2</sup> ]
<b>Current situation</b>	-	-
<b>1</b>	400	300
<b>2</b>	400	250
<b>3</b>	450	200
<b>4</b>	450	250
<b>5</b>	450	300
<b>6</b>	500	250

Table 3.22. Chambers configurations

### 3.3.2.3 Implementation of a throttle

The third and last solution proposed in this study is to implement a throttle in the downstream surge tank. The throttle creates an additional head loss applied to the water moving inside the surge tank. It dissipates the energy of the mass oscillations and dampens them.

Two types of throttle can be distinguished, depending on their design. The symmetrical throttle creates the same head loss for both flow directions while the asymmetrical throttle is designed to create more losses in one way than the other. An asymmetrical throttle is more flexible and the head loss it creates can be adapted to the needs in the downward and the upward direction. However, its design is more complex. An asymmetrical throttle is usually build as a steel cone while a symmetrical one can take the form of simple concrete plug with a hole. Both types are tested to estimate which one is optimal in this case.

The throttle is placed at the bottom of the surge tank so that the water table never goes below it and that the water flowing in the surge tank always go through it. Its implementation occupiees space in the surge tank that cannot be filled with water, and the surge tank boundaries in the model should be changed accordingly. It is estimated that the introduction of a symmetrical throttle would require around 1 meters of the surge tank height. An asymmetrical throttle would need more space to be able to produce two different head loss coefficients. A 2 meters height is deemed necessary. The new boundaries that should be taken into account when analyzing the results are summed up in Table 3.23.

	Upper boundary [m]	Lower boundary [m]
<b>With symmetrical throttle</b>	840	821
<b>With asymmetrical throttle</b>	840	822

Table 3.23. Surge tank boundaries after the implementation of a throttle

### 3.3.2.3.1 Simulated values

The effect of a throttle in the surge tank is simulated by decreasing the coefficients  $C_{vp}$  and  $C_{vm}$  in the surge tank. As seen in chapter 2.1.3.3, these coefficients can be related to the singular loss coefficient  $\zeta$  by equation 3.5. The head loss simulated is inversely proportional to the coefficient  $C_v$ . Unlike for the symmetrical throttles, the two coefficients have different values for an asymmetrical throttle.

$$C_v = \frac{Q^2}{2\Delta H_s} = \frac{A^2 g}{\zeta} \quad (3.5)$$

The optimal design of the throttle reduces the oscillations enough to keep them within the surge tank boundaries for a minimal restriction of the water. A set of different coefficient combinations is tested to identify the optimal throttle that should be implemented. Table 3.24 summed up the simulated coefficients, along with their equivalent singular loss coefficients.

Test no.	$C_{vp}$ [ $\text{m}^5/\text{s}^2$ ]	$C_{vm}$ [ $\text{m}^5/\text{s}^2$ ]	$\zeta_p$ [-]	$\zeta_m$ [-]
<b>Current situation</b>	700	700	97	97
<b>1</b>	25	25	2723	2723
<b>2</b>	40	40	1702	1702
<b>3</b>	50	50	1361	1361
<b>4</b>	40	50	1702	1361

Table 3.24. Singular loss coefficients in the surge tank

### 3.3.2.3.2 Design of a symmetrical throttle

The symmetrical throttle is considered as concrete plug with a circular hole in it. It has been estimated that the hole is 1 meter thick. Its diameter is computed from the optimal coefficient  $C_v$  found in the surge tank. This coefficient reflects the loss coefficient in the whole surge tank, and not only the throttle. First, the coefficient attributed to the throttle must then be found. The hypothesis is made that the implementation of the throttle doesn't change the head losses in the rest of the surge tank. The new global head losses can then be considered as the addition of the head losses that would be produced in the surge tank without the throttle with the head losses

caused by the throttle itself. The head loss coefficient  $\zeta$  attributed to the throttle can be estimated by the following equation:

$$\zeta_{throttle} = \zeta_{new} - \zeta_{no\ throttle} \quad (3.6)$$

where: $\zeta_{throttle} [m^5/s^2]$	Head loss coefficient attributed to the throttle
$\zeta_{new} [m^5/s^2]$	Head loss coefficient in the new surge tank on which the throttle is implemented
$\zeta_{no\ throttle} [m^5/s^2]$	Head loss coefficient in the surge tank without throttle

The design of the throttle diameter is based on the formula proposed by Idelchick<sup>7</sup> and displayed in equations (3.7), (3.8) and (3.9) to estimate the head losses induced by a thick-edged orifice in a straight tube.

$$\zeta_{throttle} = \left( \zeta_0 + \lambda \frac{1}{D_h} \right) \left( \frac{F_1}{F_0} \right)^2 \quad (3.7)$$

$$D_h = \frac{4F_0}{\pi} \quad (3.8)$$

$$\zeta_0 = 0.5 \left( 1 - \frac{F_0}{F_1} \right) + \left( 1 - \frac{F_0}{F_1} \right)^2 + \tau \sqrt{1 - \frac{F_0}{F_1}} \left( 1 - \frac{F_0}{F_1} \right) \quad (3.9)$$

where: $\lambda [-]$	Friction coefficient
$F_{0,1} [m^2]$	Cross-section of the orifice (0) and the tube (1)
$\tau [-]$	Parameter depending on the ratio $l/D_h$
$l [m]$	Thickness of the hole

Iterations are carried out to find the maximal throttle cross-section for which the head loss coefficient is higher than the optimal coefficient found in the simulations. Finally, the throttle diameter is drawn from it.

### 3.3.3 Economic analysis

The economic analysis completed in this part presents a rough estimation of the costs that could be expected in the implementation of each solution. Many uncertainties surround the construction conditions and therefore the prices exposed here should be considered cautiously.

<sup>7</sup> (Idelchick, 1960)

A cost that concerns every solutions is the cost of the halting of production that is mandatory when working inside the downstream surge tank. It is very difficult to estimate its value without doing an in-depth study of the production earnings of the Roskrepp powerplant, but also of all the other powerplants placed downstream. Roskrepp has a large upper reservoir for annual storage of water and water spill is not likely, but the optimization of the production in the power market will be reduced. As a first approximation, outage in the summer months (May-September) is estimated to cost 0.5 million Norwegian kroner per month, while 2 million Norwegian kroner per month is considered for the remaining winter months.

An additional cost that would occur in all the solutions would be the price of the design and planning of the solution. An estimated cost of 500'000 kroner is considered.

The construction costs presented in the following parts are based on a Norwegian report<sup>8</sup> cataloguing the prices related to hydraulic constructions. All of the prices are given in Norwegian kroners and will be converted into Swiss francs by using an exchange rate of 0.1222 Swiss francs for one Norwegian krone.

### **3.3.3.1 Enlargement of the surge tank**

The enlargement of the surge tank induces excavation costs that depends on the volume of excavated rocks. The estimated cost of the excavation is based on the price used in the expansion of a cavern harboring a power station. An estimation of 400 to 500 kr/m<sup>3</sup> is used.

The construction of this solution would require to remove the construction machines from the bottom of the surge tank at the end of the excavation. The addit used during the construction of the powerplant could be reopened at this end. The concrete plug should then be rebuild at the end of the construction. The machines could also be elevated inside the surge tank from its top.

First, rocks should be excavated on a height of 20 meters. Then, the machines should be taken out of the surge tank and finally the concrete plug in the addit should be rebuild if the old addit is used. The estimation of the time needed to complete those tasks depends on the volume of material that should be excavated but a minimum of one to two months should be considered.

### **3.3.3.2 Variable surge tank**

The construction of the upper chamber added to the surge tank is similar to the construction of a tunnel, with a plug at one of their extremity. The lower chamber is placed just over the tail

---

<sup>8</sup> (Stensby, 2016)

race tunnel and can be seen as an expansion of the tunnel. As a simplification, the construction price of the lower tunnel is taken similar to the one of the construction of a new tunnel. The construction machines should access the tail race tunnel. A solution would be to reopen the addit used during the construction of the powerplant and to rebuild the plug afterward. The construction cost of the variable surge tank would then consider two tunnels and two concrete plugs.

The price in kroner estimated for a meter of blasted tunnel and depending on the tunnel section is displayed in Figure 3.33.

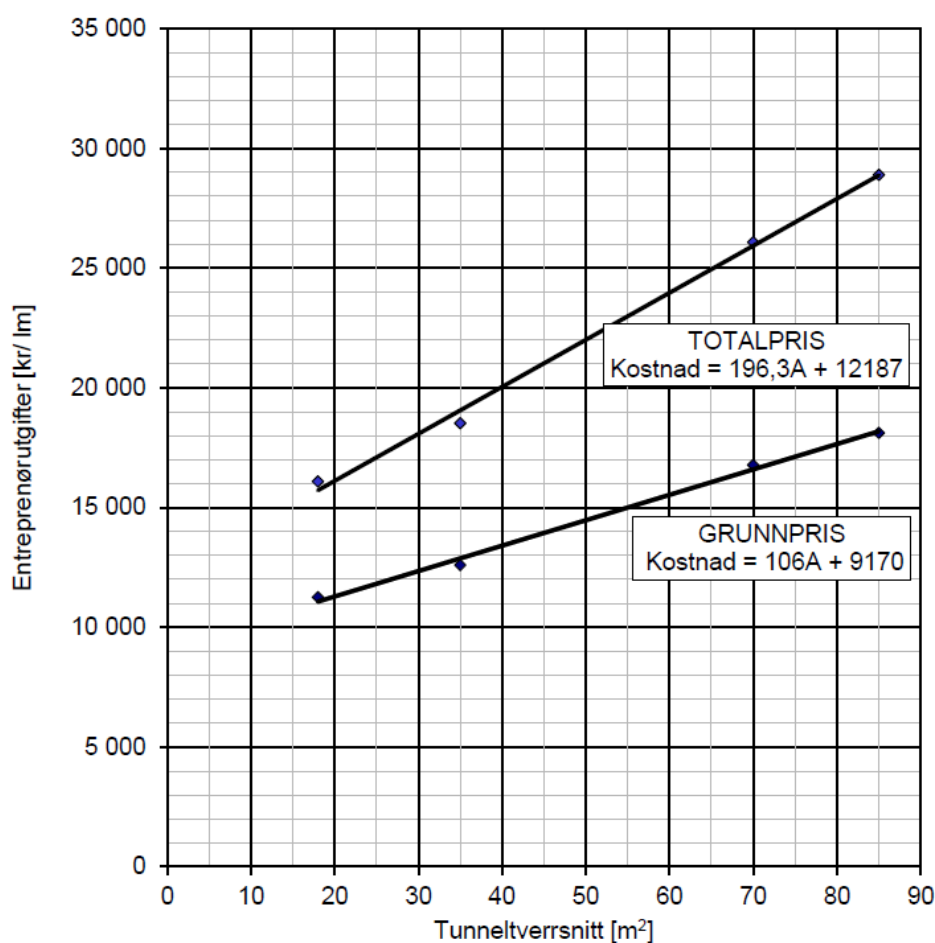


Figure 3.33. Estimated cost in NOK per meter of blasted tunnel, for different cross-section areas

The cost of a plug, depending on the design total head, is displayed Figure 3.34. The maximum head that can appear at one of the plugs level is equal to the height difference between the plug and the top of the surge tank, that is 20 meters for the lower chamber and 5 meters for the upper one. The tunnel section is larger than the largest section considered by the curves but as a first approximation, the formula for a design head of 30 meters is used.



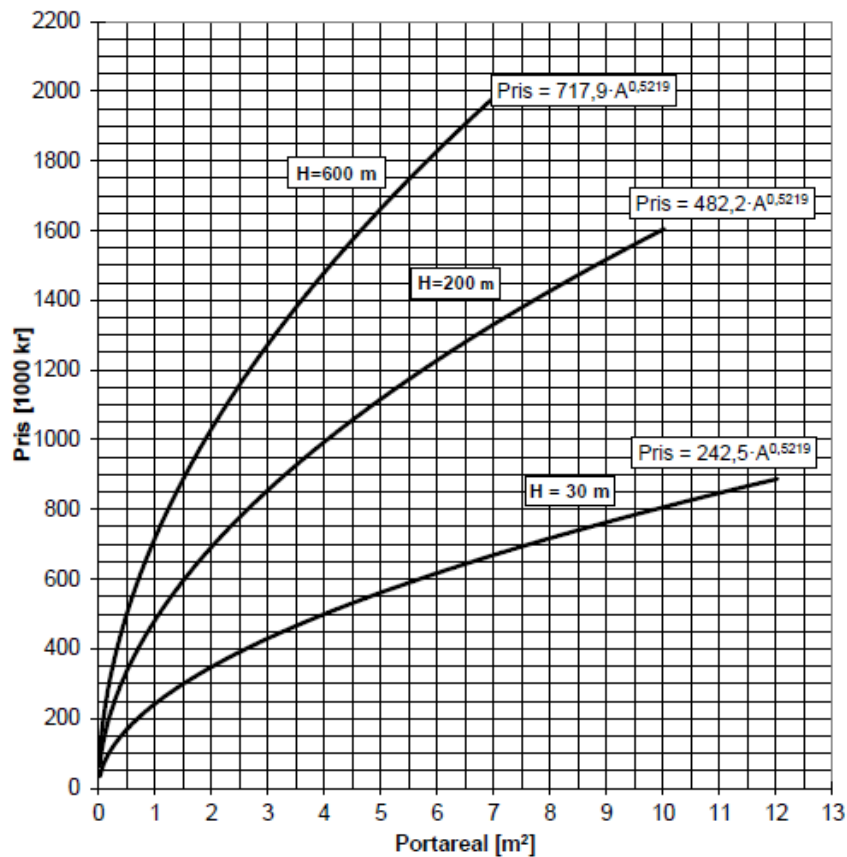


Figure 3.34. Estimated cost of a plug implemented in an addit tunnel

The construction of the upper tunnel could begin without interrupting the normal operation of the powerplant by starting the construction from the others extremities of the tunnel. This would reduce the time during which the tailrace tunnel must be empty and consequently reduce the cost of plant halt. The tailrace tunnel should however be emptied for the construction of the lower tunnel. Some time should then be taken to clean the tunnels and install the plugs. In total, the tail race tunnel should be empty for an estimated time of 4 to 8 weeks.

### 3.3.3.3 Throttle

The implementation of a throttle is not considered in the report regrouping the prices applied to hydraulic constructions. As an approximation, the throttle is treated as concrete plug, the price of which is displayed in Figure 3.34. The maximum head that can be applied to the throttle is the height difference between the throttle and the top of the surge tank, that is 20 meters. Thus, the curve for a head of 30 meters is used. The section of the surge tank is 8 times larger than the largest one considered by this curve. To have a rough estimation of the price of the throttle, the formula for the cost of a concrete plug with a total head of 30 meters is considered and tripled to take into account the largest area and the difficulties related to the vertical laying of the throttle.

The implementation of the throttle necessitates first that the construction machine access the bottom of the surge tank by reopening the addit used during the construction of the powerplant. Then a platform is built on which is placed the throttle. Its purpose is to support the throttle while the concrete plug is cast around it. Finally, the platform is dismembered, the tunnel cleaned and the plug in the addit rebuild. An estimated time of one to two months should be allocated to the construction of the throttle.

## 4 Results

Results from the simulations are presented in this chapter. The water level in the unmodified downstream surge tank, with the addition of a pump into the system, is first introduced. Then the possible designs of each solution are studied and finally, an economic analysis of those solutions is carried out.

### 4.1 Current surge tank

The current surge tank is first tested to identify the highest and lowest water level reached when a pump is added to the system. The evolutions of the water level in the downstream surge tank in the worst-case scenarios are displayed on Figure 4.1. The elevations of the actual surge tank boundaries are added as points of comparison.

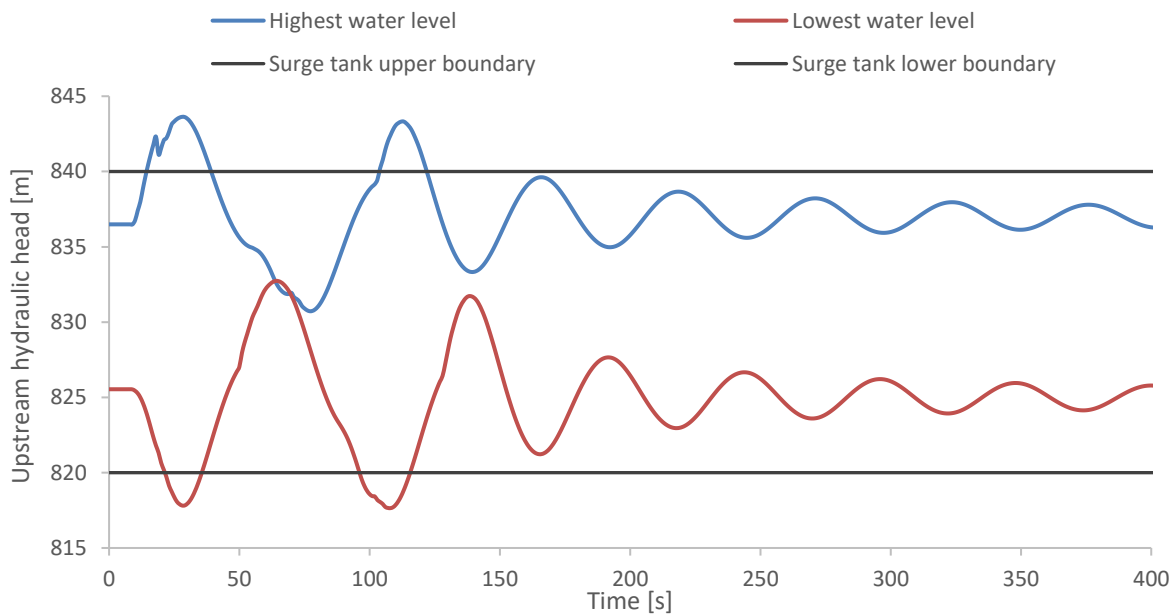


Figure 4.1. Extreme simulated water level in the downstream surge tank

As seen in the figure, the simulated water level goes way out of the boundaries of the surge tank. The water overtopping would flow inside the service cavern and could put the powerplant employees at risk. The water table moving under the surge tank lower boundary would allow air to enter and possibly damaged the tailrace tunnel. Measures must be taken to avoid those situations.

## 4.2 Solutions proposal

The purpose of the solutions proposed in this part is to keep the water table to go out of the surge tank boundaries. The simulation results are then studied to identify the optimal design of each solution that reach that goal for the smallest alteration of the surge tank. For each design, the simulations results of the scenarios summed up in Table 3.20 are plotted and compared with the surge tank boundaries.

### 4.2.1 Alternative I – Surge tank enlargement

Different diameters, listed in Table 3.21, are tested to identify the lowest one that could keep the water level inside the surge tank boundaries. Figure 4.2 and Figure 4.3 display the evolutions of the water level when simulating the worst-case scenarios.

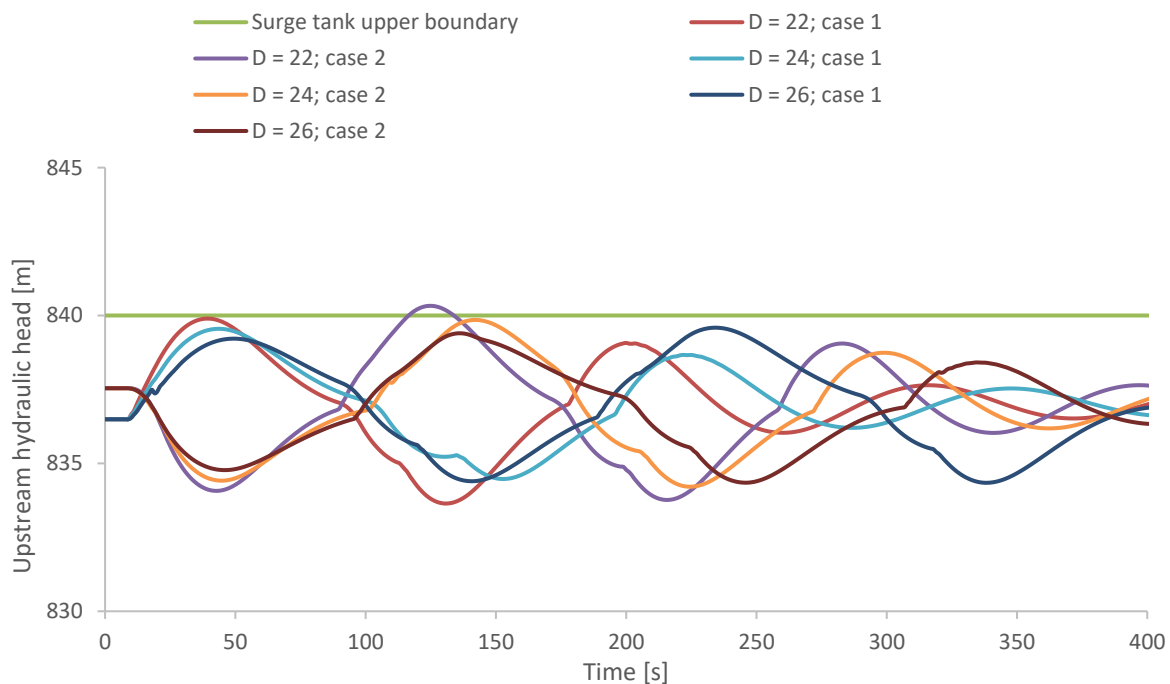


Figure 4.2. Highest water level in the surge tank for different surge tank diameters

As seen in Figure 4.2, the water level still overtops the surge tank upper boundary for a diameter of 24 meters. However, the enlargement of the surge to a diameter of 24 or 26 meters is successful in keeping the water level from overflowing. The optimal design has the lowest diameter possible. From the highest water level reached perspective, the optimal diameter would then be of 24 meters.

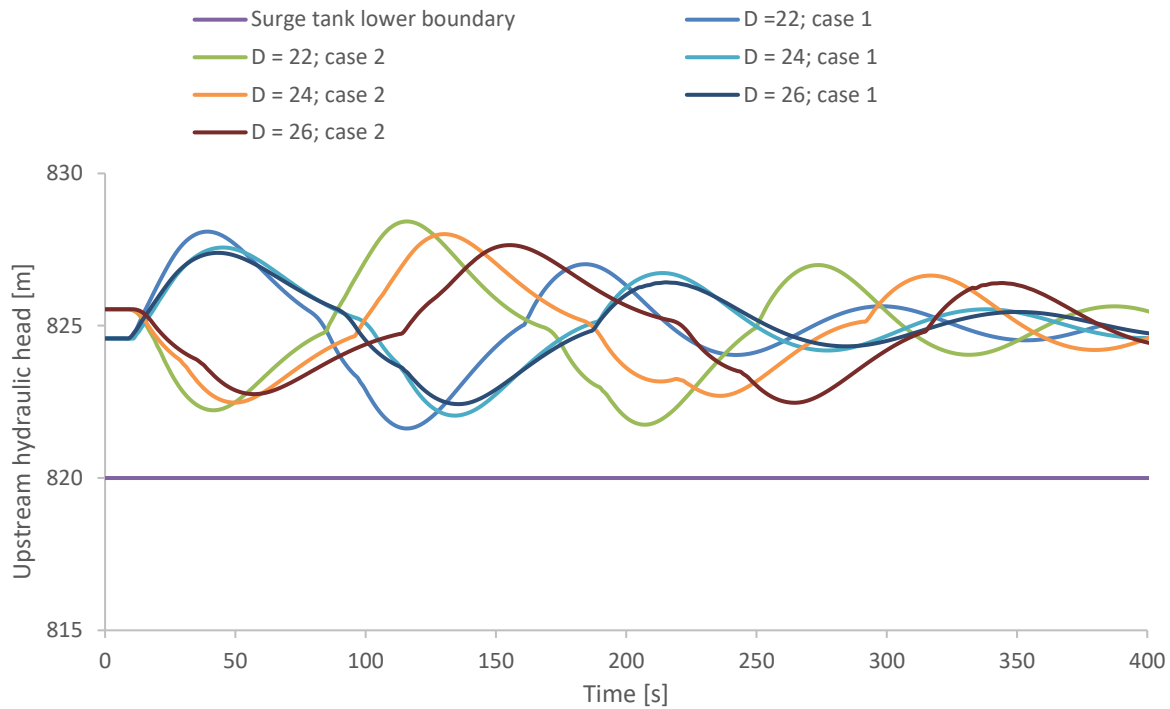


Figure 4.3. Lowest water level in the surge tank for different surge tank diameters

The lowest levels reached by the water for the tested diameters are shown in Figure 4.3. None of them goes near the lower boundary. The highest water level is then the most significant in the search of the optimal diameter and the value of 24 meters is validated.

The enlargement of the surge tank to obtain an equivalent diameter of 24 meters would increase its cross-section from  $83 \text{ m}^2$  to  $452 \text{ m}^2$ . Considering its height of 20 meters, that would imply a volume of  $7'380 \text{ m}^3$  of excavated rocks.

#### 4.2.2 Alternative II – Variable surge tank

The worst-case scenarios are simulated with several combinations of chambers to identify which one is able to contain the water level oscillations for a minimal excavation. The results of the water level simulations are displayed in Figure 4.4 and Figure 4.5. The maximum and minimum levels reached for the different combinations are summed up in Table 4.1.

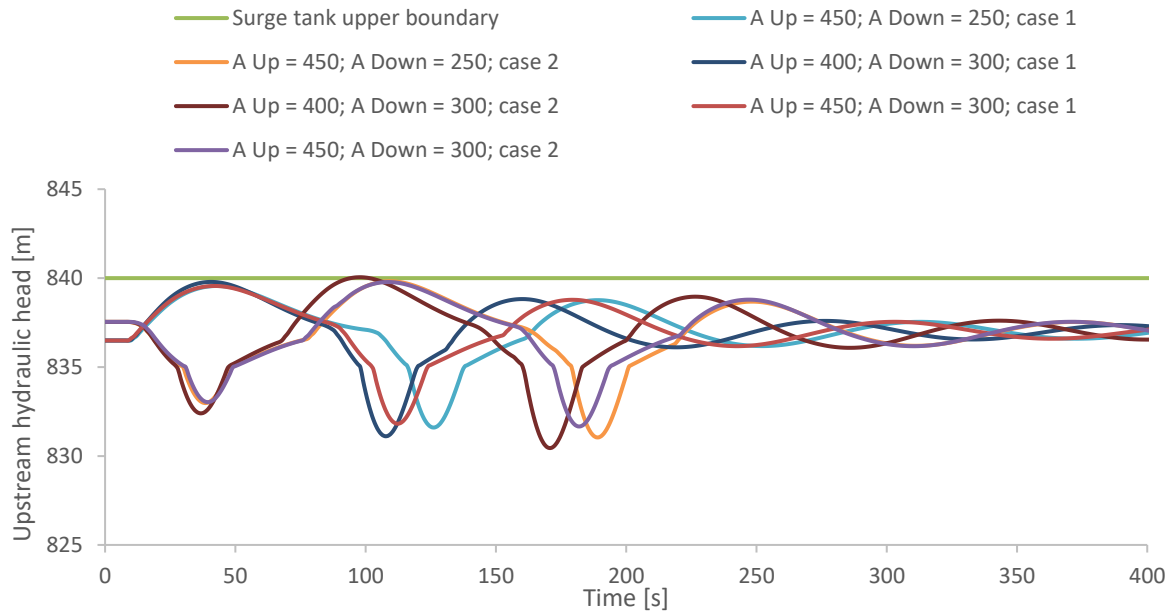


Figure 4.4. Highest water level in the variable surge tank for different chambers area

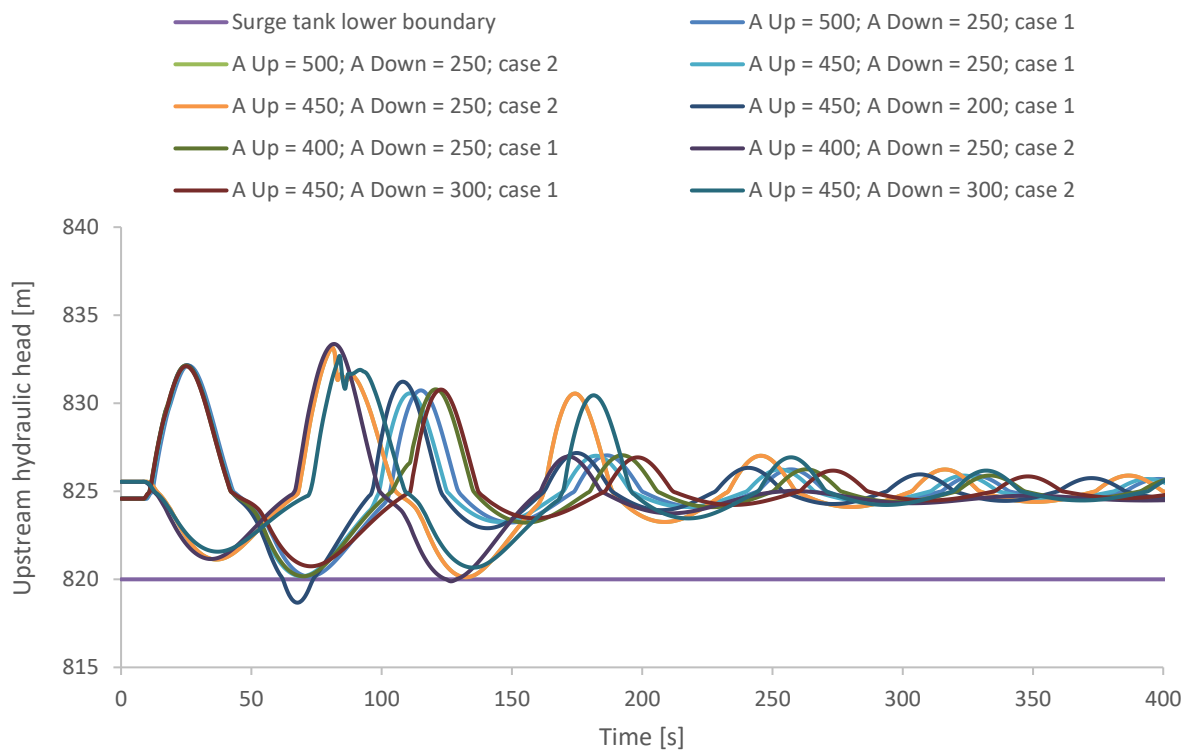


Figure 4.5. Lowest water level in the variable surge tank for different chambers area

<b><math>A_{up}</math> [m<sup>2</sup>]</b>	450	400	400	450	500	450
<b><math>A_{down}</math> [m<sup>2</sup>]</b>	200	300	250	250	250	300
<b>Max. water level [m]</b>	-	840.1	-	839.8	-	839.8
<b>Min. water level [m]</b>	818.7	-	819.9	820.1	819.9	820.7

Table 4.1. Maximum and minimum water level reached for each combination

According to the simulations results, the combination with the minimal volume of excavation for which the water is kept within the surge tank boundaries includes an upper chamber of 450 m<sup>2</sup> and a lower chamber of 250 m<sup>2</sup>. However, an additional simulation with the same lower chamber but a larger upper chamber of 500 m<sup>2</sup> results in the water level going under the lower boundary. In case the construction of the upper chamber results in an area larger than intended, the surge tank could then present the risk of the water level going too low. To prevent this from happening, a combination involving an upper chamber of 450 m<sup>2</sup> and a lower chamber of 300 m<sup>2</sup> is preferred.

The construction of such chambers, with a height of 5 meters for both, would result in the excavation of a total of 3'750 m<sup>3</sup> of rocks. This volume, while still significant, is way smaller than the one forecasted in the first alternative. If a square section with a 5 meters side is considered for the upper chamber, the length of the tunnel composing the chamber would then be of 90 meters. The lower chamber would be placed just over the tailrace tunnel and consequently have the same width of 7 meters. Its length would then be of 43 meters.

### **4.2.3 Alternative III – Throttled surge tank**

The implementation of a throttle in the surge tank is now investigated. First, the simulations involving symmetrical throttles are studied, then the implementation of an asymmetrical one is analysed. The values of  $C_v$  presented in chapter 3.3.2.3 are used.

#### **4.2.3.1 Symmetric**

As viewed in chapter 3.3.2.3, the implementation of a symmetrical throttle goes along with a 1 meters upward displacement of the lower boundary. The water levels simulated for different coefficients  $C_v$  in the worst case scenarios are displayed in Figure 4.6 and Figure 4.7. The extreme values are summed up in Table 4.2.

The simulations show that the lower boundary is never reached with the chosen  $C_v$  coefficients. However, the implementation of a coefficient  $C_v = 50 \text{ m}^5/\text{s}^2$  results in the water level reaching the upper boundary. The optimal throttle would then induce a global coefficient  $C_v$  of  $40 \text{ m}^5/\text{s}^2$  to keep the oscillations within the surge tank boundaries.

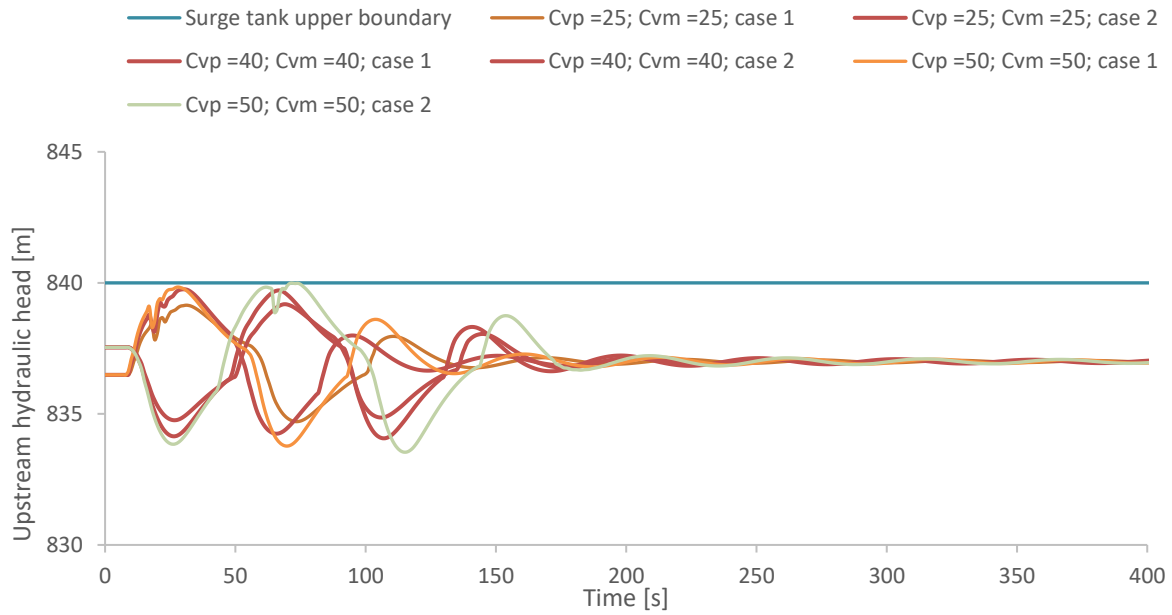


Figure 4.6. Highest water level in the variable surge tank for different throttles

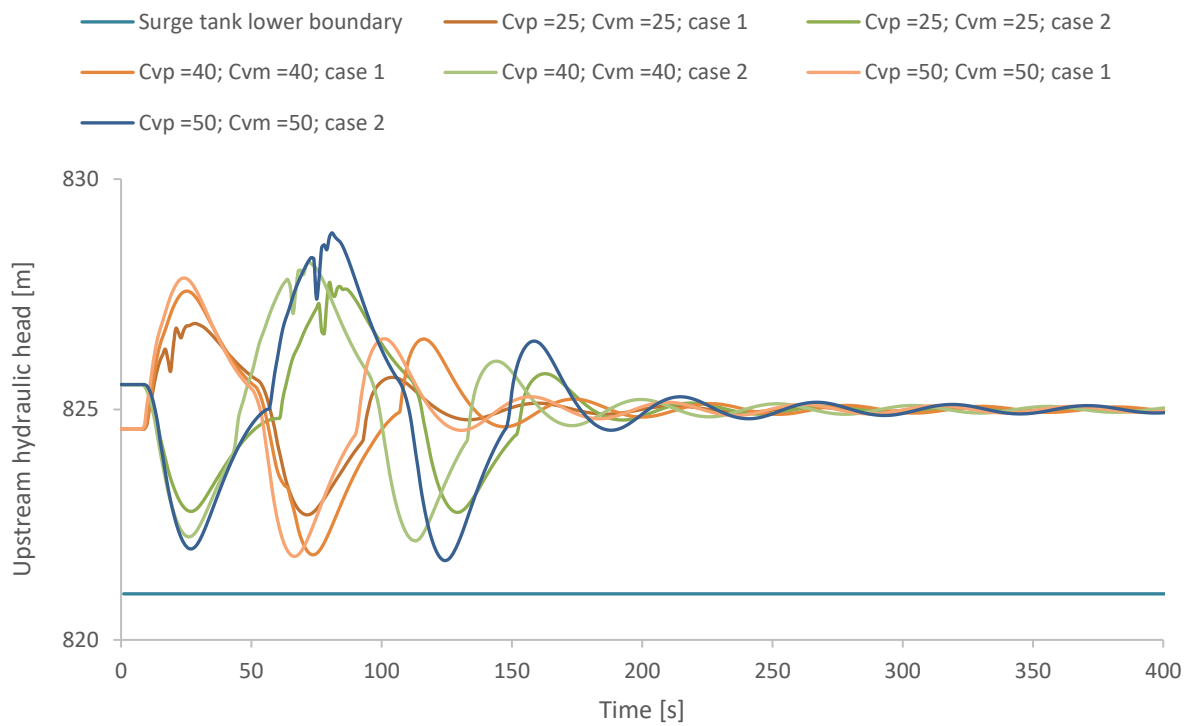


Figure 4.7. Lowest water level in the variable surge tank for different throttles

$C_v$ [ $m^5/s^2$ ]	25	40	50
Max. water level [m]	839.1	839.8	840.0
Min. water level [m]	822.7	821.8	821.7

Table 4.2. Maximum and minimum levels simulated with different symmetrical throttles



### 4.2.3.2 Asymmetric

As mentioned in chapter 3.3.2.3, a rise of the surge tank lower boundary by 2 meters is attributed to the implementation of an asymmetrical throttle. The water level should then stay above 822 meters in the surge tank.

The simulations of symmetrical throttles in the previous part showed that a coefficient  $C_v = 40 \text{ m}^5/\text{s}^2$  should be considered. For this coefficient, the water level almost reaches the upper boundary while there is a small margin between the lowest water level and the lower boundary. An asymmetrical throttle for which the head losses in the downward direction are smaller is then tested. A combination of  $C_{vp} = 40 \text{ m}^5/\text{s}^2$  and  $C_{vm} = 50 \text{ m}^5/\text{s}^2$  is considered and the results for the lowest water level reached are shown in Figure 4.8.

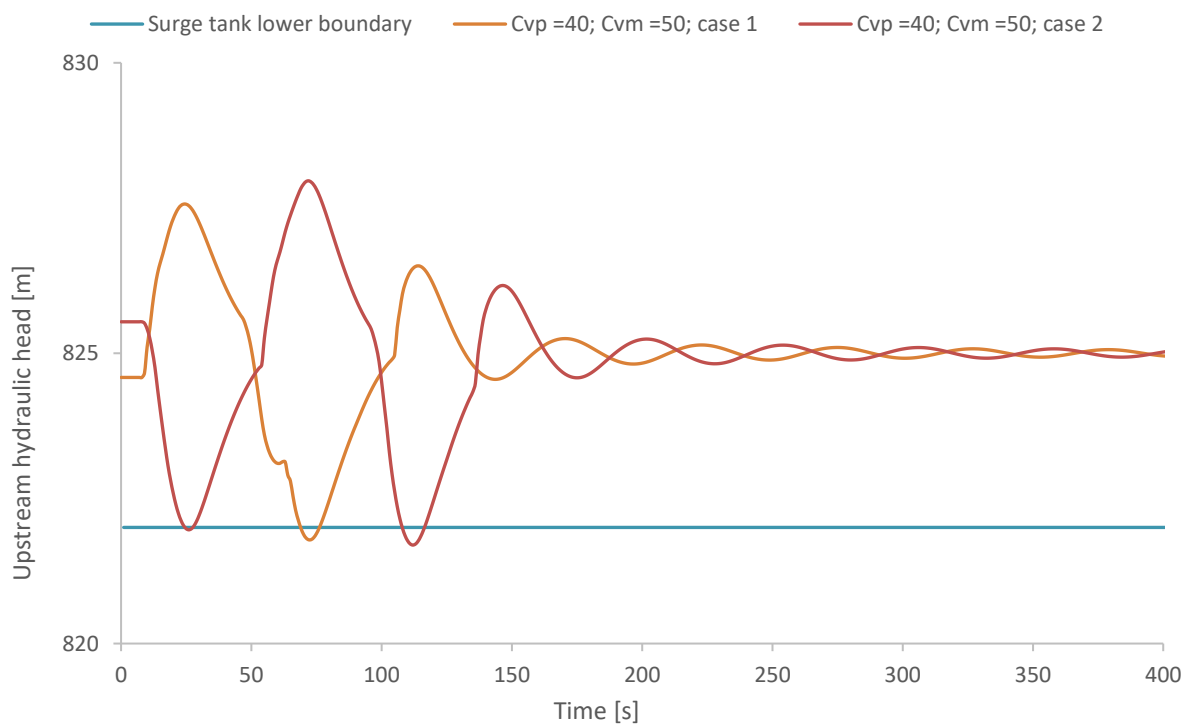


Figure 4.8. Lowest water level in the variable surge tank for an asymmetrical throttle

As seen in the results, the water level goes under the new surge tank boundary, even for a small decrease of the downward head losses. Thus, the larger space used by this kind of throttle keeps them from being implemented in this situation. A symmetrical throttle is then a better option in this case.

### 4.2.3.3 Throttle design

The symmetrical throttle associated with the optimal coefficient  $C_v = 40 \text{ m}^5/\text{s}^2$  found previously is designed by using the method described in chapter 3.3.2.3.2. According to Table

3.24, the head loss coefficient in the whole surge tank associated with this coefficient  $C_v$  is equal to  $\zeta_{new} = 1702 [-]$ . Then, the head loss coefficient related to the throttle itself is  $\zeta_{throttle} = 1605 [-]$ .

The Idelchick formula is used to estimate the diameter of such a throttle. It is assumed that  $\lambda = 0.02[-]$ ,  $F_1 = A_{surge\ tank} = 83.3\text{m}^2$  and  $l = 1\text{m}$ . After several iteration, a section of  $3.3\text{ m}^2$  for which the computed head loss coefficient would be  $\zeta_1 = 1614 [-]$  is proposed. The throttle would then have a 2 meters diameter.

### 4.3 Economic analysis

The estimated costs of each solutions are displayed in Table 4.3, Table 4.4 and Table 4.5. As a first approximation, the implementation of the throttle seems to be the most expensive solution while the two others are similar.

<b>Price per m<sup>3</sup> [kr/m<sup>3</sup>]</b>	500
<b>Excavated volume [m<sup>3</sup>]</b>	7'380
<b>Excavation price [kr]</b>	3'690'000
<b>Construction time</b>	1.5 month
<b>Production halt cost [kr]</b>	750'000
<b>Design and planning [kr]</b>	500'000
<b>Total cost [kr]</b>	4'940'000
<b>Total cost [CHF]</b>	600'000

Table 4.3. Estimated cost of the enlargement of the surge tank

The plugs in the addit and the upper tunnel are considered to have a section of 25 m<sup>2</sup>.

<b>Upper tunnel section [m<sup>2</sup>]</b>	25
<b>Price per meter [kr/m]</b>	17'000
<b>Upper tunnel length [m]</b>	90
<b>Upper tunnel cost [kr]</b>	1'530'000
<b>Lower tunnel section [m<sup>2</sup>]</b>	35
<b>Price per meter [kr/m]</b>	19'000
<b>Lower tunnel length [m]</b>	43
<b>Upper tunnel cost [kr]</b>	817'000
<b>Tunnels cost [kr]</b>	2'350'000
<b>Plugs cost [kr]</b>	2 x 650'000
<b>Construction time</b>	1.5 month
<b>Production halt cost [kr]</b>	750'000
<b>Design and planning [kr]</b>	500'000
<b>Total cost [kr]</b>	4'900'000
<b>Total cost [CHF]</b>	600'000

Table 4.4. Estimated cost of the transformation of the surge tank into a variable surge tank

The cost of the throttle is approximated by the cost of a concrete plug that would be implemented on the surge tank multiplied by a factor of 3 to take into account the construction of the steel throttle and the vertical orientation of the throttle. The considered plug is the one rebuilt in the old addit at the end of the construction. A section of 25 m<sup>2</sup> is considered for it.

<b>Surge tank section [m<sup>2</sup>]</b>	83
<b>Throttle cost [kr]</b>	3 x 2'400'000
<b>Plug cost [kr]</b>	650'000
<b>Construction time</b>	1.5 month
<b>Production halt cost [kr]</b>	750'000
<b>Design and planning [kr]</b>	500'000
<b>Total cost [kr]</b>	8'600'000
<b>Total cost [CHF]</b>	1'050'000

Table 4.5. Estimated cost of the implementation of a throttle

## 5 Discussion

### 5.1 Calibration

#### Data

The calibration of the model is largely based on the measurements carried out during the field trip in September 2017. The pressure measured for different values of power produced by the turbine allowed for a good overview of what can happen during normal operation. The shutdown situation is also covered, although with only one occurrence. An additional shutdown would have been useful to validate the calibration.

The lack of water velocity or discharge measurements add some uncertainties in the calibration. The velocity estimation in the model is based on the set of parameters that better fits the measurements in normal operation. A wrong value of efficiency in the turbine could for example lead to a poor estimation of the discharge needed to produce the demanded power, which would influence the calibration of the head loss coefficients.

A direct measurement of the water table movements in the surge tanks would have suppressed any uncertainties linked to the pressure measurements but overall, the data provided to complete the calibration of the model was very good, better than in most cases.

#### Normal operation

The calibration of the normal operation leads to good results in the upstream part of the model, with very small differences between the hydraulic head values coming from the measurements and the ones coming from the simulation. However, some uncertainties are linked to the downstream measurements, with high values of hydraulic heads that are difficult to explain. The most plausible explanation would be that the pressure repartition in the sensor section isn't homogeneous and that it causes a higher value of measured pressure than it should normally be. The simulation however fits well the measurements when the power produced reaches its maximum, 50 MW. This power is the one used in the finding of the extreme water level in the surge tanks. The calibration is then deemed acceptable.

#### Shutdown

A difficulty experienced during the shutdown calibration is the reopening of the turbine in a no-load operation that could not be replicated in LVTrans. It leads to some uncertainties about the

hydraulic phenomena taking place and to the adjustment of the measured pressure in the downstream part. The hypothesis is made that the amplitude and period of the oscillations observed in the measurements are consistent with the oscillations of the water table inside the downstream surge tank. The effect of the turbine reopening is then viewed as a constant and local increase of pressure at the sensor level and the adjustment consists in a simple vertical translation of the measurements. However, the reopening of the turbine could also influence the water table movements and increase or decrease their amplitude. The friction coefficient of the surge tank established by the calibration could then be incorrect.

The calibration for the shutdown presents some surprising parameters values. First, the diameter of the upstream creek shaft is way larger than the one estimated from the drawings. The imprecision of the drawings in itself does not explain such a difference. However, it has been shown that simulating a smaller diameter leads to an oscillation with a way too large amplitude and period. It would then be necessary to reduce drastically the diameter of the surge tank to decrease the period and its coefficient  $C_v$  to decrease the amplitude. This would lead to completely unrealistic values for the surge tank.

The friction coefficients are generally too low to be realistic in the surge tanks and the creek shaft. However, they can't be increased without having completely different results that don't fit the measurements as well as the calibrated model does. Furthermore, it has been noted in other thesis working with LVTrans, such as the one written by Daniel Gomsrud<sup>9</sup>, that the method of characteristics used in the software can underestimate the transient friction. It is then possible that the need to use low friction coefficients is due to the need to compensate the underestimation of the transient friction.

Overall, the hydraulic head oscillations issued by the surge tanks movements upstream and downstream the turbine seem well represented by the model for the purpose of this work. It can then be assumed that the simulated water level in the surge tanks are a good depiction of the reality.

## **5.2 Upgrade of the model**

### **Considerations on the model**

---

<sup>9</sup> Invalid source specified.

The upgrade of a powerplant into a pumped storage system can take many forms. For the purpose of this study, only one case was explored for the Roskrepp powerplant with a 50 MW pump placed in parallel with the turbine. It is however a simplification and the design of the pump should consider the implementation of a reversible pump turbine or a pump with another characteristics. In the same way, the pump is placed 10 meters below the turbine in the model to avoid cavitation whereas its actual position should be optimized.

Furthermore, it is recommended to avoid very small lengths in the model pipes as computational mistakes could distort the results. The positions of the junctions between the pipes leading to the turbine and the ones leading to the pump are chosen accordingly and do not reflect reality.

In those aspects, the model does not represent what would actually happen if the powerplant was upgraded into a pumped storage plant. However, it presents a good first assessment of the behaviour of the surge tanks when a pump is introduced in the system, which is the purpose of this study.

### **Load case scenarios**

The scenarios used to identify the lowest and highest water levels that can be reached in the surge tanks take into account different combinations of pump and turbine operations and water levels in the reservoirs. It is not likely that all the conditions simulated in those scenarios occur in a same event in reality as it would mean that several start up and shutdown of the pump and turbine would occur at the worst moments while having the highest and/or lowest water levels in the reservoirs. In this regard, the load case scenarios are considered conservative.

### **Results**

The simulations results state that the upstream surge tank would be able to absorb the mass oscillations in an upgraded plant while the downstream surge tank would be insufficient. The much larger capacity of the upstream surge tank make it less sensitive to the addition of a pump. Furthermore, the secondary intake acting as a second surge tank adds to the global capacity of the upstream part of the powerplant to absorb or supply water. The downstream part on the other hand can only rely on its small surge tank, which is not enough when the pump add an extra-demand.

## 5.3 Solutions

This study limits itself to three solutions to keep the water level from going out of the downstream surge tank boundaries. However, more could be explored such as the displacement of the surge tank boundaries or its transformation into a closed surge tank or a differential surge tank.

All the solutions should be built in summer, when the production is at its lowest to reduce the halting costs.

The solution designed in this part are considered as a first approximation and do not take into account any margin of error on the simulation results. In more detailed future studies, the fact that the water table is not completely flat should be considered and safety factors should be applied to the simulation results.

### 5.3.1 Surge tank enlargement

The enlargement of the surge tank would lead to an equivalent diameter of 24 meters and a section of 452 m<sup>2</sup>. The surge tank would then have its volume multiplied by 5. Such a big section for a height of only 20 meters would be unusual and not necessarily the most optimized solution in a hydraulic point of view. A proposed section is a rectangle of 15 by 30 meters, according to the drawing displayed in annex A.

The excavation of the additional space in the surge tank should start at the access point at the top of the surge tank. The machines would then excavate from the top toward the bottom, in the same way as for the construction of a shaft. At the end of the excavation, the machines should be evacuated by elevating them through the surge tank or by opening the old addit and rebuilding the plug at the end of the construction.

### 5.3.2 Variable surge tank

The transformation of the surge tank into a variable surge tank would require the construction of a tunnel with a length of 90 meters to form the upper chamber, and the expansion of the tailrace tunnel on a 43 meters length from the surge tank. A solution would be to start the excavation of the upper tunnel from the service tunnels of the powerplant as shown in the drawing in annexes B and C and then place a plug to close it. The lower tunnel would be built by excavating the top of the tailrace tunnel and expanding its height until it reaches 11.2 meters instead of 6.2 meters. The construction machines could access the tunnel by removing the plug and using the old addit. The plug should then be rebuilt afterward.



### **5.3.3 Throttle**

The optimal throttle that should be implemented is a symmetrical throttle with a diameter of 2 meters. The considered design would be a concrete plug placed at the bottom of the surge tank with a hole in it. The hole would have a diameter of 2 meters and should be covered by steel to keep the water from damaging its edges. Drawings of it are available in annexes D and E.

The construction of such a throttle could take place as following: The tail race tunnel would first be emptied by lowering the downstream reservoir and closing the ball valve upstream of the turbine. The construction machines would then access the bottom of the surge tank by removing the plug in the old addit. A platform would then be built on which the steel outline of the throttle would be placed. The platform would then support the throttle while the 1 meter thick concrete is cast around it. Finally, once this part finished, the platform and machines would be removed, the tunnel cleaned and a new plug would be installed in the old addit.

The implementation of a throttle inside the surge tank could diminish the protection brought by the surge tank to the tail race tunnel against the water hammer. The surge tank close proximity to the turbine reduces the risk of it being an issue, however, it should be examined by a more in-depth study of effect of the upgrade of the Roskrepp powerplant on the water hammer.

It should be noted that the design of the throttle is based on a simplified method of estimation of the head loss coefficient. Even though the diameter value computed from it is considered valid for the purpose of this study, a more accurate design of the throttle should be carried out by using for example a 3D modelling software.

### **5.3.4 Economic analysis**

The economic analysis is based on very rough estimations of the costs related to the constructions of the solutions. Number of approximations have been realized and the actual conditions of construction are not taken into account. The prices used in this study are average prices and could be largely different in reality. For those reasons, this economic analysis should be taken cautiously and viewed as a very first approximation of the costs that could be expected in the construction of the solutions.



## 6 Conclusion

In this study, the numerical model of the Roskrepp powerplant has been built with the 1D software LVTrans to simulate the effect on the surge tanks of the upgrade of the powerplant into a pumped storage system. The calibration of the model, based on the data collected during the field trip, showed that the model gives an accurate enough estimation of the water level movements in the surge tanks.

The model has been upgraded to reproduce the addition of a 50 MW pump in parallel with the turbine. Worst case scenarios were then established for the water levels in both surge tanks. They propose different combinations of water level in the reservoirs and of pump and turbine operations that should lead to the largest amplitude that could be experienced by the surge tanks. The simulation of those scenarios showed that the upstream surge tank supports the upgrade of the powerplant without any modification needed. The downstream surge tank on the other hand is not able to keep the water table oscillations within its boundaries and should be upgraded.

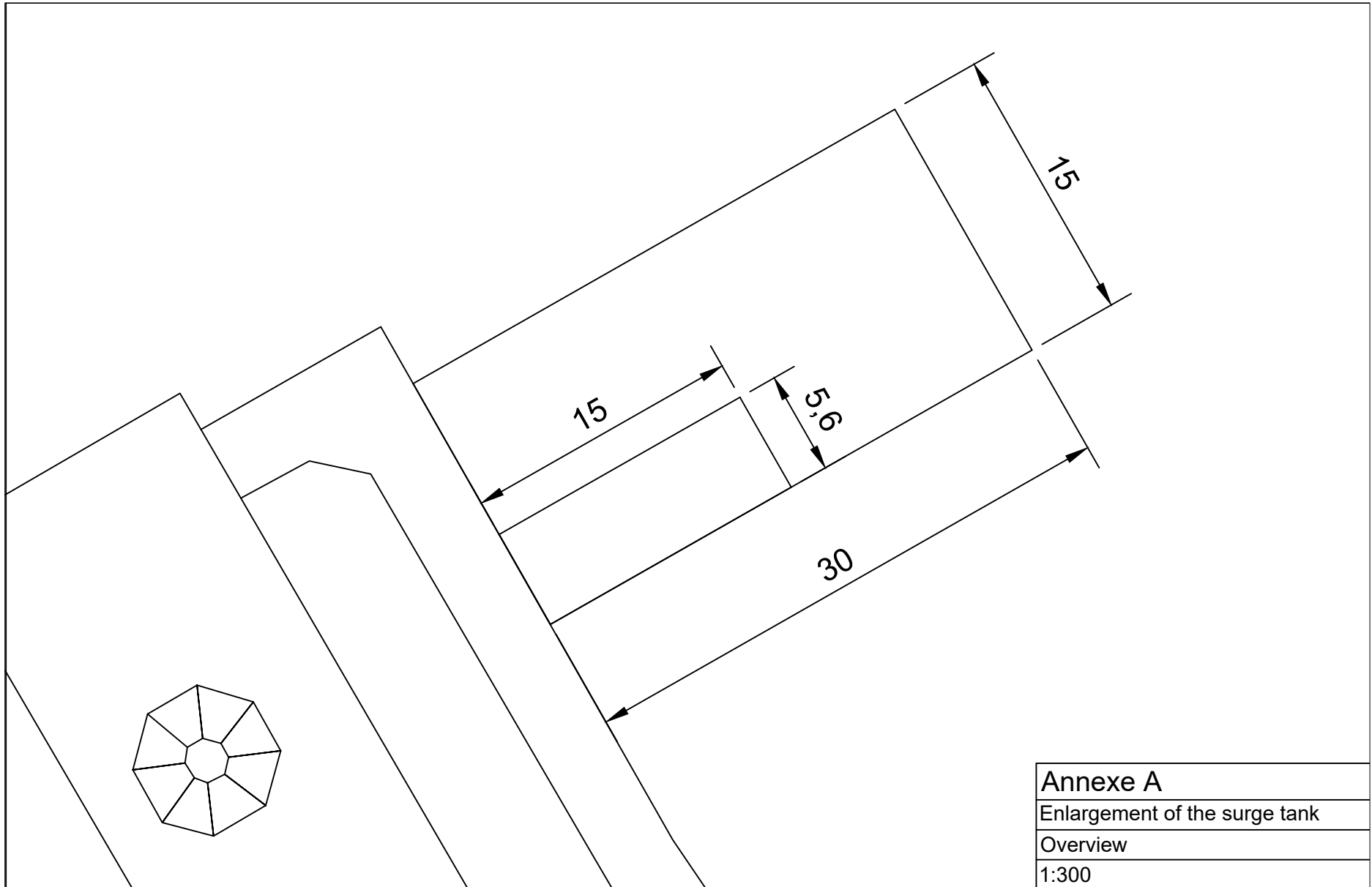
Three solutions were proposed in this study and implemented in the model. The first one was the enlargement of the surge tank. The second one was the transformation of the surge tank into a variable surge tank. The third one was the implementation of a throttle at the bottom of the surge tank. All three of them increased the surge tank capacity and an optimal design for each of them was proposed.

Finally, an economic analysis of the solutions was proposed and a rough estimation of the cost of each of them was presented.

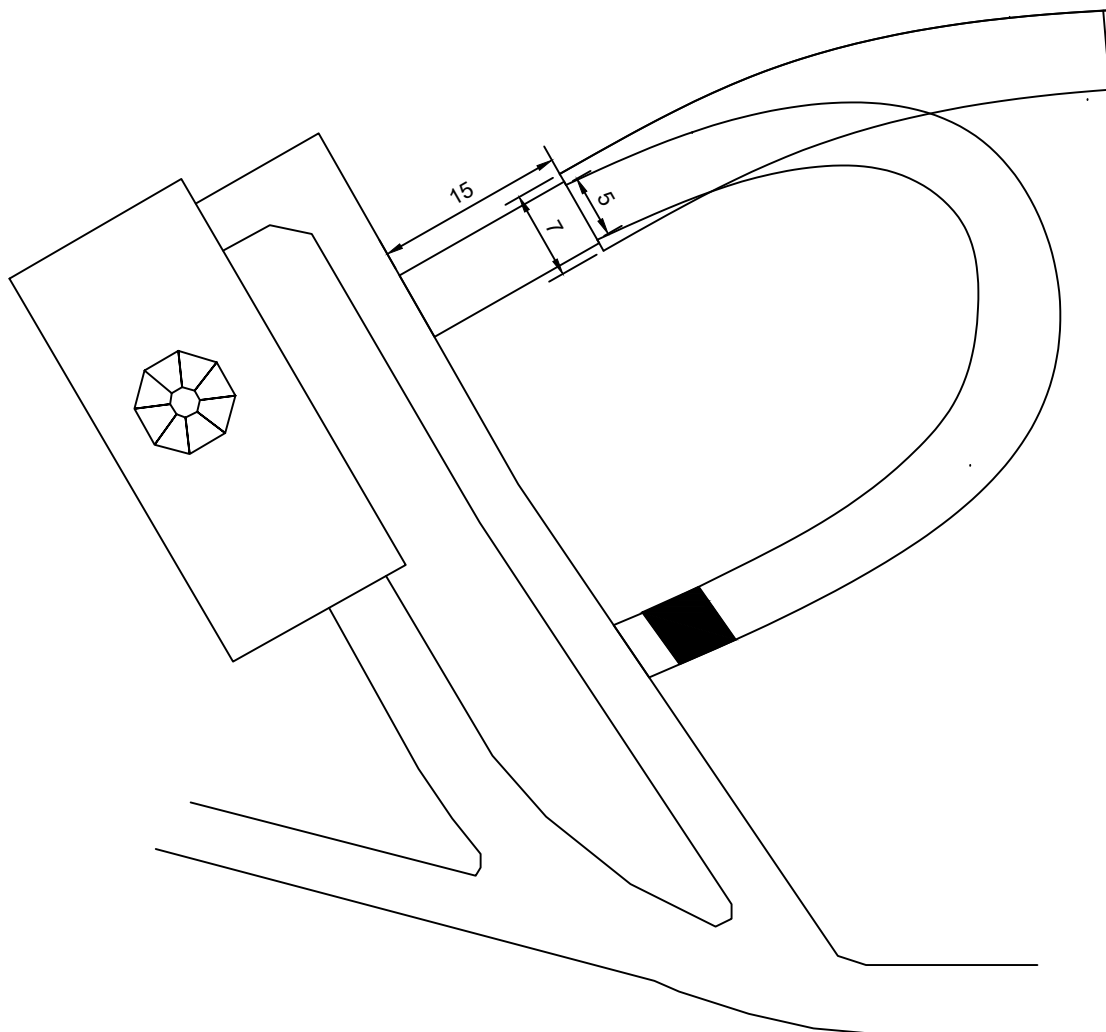
## 7 Bibliography

- Adam, N., De Cesare, G., & Schleiss, A. (n.d.). *Surge tank throttles for safe and flexible operation of storage plants*. Laboratory of Hydraulic Construction (LCH) - EPFL.
- Ancey, C. (2014). *Mécanique des fluides - Une introduction à l'hydraulique pour les ingénieurs civils*. Laboratoire hydraulique environnementale (LHE) - EPFL.
- Bandi, A.; Bogenrieder, W.; Braitsch, W.; Clauser, C.; Dafu, Y.; Fisch, M.N.; Gökler, G.; Goetzberger, A.; Haas, H.; Hein, D.; Heinloth, K.; Huckermann, V.; Karl, J.; Laue, H.J.; Neumann, A.; Pürer, E.; Richter, S.; Rosillo-Calle, F.; Shuqing, W.; Song, Won-Oh; Specht, M. (2006). *Energy Technologies - Subvolume C : Renewable Energy*.
- Boillat, J.-L., & De Souza, P. (2004). *Modélisation des systèmes hydrauliques à écoulement transitoire en charge*. Communication 16, LCH, Lausanne.
- Chaudhry, H. (2014). *Applied Hydraulic Transient*.
- Dinçer, A. E., & Bozkus, Z. (2014). *Investigation of water hammer problems in the penstocks of pumped - storage power plants*.
- Elie, F. (2014, mai). Coup de bélier et cheminée d'équilibre.
- Hachem, F., Nicolet, C., Duarte, R., De Cesare, G., & Micoulet, G. (2013). *Hydraulic design of the diaphragm's orifice at the entrance of the surge shaft of FMHL pumped-storage power plant*.
- Idelchick, I. (1960). *Handbook of hydraulic resistance - Coefficient of local resistance and of friction*.
- Jaeger, C. (1933). *Théorie générale du coup de Bélier - Application au calcul des conduites à caractéristiques multiples et des chambres d'équilibres*. Ecole Polytechnique Fédérale de Zürich.
- Jaeger, C. (1977). *Fluid transient in hydro-electric engineering practice*.
- Nabi, G., Habib-ur-Rehman, Kashif, M., & Tariq, M. (2011). Hydraulic Transient Analysis of Surge Tanks: Case Study of Satpara. *Journal of Engineering & Applied Science, Vol 8*, 34-48.
- Richter, W., Zenz, G., & Vereide, K. (2015). *Hydraulic design and modelling of large surge tank*.
- Richter, W., Zenz, G., Schneider, J., & Knoblauch, H. (2015). *Surge tank for high head hydropower plants - Hydraulic layout*.
- Schleiss, A. (2015). *Aménagement hydrauliques*. Section de Génie Civil - EPFL.
- Schleiss, A. (n.d.). *Polycopié postgrade*.
- Stensby, K. E. (2016). *Kostnadsgrunnlag for vannkraft - Kostnadsnivå januar 2015*.
- Travas, V. (2014). *Water mass oscillations in a generic surge chamber*.
- Vereide, K., Lia, L., & Nielsen, T. K. (2015). *Hydraulic scale modelling and thermodynamics of mass oscillations in closed surge tanks*.
- Vereide, K., Richter, W., & Lia, L. (2015). *Surge tank research in Norway and Austria*.
- Wang, C., Yang, J., & Nilsson, H. (2015). *Simulation of water level fluctuation in a hydraulic system using a coupled liquid-gas model*. Retrieved from MDPI: <http://www.mdpi.com/2073-4441/7/8/4446/htm>

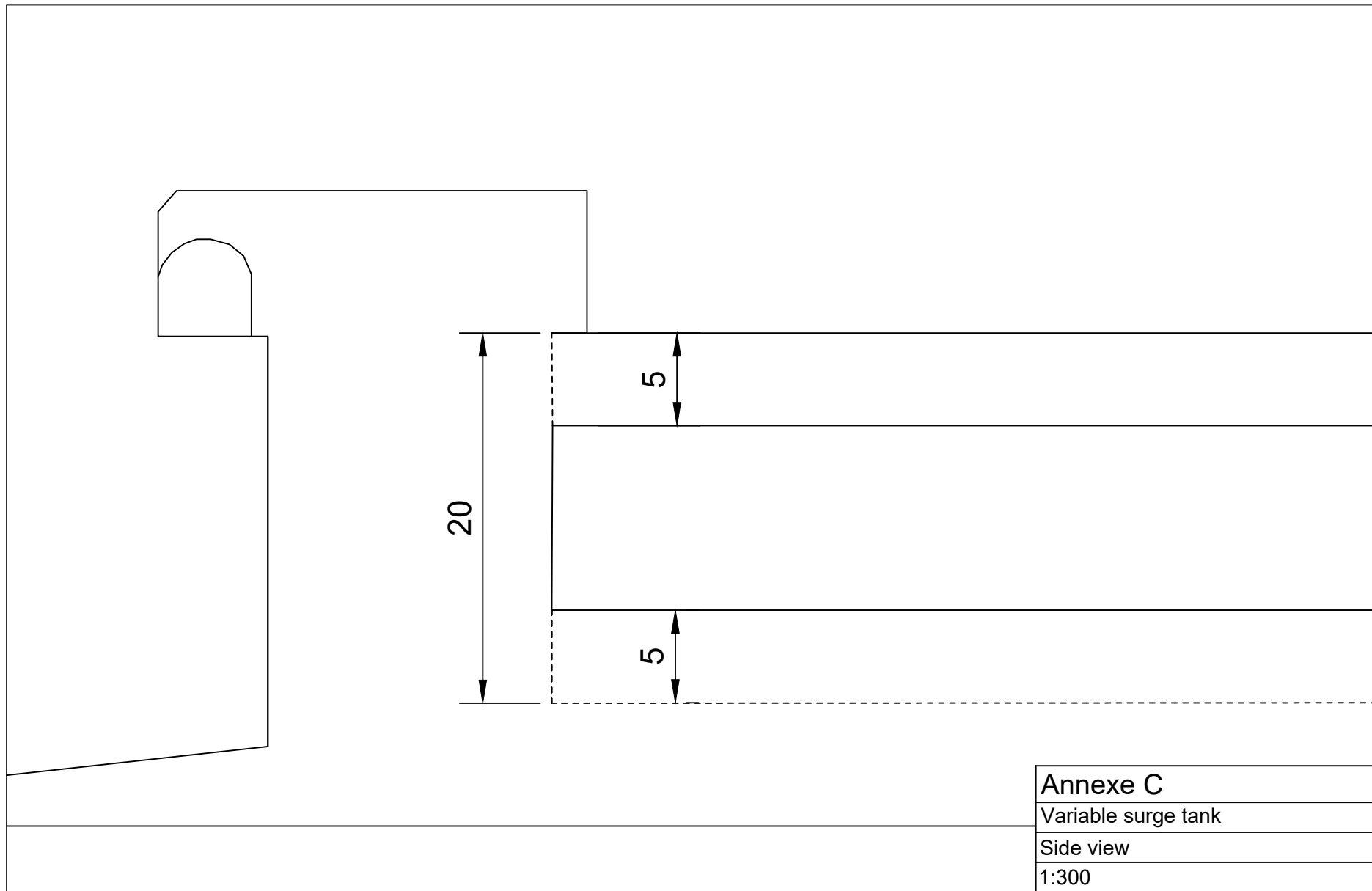
# ANNEXES



Annexe A
Enlargement of the surge tank
Overview
1:300

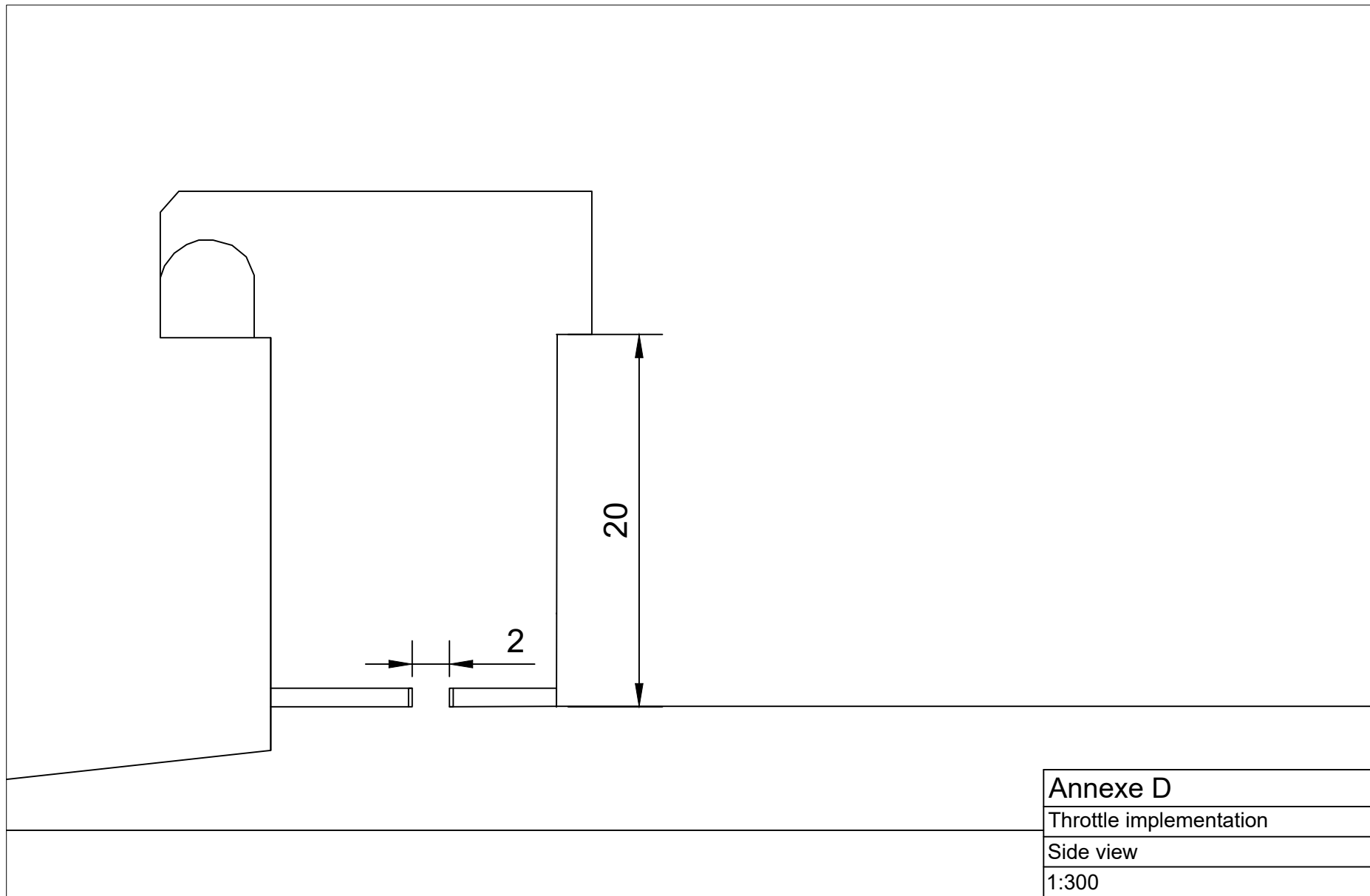


<b>Annexe B</b>
Transformation into a variable surge tank
Overview
1:600

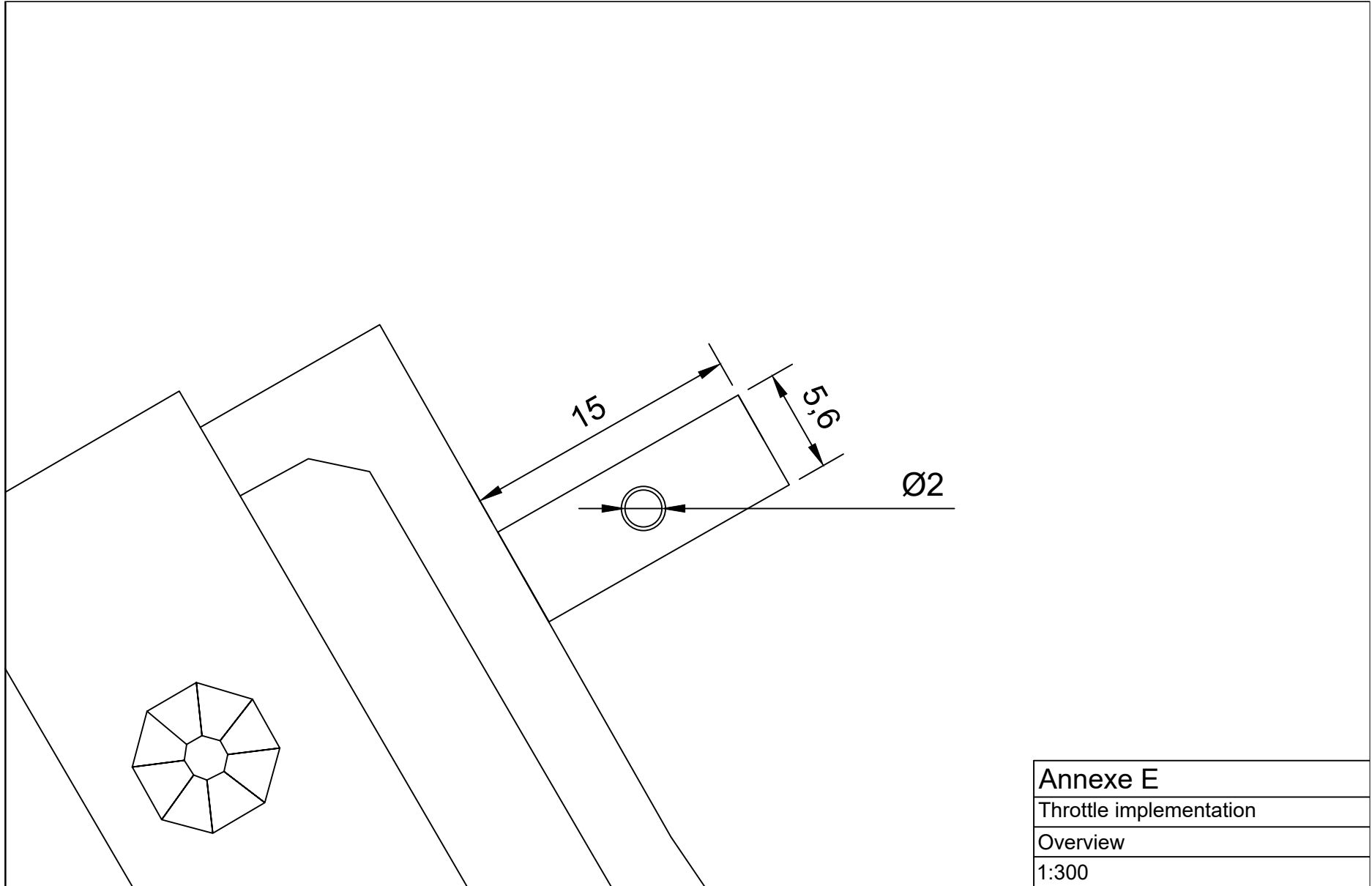


Annexe C
Variable surge tank
Side view
1:300



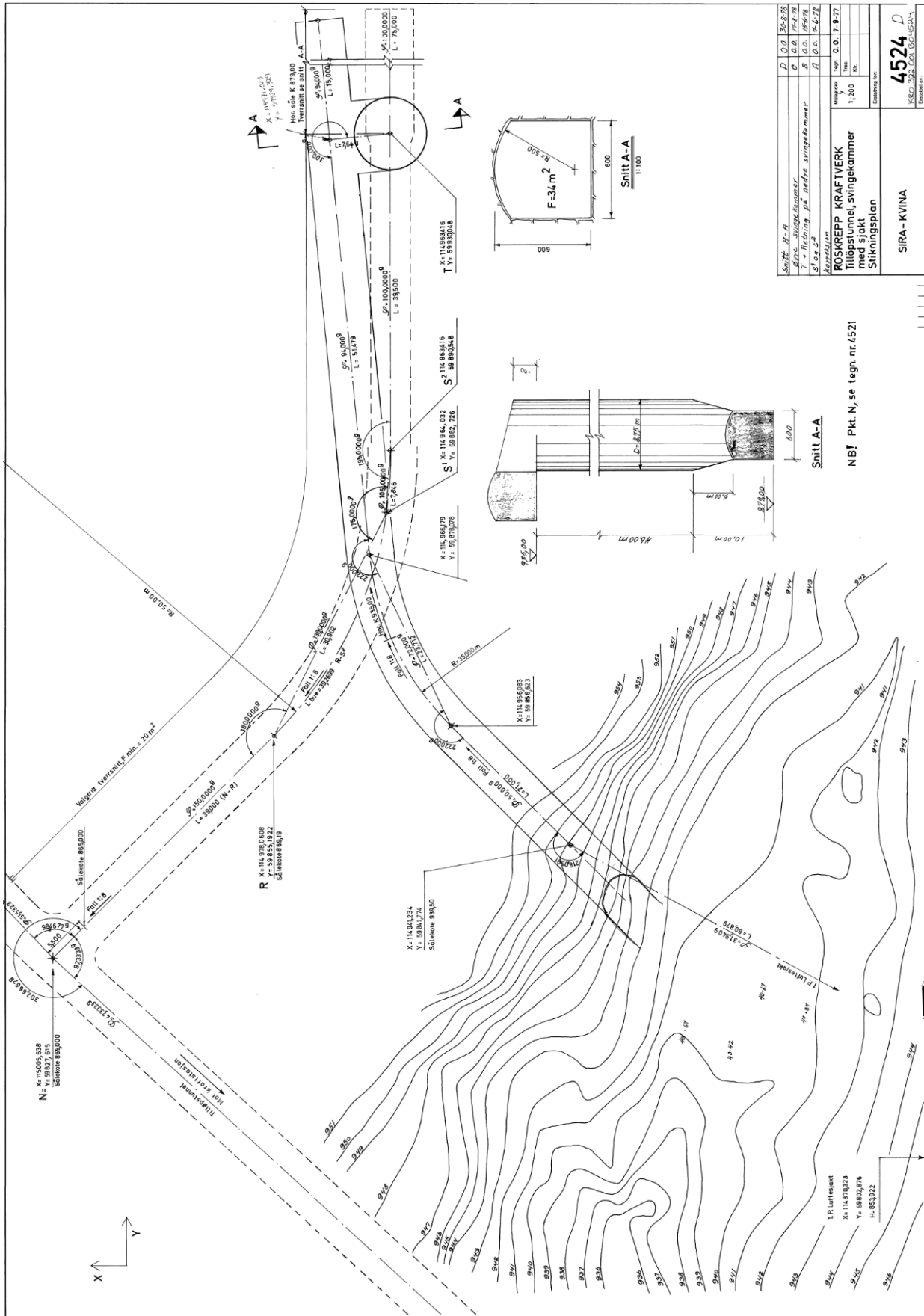


Annexe D
Throttle implementation
Side view
1:300



Annexe E
Throttle implementation
Overview
1:300

# Annex F – Upstream surge tank drawing



Snitt A-A	D	0.0	30.878
Blive - svingekammer	C	0.0	17.478
T - Røtting på nedre svingekammer	B	0.0	15.978
Stig 3	A	0.0	14.678

Skala	1:200	1:100
Blive	1:200	1:100
Stig 3	1:200	1:100

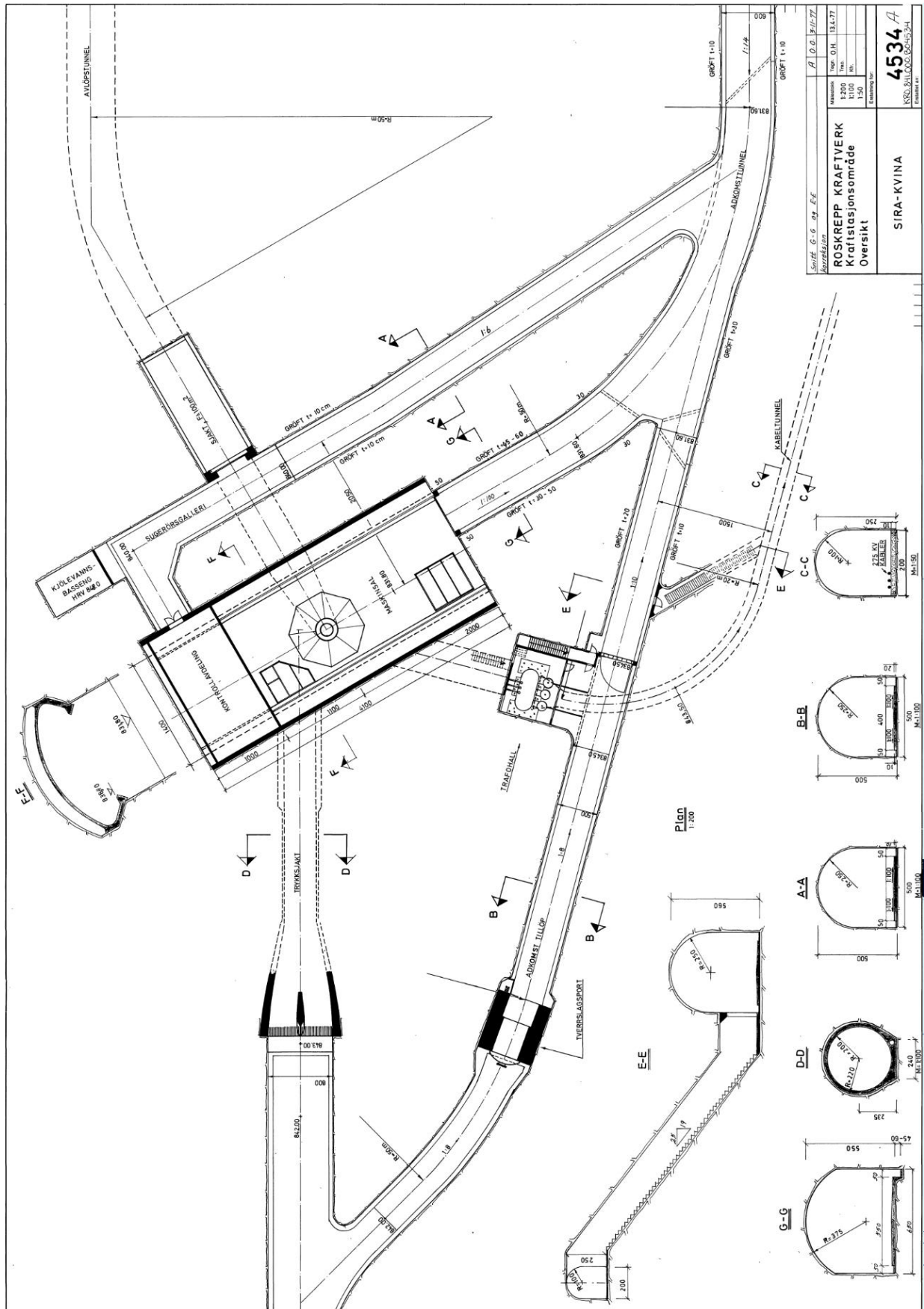
  

Prosjekt	ROSAREPP KRAFTVERK
Oppdragsnr.	11497323
Oppdragsnavn	Tilførselstunnel, svingekammer med sjøtt
Oppdragsleder	Stikkingsplan
Oppdragsnr.	4524
Oppdragsnavn	SIRA - KVINA

NBT Pkt. N, se tegn. nr. 4521



# Annex H – Power station drawing



Side: G-G, 1:100	Scale: 1:100	Project: ROSKREPP KRAFTVERK Kraftstasjonsområde Oversikt	Sheet: 4534 A
Author: O.E. 1/11/22	Scale: 1:100	Client: SIRA-KVINA	Project No: KSS-2010-02-0524
Revision: 1.000	Scale: 1:100	Project Name: ROSKREPP KRAFTVERK Kraftstasjonsområde Oversikt	Project No: KSS-2010-02-0524
Revision: 1.000	Scale: 1:100	Project Name: ROSKREPP KRAFTVERK Kraftstasjonsområde Oversikt	Project No: KSS-2010-02-0524
Revision: 1.000	Scale: 1:100	Project Name: ROSKREPP KRAFTVERK Kraftstasjonsområde Oversikt	Project No: KSS-2010-02-0524

